Ghent University
Faculty of Sciences
Department of Inorganic and Physical Chemistry

# Innovative Indium Phosphide-Based Colloidal Quantum Dots Synthesis Designed for Luminescent Down-Conversion

Dorian Dupont

Thesis submitted in fulfillment
of the requirements of the degree of
Doctor in Science: Chemistry
2017

Ghent University
Faculty of Sciences
Department of Inorganic and Physical Chemistry

| Promotor | Department |
|---|---|
| Prof. Dr. Ir. Z. Hens | Inorganic and Physical Chemistry |

| Co-promotor | Department |
|---|---|
| Dr. M. D. Tessier | Inorganic and Physical Chemistry |

| Jury members | Affiliation |
|---|---|
| Dr. P. Reiss | CEA |
| Prof. Dr. P. F. Smet | UGent |
| Prof. Dr. I. Moreels | UGent |
| Dr. Y. Meuret | KU Leuven |
| Dr. Shalini Singh | UGent |

This work was realized with the support of the
Agency for Innovation by Science and Technology
(IWT)

La Materia Prima qu'il ne faut surtout pas confondre avec la matière au sens moderne du terme doit être envisagée dans la perspective thomiste. Nous nous répétons au risque d'être mal compris, la Materia Prima ne doit absolument pas être confondue avec la matière au sens moderne qui n'ont en commun que l'étymologie.

-

Antoine Sabatier

# Acknowledgements

Knowing that most of the people will tend to search for their own acknowledgments rather than taking time to read all the text, I will put your name or surname in bold for your convenience.

First of all, I would like to thank **Prof. Hens** who gave me the opportunity to pursue my doctoral study in his group and trusted me despite of my very bad English level the first time we met. I remember when you explained me the content of the project I was only able to answer "Yes, it is a very good project!" which I repeated at least a dozen times since I did not really fully understand what you said. But I knew I would enjoy to tackle the challenge of the synthesis and I was really motivated to start and carry out this project. This work would not have been possible without our scientific discussions and the bright ideas that you proposed during the group meeting. Speaking of which, I am always impressed by your ability to process a large amount of information and to provide constructive inputs in a very short time, I think you can surpass the processing power of a quantum computer. I would also like to express my sincere thanks to **Prof. Smet** for allowing me to use his lab equipment and for his help, when I struggled to set up the devices. It has also been very instructive, in the style and content, to attend your oral presentations about the history of lighting. I would also like to express my gratitude to the chairman **Prof. De Buysser** and the jury members, **Dr. Reiss**, **Prof. Smet**, **Prof. Moreels**, **Dr. Meuret** and **Dr. Singh** for the constructive comments which allowed me to improve the thesis. Thanks also to the contribution of the co-authors and collaborators, **Prof. Lange**, **Prof. Brainis**, **Jana**, **Mona**. This work would not have been possible without funding. Therefore, I would also like to thank the **Innovation by Science and Technology (IWT)**.

I want to thank my PCN's colleagues for these amazing four years. Special shout out to the sick office team. **Kishu**, cheers to all the good times we had together. I liked to listen to your stories about India and life in general even if it was sometimes made-up stories. I wish you the best of luck in your new journey in Canada and I hope to see you again. Don't forget to register at the gym! **Arnau**, I liked to hang out and drinking beers with you. Thank you for the amazing centrifugations of copper nanoparticles that raised the oxygen level inside the glovebox. Also, thank you for the multiple invitations to your basketball matches but I was obliged to decline since you don't know how to make slam dunk. Now, you will be able to fully enjoy Solobasket at your new spot. Thanks **Pieter S**. aka Clark Kent. You will need the powers and abilities of Superman to take care of the glovebox and also to clean your office space. Thank you also for writing my Dutch summary and I wish you the best of success with your research. **Hannes**, I enjoyed the funny meme pictures of you as well as your contagious laugh. I hope you will get rid of the jelly stuff in your syntheses and I wish you all the best in your project.

Thanks to the cool office crew. **Kim**, I really enjoyed to work with you even if we had some difficulties to communicate at the beginning. I very much enjoyed your company especially during our trip before the conference in Phoenix. Thank you for all your work and explanations about NMR and for your precious help during the writing of this manuscript. Thanks also to remind me all the administrative stuff I needed to take care of, I'd be lost without you. I am looking forward to work again with you and I wish you good luck for your project. **Jorick**, thanks for your XRD expertise and your good musical taste. Cheers to all the nice moments we spent during conference and outside of the lab. I really enjoyed the night when I hit my head after falling off my bike when I tried to find you in the street close to Vooruit. Thank you **Willem** for taking initiative to keep the lab clean and functional. I wish you all the best in building your new house. Thanks to **Valeriia** for your TEM and NMR work and the funny pictures that we send to each other. Cheers to all the good times we had drinking Rocherfort 10 when we hung out with the lab mates. Thank you also for your invaluable help during the writing of the manuscript. **Suzanne**, thanks for organizing badminton sessions and LAN party. I must say that I am a better badminton than Age of Empire player. **Vignesh**, thanks for our discussions about single spectroscopy of InP/ZnSe quantum dots and once

again congratulations for your recent paper.

Now I would like to acknowledge people from the fun office. **Shalini**, I really appreciate your interest and the time you have taken to correct the typing and grammatical errors of my manuscript. Congratulations on your new grant and thanks a lot for your stunning dancing performances. I hope that one day you will teach me how to move like you. **Emile**, thank you for our scientific discussions and our common passion for JCVD quotes. I hope you will not be hit too much by Lacrosse sticks in the coming years. **Igor**, thank you for your help related to the photo and thermal stability measurements as well as for the installation of the Avantes spectrometer that I almost never used. Also, thank you for filling my Facebook news feed with all your Facebook posts. I wish you good luck with your new project. Thanks to **Natalia** who was always up for a party and **Pengshang** who will probably break the record for the number of syntheses performed during one PhD. Thanks also to **Tangi** for our discussions about the beer making process and for the two-year-old Westvleteren 12 that you gave me. **Pieter G.**, I hope you enjoy your stay in the US and I wish you good luck with all your future projects. Thank **Jakob** for our discussions about South America and for our amazing paintball sessions.

I would like to thank all my former PCN's colleagues. Thanks **Chen** for giving me food sometimes and I apologize once again for my mistake when I removed your unique PbS sample during the glovebox cleaning. **Jonathan**, thanks for your help in finding the chemical mechanism of InP synthesis. Enjoy your stay in New-York and I wish you all the best in your future scientific career. **Sofie**, I really appreciate your help concerning the experimental measurements on remote phosphor layer. I wish you all the best in your new job and your new house. I want to thank **Yolanda** for all the good times we had outside the lab at the beginning of my PhD. I wish you all the best in your life. Thanks also to **Antoine** who was my co-pilot when we used to go back to France during the weekend. I don't know what you are up to but I wish you all the best. Thanks also to **Daniel**, you left too soon. I didn't have time to know you but thanks for the beers and soups that we shared. Thanks **Justin** for our interesting discussions about electroluminescence and red wine. Thanks to **Stijn** for your availability and help when I was working in the lab. Thanks also to **Ruben** who taught me how to use and maintain the glovebox and for all the discussion we had

about the Flemish daily newspapers during lunch time. **Jose**, you did an amazing work during your master thesis and you would have been a great doctoral student. Thanks for your explanations about the chemical yield calculations. Thank you **Nurullah** for the quantum dots explosions when you performed synthesis and I have really appreciated when you gave us back our precious gifts before the Christmas dinner. Finally, I would like to thank **David** for his expertise in online role playing game and Coca-Cola Zero. Best regards for yourself and your family.

Thank you **Eleni** for your kindness, your advices and the delicious dishes that you made, especially the pizza. I wish you all the best in your life and your new work with Tam-Tam. Thanks to **Amrou** who supported me during the last days of my PhD. I hope you will find a nice job in the south of France. Thanks also to **Fady** aka Tonton Pipo for your support and all the discussions we had during and outside the working hours. Thanks to **Yesid**, **Inge** and **An-Sophie** for all the good times we spend together. Thanks also to **Louis**, **Emmanuel** for the great moments we had during conferences.

I also want to express my sincere thanks to the scientific staff which helped me to accomplish this work. Thanks to **Katrien** for your wonderful TEM images, you know how to handle the TEM controller. Special thanks to **Bart** who was my glovebox buddy and who helped me a lot in trying to maintain the glovebox operational. Be careful when you ride your motorbike! **Pat**, thank you for fixing my issues with computers. Thanks to the **Pierre**, **Kathleen**, **Ann**, **Claudine** that took care of the administrative stuff and for organizing the life of the department. Thanks to **Chokri** for keeping me informed about French news and I apologize to your wife for the times I started to eat after you had clean the kitchen. Enjoy your rides in your brand new car.

I also thank **my family** and **friends** for their support through all the ups and downs.

Like the saying goes, I "save the best for last", **Mickaël**. Thank you for putting your trust and confidence in me since the day I met you. It hasn't always been easy to supervise me during my internship in Paris as I was making a lot of redshift but I really enjoyed my stay and particularly my first nanocrystal synthesis. Shortly after my improbable graduation and the

end of your successful PhD, you moved to Ghent to work as post-doctoral researcher within this project and informed me about this PhD position. You also convinced Zeger that I would be the ideal candidate and asked me to join but I first declined as I did not want to start PhD studies. Still, due to your perseverance and a combination of circumstances, I decided to follow you. I must say that it was one of my best decision and I don't regret it given the excellent work we have accomplished in line with what we realized in Paris. Indeed, all the project requirements have been completed but this would not have been possible without you and your guidance. My work with you also made me realize that a positive team relationship is the key to success. Therefore, I am deeply grateful for your continued support over these years and I look forward to continue working with you.

*Ghent, October 2017*
*Dorian "Doud" Dupont*

# Contents

# List of Acronyms

## C

**C.Y.** ..... Chemical yield

## D

**DDT** ..... 1-Dodecanethiol

**DMF** ..... N,N-Dimethylformamide

**DOSY** ..... Diffusion ordered spectroscopy

## F

**FWHM** ..... Full width at half maximum

## I

**ICP-OES** .. Inductively coupled plasma optical emission spectrometry

## L

**LCD** ..... Liquid crystal display

**LED** ..... Light emitting diode

## M

**MSC** ..... Magic-sized cluster

## N

**NC** ..... Nanocrystal

**NMR** ..... Nuclear magnetic resonance spectroscopy

**nOe** ..... Nuclear Overhauser effect

**NOESY** ..... Nuclear Overhauser effect spectroscopy

## O

**ODE** ..... 1-Octadecene

**OLA** ..... Oleylamine

**OLED** ..... Organic light-emitting diode

## P

**PL** ..... Photoluminescence

**PLQY** ..... Photoluminescence quantum yield

**P(NEt$_2$)$_3$P** ..... Tris(diethylamino)phosphine

**P(NMe$_2$)$_3$P** ..... Tris(dimethylamino)phosphine

## Q

**QD** ..... Quantum dot

## R

**RBS** ..... Rutherford backscattering spectrometry

## T

**TEM** ..... Transmission electron microscopy

**TOP** ..... Tri-*n*-octylphosphine

**TOPO** ..... Tri-*n*-octylphosphine oxide

**TOP-S** ..... Tri-*n*-octylphosphine sulfide

**TOP-Se** ..... Tri-*n*-octylphosphine selenide

**(TMS)$_3$P** ..... Tris(trimethylsilyl)phosphine

## U

**UV-Vis** ..... UV-Visible spectroscopy

## W

**wLED** ..... White light emitting device

## X

**XPS** ..... X-ray photoelectron spectroscopy

**XRD** ..... X-ray powder diffraction

**XRF** ..... X-ray fluorescence spectroscopy

## Y

**YAG:Ce** ..... $Ce_3^+$-doped yttrium aluminum garnet aluminum garnet

# Nederlandse Samenvatting
# –Summary in Dutch–

Colloïdale halfgeleider nanokristallen (NCs) of quantum dots (QDs) zijn veelbelovende materialen voor een gamma aan toepassingen waarbij absorptie of emissie van licht een prominente rol speelt. De combinatie van hun nauw en grootte-afhankelijk emissie spectrum, hun breed absorptie-en excitatiegebied en hun verwerkbaarheid in oplossing maakt ze uitermate geschikt in verlichting en beeldschermen. In dit laatstgenoemde wordt wit licht genereerd door middel van de combinatie van een blauwe light-emitting diode (LED) en een remote phosphorfilm bestaande uit QDs die groen en rood licht uitzenden. De QDs absorberen een gedeelde van het blauwe licht, afkomstig van de LED, en zetten dit om in nauwbandig groen en rood licht. Op deze manier wordt wit licht genereerd wiens emissiespectrum opgebouwd is uit drie nauwe emissiebanden: blauw afkomstig van de pomp-LED, groen en rood afkomstig van de emissie van de QD. Het gebruik van QDs als een luminescente kleurconvertor is hiervoor uitermate geschikt aangezien hun nauwbandige emissie het kleurengamma van een LCD beeldscherm aanzienlijk kan verbeteren.

Cadmium gebaseerde QDs springen in dit opzicht in het oog, ze vertonen uitstekende optische eigenschappen en zijn relatief eenvoudig in oplossing te synthetiseren. Echter zorgen strenge beperkingen op het gebruik van cadmium in consumentenproducten voor een verschuiving naar cadmium-vrije alternatieven zoals InP QDs die vergelijkbare emissie karakteristieken als CdSe QDs combineren met een verminderde toxiciteit. Echter vertonen InP gebaseerde kern/schil QDs, in vergelijking met cadmium gebaseerde QDs, een lagere absorptie cross-sectie en een beperkte foto-stabiliteit. In dit opzicht kan controle over de kern/schil interface, de schil samenstelling en het schil oppervlak de eigenschappen van InP gebaseerde QDs drastisch verbete-

ren. Bovendien belemmert een moeilijke synthese, waarin gebruik gemaakt wordt van dure en gevaarlijke forsforprecursoren, het wijdverspreide gebruik van InP-gebaseerde QDs. Daarom is er nood aan een efficiëntere en goedkopere synthesemethode. Dit proefschift heeft tot doel deze problemen aan te pakken.

In hoofdstuk 3 ontwikkelen we economische manier om InP QDs te produceren met behulp van een aminofosfine, een aanpak afgeleid uit initiële literatuurresultaten die in hoofdstuk 2 uitgezet zijn, bijvoorbeeld een publicatie door Song et al. We tonen aan dat de omzetting van de indium precursor naar InP QDs sterk aanhangt van de molaire verhouding P/In, waarbij een overmaat van de aminofosfine precursor (P:In ratio van 4) tot een volledige omzetting leidt. Dit standpunt wordt ondersteund door bijbehorend onderzoek naar het reactiemechanisme. Analyse van de reactieproducten met behulp van nucleaire magnetische resonantie (NMR) spectroscopie demonstreert dat de reactie geïnitieerd wordt door middel van een transaminatie reactie. Hierbij worden de aminegroepen van het solvent uitgewisseld met de amino groepen van de oorspronkelijke precursor. Vervolgens staven we aan dat een overmaat aminofosfine noodzakelijk is voor een volledige conversie aangezien het zowel als reductiemiddel en fosforprecursor fungeert. Dit wordt bevestigd door middel van massa en NMR spectroscopie die aantonen dat één aminofosfine eenheid wordt gereduceerd van $P^{III}$ naar $^{-III}$ bij de vorming van één InP eenheid, waarbij de overige drie eenheden als reductiemiddel aangewend worden en hierbij tijdens de synthese omgezet worden in fosfonium zouten ($P^{V}$).

In hoofstuk 4 tonen we aan de grootte van de InP kern QDs, gesynthetiseerd bij een volledige opbrengst, afgestemd kan worden door variatie van het indium halide als indium precursor. De InP QDs geproduceerd via deze methodes vertonen echter een lage fotoluminescentie. Als er echter een schil, bestaande uit een II-VI materiaal met een wijdere verboden zone, rond de kern wordt gegroeid, worden fotoluminescente kern/schil QDs verkregen die zichtbaar licht uitzenden. Dit, in combinatie met een hoge chemische reactie opbrengst, geeft aanleiding tot fotoluminescente InP/ZnS en InP/ZnSe kern/schil QDs die tussen 510 en 630 nm licht uitzenden. Verder wijzen we erop dat de emissie karakteristieken afhangen van de aard van de schil. Zo leidt een ZnS schil tot bredere emissielijnen dan een ZnSe schil, maar geeft het aanleiding tot hogere kwantumopbrengsten.

In hoofdstuk 5 beschrijven we een methode om InP gebaseerde QDs in een polymere laag in te bedden, waarvan we vervolgens hun emissie karakteristieken in een remote fosfor configuratie analyseren. We tonen aan dat InP/ZnSe QDs een relatief lage absorptie coëfficiënt hebben bij 450 nm, de centrale golflengte voor een blauwe pomp-LED in displays en verlichtingstoepassingen. Dit verhoogt de hoeveelheid materiaal die noodzakelijk is om een vooraf gedefinieerde kleuromzetting te behalen en maakt InP/-ZnSe QDs bijgevolg vatbaar voor zelfabsorptie, twee elementen die de prestaties en de kosten van kleurconvertoren negatief beïnvloeden. Dit probleem kan worden aangepakt door kleine hoeveelheden Cd in de ZnSe schil in te corporeren, tot gevolg hebben de (Zn,Cd)Se schillen een kleinere verbonden zone dan ZnSe schillen. Vergelijking van de fotoluminescente efficientie van InP/ZnSe en InP/(Zn,Cd)Se lagen toont aan dat deze laatsten een significant hogere absorptie van het blauwe LED licht vertonen – ze bereiken dezelfde kleuromzetting als InP/ZnSe QD geladen films met 74 % minder QDs per massa – en lijden niet aan efficiëntieverliezen door zelfabsorptie.

In hoofdstuk 6 tonen we ten slotte aan dat blootstelling van InP/ZnSe QDs aan dodecaanthiolen resulteert in een verhoogde fotostabiliteit. Met behulp van NMR spectroscopie en elementaire analyse staven we dat blootstelling aan dodecaanthiolen de samenstelling van de ligandschil verandert; van de oorspronkelijke combinatie van oleylamines en een overmaat aan haliden naar een mengsel van dodecaanthiolen en dodecaanthiolaten met resterend oleylamine en haliden. Terwijl de relatie tussen een aangepaste ligandschil en een verbeterde fotostabiliteit onduidelijk blijft, speculeren we dat de opname van dodecaanthiolen de foto-oxidatie van het ZnSe buitenoppervlak onderdrukt.

# 1 Introduction

## 1.1 Problem definition

The aim of sustainable development encourages scientists to improve lighting solutions since lighting represents a significant proportion of the world electricity consumption.[1] Incandescent and fluorescent lamps were for long considered as a revolution as compared to candles or oil lamps and they have become ubiquitous in public or private area. However, they still pose energy saving and environmental issues. Incandescent lamps have a notoriously low electrical-energy-to-light conversion efficiency and fluorescent lamps contain hazardous elements such as mercury.[2;3] Therefore, research has focused on light emitting diodes (LEDs) as a lighting alternative, which provides many environmental advantages in term of efficiency, toxicity and lifetime as compared to incandescent or fluorescent lamps.[4;5] Thanks to the development of an efficient blue LED by Nakamura, an invention awarded by the 2014 Nobel Prize in Physics,[6] the use of LEDs shifted from mere indicator lamps to indoor and outdoor illumination and display backlighting.[7] However, since no LED with intrinsic white emission exits, two fabrication strategies are used to obtain white light emission. A first approach produces white light by combining the output from red, green and blue LEDs. This

strategy has numerous disadvantages. For example, each of these LEDs comes with a different lifetime and temperature behavior, which can result in undesired variations of light intensity and color.[8–10] In a second approach, a lanthanide-doped yellow-emitting phosphor is used to convert part of the blue LED light into a sufficiently broad emission band to achieve an overall white light emission. Typically implemented using $Ce_3^+$-doped yttrium aluminum garnet (YAG:Ce) as the yellow phosphor, this configuration has several advantages, such as a high brightness and a low cost fabrication process.[11;12] On the other hand, a YAG:Ce based white LED yields a white light spectrum that lacks in red light, resulting in a high color temperature and a poor color rendering. So-called warm white LEDs can be made by including an additional red-emitting material such as $Eu_2^+$-doped nitride phosphor. These, however, often result in a tailing of the emission spectrum into near infrared, which reduces the luminous efficacy of the LED.[13]

Recently, new luminescent materials have been put forward as an alternative to more conventional powder phosphors to be combined with blue LEDs in display and lighting. In particular, semiconductor nanocrystals or quantum dots (QDs) have attracted great attention over the last years thanks to their fascinating opto-electronic properties. QDs are of particular interest here since they feature a spectrally narrow emission that can be tuned by modifying the size and shape of a QD.[14;15] Early proof-of-concepts have already shown that an emission spectrum containing different emission bands can be easily obtained by dispersing QDs with different emission lines in a single film or coating.[16] This principle is particularly useful to make high color gamut liquid crystal display (LCD) in which the narrow blue emission of a pump LED is combined with narrow green and red emission lines from colloidal QDs.[17;18] In this case, the emission wavelength of QDs can be finely tuned in order to closely match the spectral transmittance of the LCD color filters.[19] A drawback of using QDs as luminescent materials for optical down-conversion is, however, that the best performing QDs all involved cadmium-based II-VI semiconductors. Cadmium is a toxic heavy metal and its use in consumer products is subject to regulation by, for example, the European Commission. In this context, indium phosphide (InP) QDs offer a cadmium-free alternative. At the moment, however, InP QDs lag behind Cd-based QDs in terms of performance – typically measured using the photoluminescence quantum yield.[20] Moreover, a widespread deployment of InP-based QDs will require cheaper and easier synthesis methods.

This thesis addresses the issues InP-based QDs face as a replacement of Cd-based QDs in view of its application as a luminescent material for luminescent down-conversion. To begin with, an overview of InP QDs synthesis methods will be presented. In fact, InP QDs are generally made with an expensive and pyrophoric phosphorus-containing precursor which hinders a large scale product development. Moreover, the material properties arising from each InP QDs synthesis will be explored where a control over the QDs diameter along with a high chemical yield is a key to achieve economical InP synthesis. Following this study, we will propose an innovative method based on a cheap and easy to handle phosphorous precursor which enable the production of high quality and economical InP QDs. The reaction chemistry of such synthesis will be explored and an approach to develop InP-based QDs with equal or better performance as compared to Cd-based QDs will be proposed.

## 1.2 Physical properties of quantum dots

Semiconductor nanocrystals (NCs) or quantum dots are nanometer-sized crystallites, typically of so-called II-VI, IV-VI, or III-V semiconductors, that exhibit size-dependent optical and electronic properties.[21] With sizes most often in between 1 to 10 nm, they generally contain a few hundred to a few thousand of atoms.[22] Therefore, QDs are often described as a state of matter intermediate between bulk materials and molecules. They have discrete energy levels, similar to molecules, while already having a crystal structure comparable to that of the corresponding bulk material.[23] For this reason, QDs are often called artificial atoms and they have a number of valuable properties. Indeed, bulk semiconductors are known to have a set band gap, which correspond to the minimum energy required to excite an electron from the valence band to the conduction band (see Figure 1.1). When a photon with an energy exceeding the energy band gap of the bulk semiconductor is absorbed, a valence-band electron can be promoted to the conduction band, a process leaving a hole in the valence band. Whereas for a bulk semiconductor, conduction-band electrons and valence-band holes can be seen as free particles characterized by an effective mass, the crystal boundaries will create a particle-in-a-box potential for both charge carriers when the crystal size is reduced to a few nanometers. This makes that the quasi-continuous energy bands are replaced by a set of discrete levels, separated by energy gaps. Most strikingly, this leads to an increase of the band gap energy with decreasing particle size.[14] A further tailoring of the electronic energy levels and the optical properties is possible by adjusting the shape of the NCs. Especially in the case of Cd-based QDs, colloidal

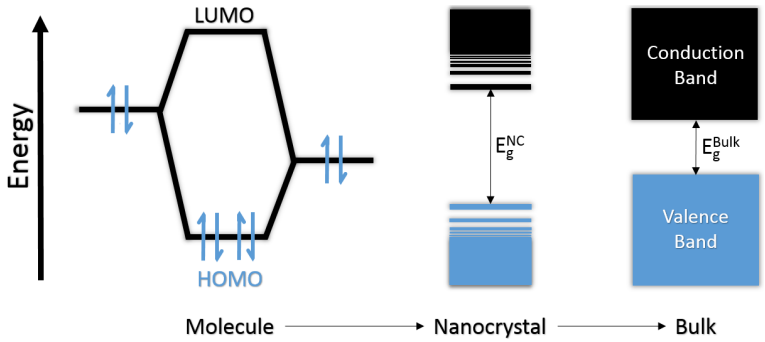


**Figure 1.1:** The electronic structure of semiconductor QD is intermediate between single molecule and bulk semiconductor. The blue color represents the ground state electron occupation.

synthesis methods enable QDs to be synthesized as rod-like particles where charge carriers are only confined in two dimensions, or as so-called platelets, where confinement only takes place in a single dimension.[14;24]

## 1.3 Synthesis of quantum dots

As discussed above, optical properties of quantum dots are known to vary according to their sizes and shape. A careful control over their diameters is a key parameter to achieve monodisperse QDs batches. In this respect, the best results are obtained when QDs are synthesized by a chemical route referred to as the hot injection method.[25] In this approach, the reaction is conducted in a high boiling solvent where molecular precursors are mixed with surfactant molecules that stabilize the nanocrystals surface and prevent aggregation during and after the synthesis. After a purification process where the reaction mixture is put under vacuum to remove impurities or volatile compounds, the latter is subsequently heated under inert atmosphere to a temperature of 150-300 °C. When the desired temperature is reached, an organometallic precursor is swiftly injected into the mixture and the nanocrystal formation starts. Several studies have been carried out on the nucleation and growth of QDs,[26;27] which often use the LaMer model to rationalize the different stages of the synthesis (see Figure 1.2).[28] Briefly, after the injection of the organometallic precursor in the hot reaction mixture, the concentration of monomers – reactive precursors – increases rapidly to reach a state of supersaturation. The increase of monomers concentration continues until it reaches a point where critical nuclei can form in large numbers. Once this stage is reached, particles growth will help

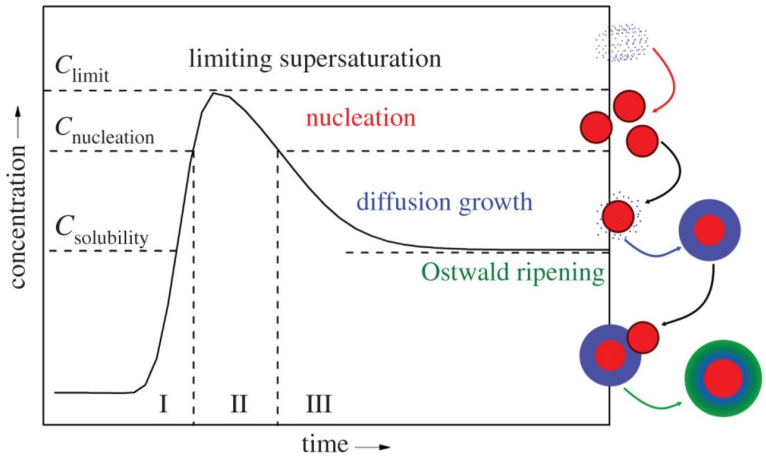


**Figure 1.2:** Schematic representation of the LaMer model in a colloidal QDs synthesis with a generation of monomers, nucleation and growth of colloidal nanocrystals. (Reprinted from reference [29]).

reducing the supersaturation, such that further nucleation of particles is stopped.

Since the emission spectrum of QDs depends on their size, QD syntheses should enable the average radius of the QDs to be controlled and the distribution of different sizes within a QD ensemble should be as low as possible. From this perspective, the LaMer model promotes the concept of "burst nucleation", which implies that nucleation and growth should be two stages in a reaction that are well separated in time.[30–32] Suppose for example that nucleation and growth coincide. In such a case, small nuclei would be formed while larger nanoparticle would already be growing, a combination that is bound to lead to polydisperse nanoparticle ensembles. In contrary, a "burst nucleation" event supposedly leads to a high degree of supersaturation resulting in a short nucleation period where all the nuclei are formed at the beginning of the reaction. The latter is subsequently stopped by the drop of the supersaturation and the temperature and is followed by a growth period during which no new particles form. In this case, a more narrow size distribution can be expected. It must be emphasized that an additional stage called Ostwald ripening can occur after long annealing times, when the production of new monomers has stalled.[33] In this regime, the larger particles grow at the expense of the smaller particles, which typically leads to an increase of the size dispersion. The synthesis has to be stopped before this stage to prevent a broadening of the QDs size distribution.[34;35]

Until now, the concept of "burst nucleation" is often the first way to reach monodisperse nanoparticle ensembles. In this context, recent studies have demonstrated that the hot injection synthesis involves the conversion of reaction precursors into solutes or monomers prior to the nucleation and growth of the NCs.[36;37] This leads researchers to develop simulation models which correlate established expressions for the rate of NC nucleation and growth and the rate of monomer formation.[38;39] According to these reaction simulations, the size-tuning of NCs at the end of the size distribution focusing is possible either by tuning the rate of monomer formation or by changing the time span of nucleation. In the case of CdSe and CdS QDs synthesis, an increase of the precursor concentrations results in a faster reaction and a decrease of the NC size, in line with the predicted link between monomer formation rate and nanocrystal size.[38] In addition, increasing the concentration of free carboxylic acid in CdSe QDs synthesis leaves the reaction rate constant although resulting in larger NCs and a deterioration of the size distribution. This is explained in accordance with the reaction simulations by a reduction of the time span of nucleation linked to an enhanced monomer solubility.[39] Therefore, understanding the relations between the reaction conditions and the properties of the synthesized NCs is of critical importance for developing size tuning strategies for the hot injection synthesis.

However, numerous hot injection syntheses still rely on reaction time to control the final QD radius, which means that a reaction is stopped the moment the growing QDs reach a specific QD diameter.[25;40] This can be an issue in, for example, small QD synthesis where the reaction is stopped while the growth stage has not ended. This induces a partial loss of the molecular precursors resulting in a low chemical yield, *i.e.*, the amount of molecular precursors incorporated into QDs. From an economic perspective, such a low yield approach will quickly raise the synthesis cost especially in view of large scale production. In this context, researchers started to optimize synthesis protocols in order to produce QDs with a desired size at near unity chemical yield. To achieve this, several parameter in a hot injection synthesis can be tuned, such as the composition of the reaction mixture, the temperature or the precursor concentration.[38;41–43] In addition, the large volume production of QDs may require considerable changes to the typical hot-injection approach, which is typically optimized for the production of lab-scale volumes, *i.e.*, 50-500 mg scale. Especially the rapid injection of large volumes might be difficult to achieve on a larger scale. Therefore, researchers have developed non-injection approaches, in which all the precursors required for a typical QD synthesis are included in the reaction mixture from the start.[44;45] In this method, the nature of the chemical precursor has to be

**Figure 1.3:** Photoluminescence of cadmium selenide (CdSe) QDs with particle diameters increasing from left to right.

carefully selected to initiate nucleation at a desired temperature in order to produce QDs with narrow size distribution.[46] As an alternative approach, the use of specific molecular precursor like for example magic-size cluster allow for the production of high-quality monodispersed QDs.[47;48] However these molecular precursors can be difficult to synthesize and are limited to specific material systems. Another possible approach towards large-scale QDs synthesis is the use of microfluidic reactors which offer advantages over batches synthesis in term of processing.[49;50] This synthesis method has enabled production of high-quality colloidal semiconductor nanocrystal similar to that of comparable batch-synthesized nanoparticles.[25;34]

## 1.4 Optical properties of quantum dots

Quantum dots are photoluminescent materials that have a broad absorption spectrum characterized by an onset at a wavelength corresponding to the band-edge transition. Light absorption by a QD results in the formation of an electron-hole pair, which is a combination of a conduction-band electron and a valence-band hole. Very often, such an electron-hole pair is called an exciton, a somewhat unfortunate wording since the confinement energy of the electron and the hole typically exceeds to Coulomb attraction between electron and hole. Upon recombination, the electron-hole pair can emit light with a wavelength characteristic of the QD band-edge transition. This makes that ensembles of monodisperse QDs emit light with a highly saturated color that is tunable by varying the QD size (see Figure 1.3). This effect can also be observed in the absorption spectra, where a narrow

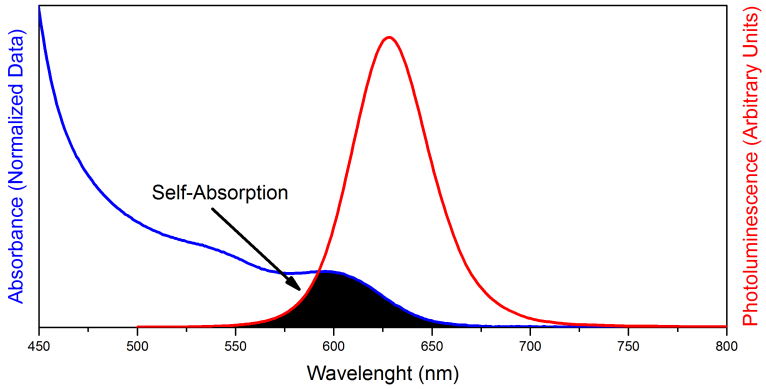


**Figure 1.4:** Self-absorption in concentrated QDs solution with partially overlapping absorption and emission spectra.

feature corresponding to the band-edge transition exhibits a blue shift when the particle size decrease. Moreover, the shape and width of the excitonic peak will be influenced by the size distribution, the shape and the composition of the QDs, with polydisperse nanocrystal samples typically yielding broadened features in the absorption spectrum.

Another aspect of the QD photoluminescence is the red shift of the peak wavelength of the emission spectrum relative to that of the band-edge absorption, a shift often referred as the Stokes shift.[51] According to the available literature on colloidal QDs, the Stokes shift – when the emitted photon has less energy than the absorbed photon – could arise from electron-phonon coupling,[52] fine structure in the band-edge emitting states,[53;54] polaron states (at low temperature)[55] or in certain cases the emission from trap states or localized emission centers.[56;57] Although the origin of the Stokes shift is the subject of many researches, its impact on luminescent wavelength conversion can be pronounced. Since the Stokes shift is typically rather small, the emission and absorption spectrum show a considerable overlap. This makes that light emitted by one QDs can be reabsorbed by other QDs (see Figure 1.4). Unless the photoluminescence quantum yield (PLQY) is 100 %, this self-absorption can significantly lower the down-conversion efficiency. A typical fingerprint of self-absorption is a red shift of the emission spectrum caused by the stronger absorption of photons at the blue side of the emission band.[58]

The radiative recombination of electron-hole pairs competes with nonradiative recombination pathways, for example through localized energy levels at the QD surface. These so-called trap states can lead to deep-trap emission

at the low-energy side of the band-edge photoluminesence, or they can simply convert the excess energy of the electron-hole pair into heat.[59] Clearly, non-radiative recombination will lower the PLQY, which is generally defined as the ratio between the number of absorbed photon over the number of emitted photons.[60] Typical approaches to enhance the PLQY therefore focus on a better termination of the QD surface. These can involve the use of appropriate ligands or dedicated etching steps,[61] yet such approaches rarely lead to a high and stable photoluminesence quantum efficiency.[62]

To further protect the QDs surface, an inorganic shell material with a wider bandgap energies can be grown on top of the core material. This can be accomplished by various synthesis method where a common approach is to combine both core and shell synthesis in a single reaction. Especially when core and shell have a commensurate crystal structure, the core/shell interface can be free of trap states. Moreover, a core/shell system can confine the electron and the hole within the core, which strongly helps to decouple both charge carriers from remaining trap states at the outer surface of the shell. As a result, specific core/shell combinations exhibit a markedly increased PLQY since non-radiative recombination is effectively suppressed.[63;64] Especially in the case of Cd-based QDs, core/shell structure with a close to 100 % PLQY have been reported.[65;66]

## 1.5 Quantum dots heterostructures

The properties of core/shell QDs strongly depend on the relative alignment of the core and shell energy levels. In general, three configurations are possible, which are commonly referred to as type-I, reverse type-I, and type-II heterostructures (see Figure 1.5). A type-I structure or straddling band alignment, for example CdSe/CdS and InP/ZnS QDs, is formed when the conduction and valence-band edge of the shell material are above and below the conduction and valence-band edges of the core, respectively. In this case, electron and hole will be confined to the core QD. In a reverse type-I structure, for example CdS/CdSe and ZnSe/CdSe QDs, the situation is exactly the opposite, and the electron and hole will be partially or completely confined in the shell. Finally, a type II structure, for example ZnTe/CdSe and CdS/ZnSe QDs, corresponds to a staggered configuration, where the valence and conduction band of the core are lower or higher than the band edges of the shell. In this configuration, one of the charge carriers is confined to the core, whereas to other is confined to the shell.

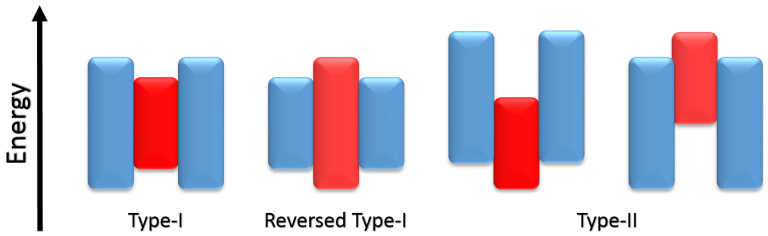


**Figure 1.5:** Schematic representation of different core/shell QD heterostructures. The upper and lower edges of the rectangles correspond to the positions of the conduction and valence band edge of the core (red) and shell materials (blue), respectively.

As discussed above, a type-I configuration is preferred to a core QDs with the aim of enhancing its optical properties. Doing so, the core material becomes less sensitive to the surrounding medium where oxygen and moisture are known to quench the PLQY. Often, the formation of a type I core/shell heterostructure results in a small redshift of the band-edge transition, which is mostly assigned to the partial leakage of the electron or the hole wavefunction into the shell.[34] In a reverse type-I systems, electrons or holes are partially delocalized in the shell and the emission wavelength can be tuned by changing the shell thickness. Increasing the shell thickness will generally results in a red shift of the emission wavelength. The optical properties of a reverse type-I system can be improve by coating a second shell with a wider bandgap than the core/shell QDs.[22] In a type-II configuration, one of the charge carriers is located in the shell and an increase of the shell thickness will induce a significant red shift of the QDs emission wavelength. Therefore, a type-II system is of particular interest in applications that rely on infra-red emission. Similar to reverse type-I system, overgrowing an appropriate shell material on a type-II system can enhance the optical properties of the QDs. Therefore, QDs are versatile materials where for example a type-I system can be use in application relying on light emission, while on the other hand a type-II heterostructure can be of interest in photovoltaic and photoconduction devices.

The materials band offsets is not the only parameters to take into account when designing core/shell QDs. Apart from a few combinations, core and shell never feature the same crystal structure with the same lattice parameter. Lattice mismatch results in strain, which can inhibit further shell growth, induce defects at the core/shell interface and shift the band-edge transition.[67] Such effects are minimized the more the lattice spacing of core and shell is similar. An additional parameter is simply the shell thicknesses.

Thin shells, for example, result in an insufficient passivation of the core material, whereas a thick shell can deteriorate the QDs due to the increasing strain induced at the core/shell interface creating defects and lowering the PLQY.[34;68]

## 1.6 Quantum dots in white light-emitting devices

Current white light emitting devices (wLEDs) are based on the combination of a blue LED together with one or more luminescent materials which convert part of the blue light in order to obtain an overall white light spectrum. This so-called "phosphor-converted LED" is widely used today in solid state lighting and is typically based on a combination of a blue LED with two broad emitting phosphors that cover the green and red part of the visible spectrum. The former is generally $Y_3Al_5O_{12}:Ce_3^+$ (YAG:Ce) or $Lu_3Al_5O_{12}:Ce_3^+$ (LuAG:Ce) and the latter a $Eu_2^+$ doped nitride based phosphor.[69] Two phosphor-converted LED configurations exist where the phosphor materials is either directly deposited on top of the blue LED (the on-chip configuration) or where the phosphor materials is displaced from the blue LED (the remote phosphor configuration). The later has the advantage that the operating temperature at the level of the phosphor is lower compared to the on chip system.[70;71] Moreover, thanks to the light distribution over far larger areas, the phosphor is exposed to a lower light flux and heating is less of an issue.[72] In the case of QDs as the down-conversion material, higher performances can be achieved in a remote-phosphor configuration as a rising temperature tends to deteriorate the photoluminescence efficiency, shift the QD emission and reduce the QD lifetime.[73;74] However, remote phosphor designs require a larger amount of luminescent material as compared to the on-chip approach, which can quickly raise the wLEDs cost.

In this context, most liquid crystal display televisions (LCD TVs) use wLEDs in a phosphor converted approach for backlight purposes, where they typically combine a blue LED with two luminescent lanthanide-doped phosphors emitting in the green and red part of the visible spectrum. However, since primary colors are created by filtering the white backlight, an LCD has an intrinsic trade-off between color gamut – which requires narrow filters – and optical efficiency – which requires as little filtering as possible.[2] This underlines the need to develop new phosphors with a narrow red and green emission since common wLEDs exhibit broad emission band that leads

to important filtering losses.[75–78] Another promising alternative to improve LCD backlighting is the use of QDs. In so-called QD-LCDs, the white backlight is replaced by the combination of a blue LED and a remote phosphor bar or sheet that contains QDs emitting in the green and the red part of the visible spectrum. The QDs absorb part of the blue LED light and convert it into narrow green and red light that match the color filters behind the LCD screen, thereby increasing useful light throughput and providing a better color gamut.[17;19] At the same time, such narrow red emitters can be used to reduce the color temperature of phosphor converted white LEDs based on YAG:Ce, without introducing the infrared tailing that compromises the luminous efficacy of current warm white LEDs. Sony was the first company to use green and red QDs to enhance LCD backlighting in their Triluminos LCD TVs. Since QDs durability can be affected by exposure to heat, oxygen and water vapor, compatible matrix materials and packaging solutions are needed to fulfill the customer lifetime requirement.[79;80] In this respect, Sony embedded their QDs in acrylate polymer and encapsulated them in thin glass tubes to avoid any oxygen and moisture contamination ensuring a long-term photoluminescent stability.[81]

Although LCD TVs are the most common type of technology used in households to produce images, they still suffer from color saturation and black level performance as liquid crystals can be prone to backlight leakage. Even with advanced dimming technology, which can increase the contrast ratio by selectively dims LEDs that don't need to be on,[82] LCD TVs still suffer from "backlight bleeding" where the backlight is not 100 % blocked and spills through on area that are supposed to be a black of the screen. In this context, emissive display technology such as OLED TVs does not experience such problems.[83] The latter, which stands for organic light-emitting diode televisions is based on organic compounds that self-emit light when an electric current is passed through. Therefore, each OLED TV's pixels can be shut off independently such as to obtain deep, dark black levels leading to higher contrast and thus a more realistic image as compared to LCD-based TVs. Other advantages of OLED TVs are that the panels are thinner than a typical LCD configuration, response times are faster and viewing angles tend to be significantly wider.[83] However, when it comes to capable brightness, QD-LCDs stand out thanks to the addition of the QD enhancement film. Therefore, the color volume – a three-dimensional representation that depicts how the display reproduces colors at different luminance levels – is higher for QD-LCDs which allows to make all colors in the available spectrum brighter without losing saturation. Finally, unlike OLED materials, QD-LCDs aren't susceptible to image burn-in problems – image retention – owing to the inorganic nature of the QDs. Therefore, QD-LCDs have

a longer lifespan than OLED TVs and are capable of producing an image quality that does not degrade over time. Hence, the future looks bright for QD-LCDs and the next display technology will certainly use the electroluminescence propreties of QDs such as to obtain emissive displays, similar to OLED TVs.

## 1.7 Thesis outline

This thesis discussed the development of an alternative method to form InP-based QDs to be used as luminescent material for wavelength down-conversion in display and lighting applications.

In the second chapter, a literature overview of the synthesis of InP-based QDs is given. It is made clear that the best performing syntheses all use tris(trimethylsilyl)phosphine [$(TMS)_3P$] as the phosphorous precursor, an approach that has significant disadvantages. $(TMS)_3P$ is a costly precursor that is pyrophoric and can produce phosphine, a highly toxic gas, in contact with air. We believe these features explain why InP nanocrystals have been studied considerably less than CdSe nanocrystals.

In the third chapter, we propose protocols based on a new phosphorus precursor that creates a pathway towards the cost efficient, up-scaled synthesis of InP nanocrystals. We investigate the chemical reactions leading to InP formation starting from $InCl_3$ and tris(dialkylamino)phosphines. Using nuclear magnetic resonance spectroscopy (NMR) and single crystal X-ray powder diffraction (XRD), we demonstrate that injection of the aminophosphine in the reaction mixture is followed by a transamination with oleylamine, the solvent of the reaction. In addition, mass spectrometry and NMR indicate that the formation of InP concurs with that of tetra(oleylamino)phosphonium chloride. The chemical yield of the InP formation shows that a full conversion of the In precursor was only attained for a 4:1 P:In ratio. Hence, this work underscores the double role of the aminophosphine as both precursor and reducing agent.

In the fourth chapter, we demonstrate that size tuning at full chemical yield is possible by changing the nature of the indium halide salt. In addition, we present ZnS and ZnSe shell growth procedures that lead to InP/ZnS and InP/ZnSe core/shell QDs that emit from 510 to 630 nm with an emission linewidth between 46 and 63 nm. This synthetic method is an important step towards performing Cd-free QDs, and it could help the transfer of colloidal QDs from the academic field to product applications.

In the fifth chapter, InP-based QDs with shell-enhanced absorption for a more efficient luminescent down-conversion are proposed. Synthetic methods to coat InP QDs with a ZnSe shell containing small amounts of Cd are developed. This enables to enhance the QD absorption at 450 nm, the typical pump wavelength for optical down-conversion, and concomitantly suppress self-absorption and reduce QD loading in QD-in-polymer based luminescent down-convertor coatings.

In the final chapter, the surface chemistry of InP/ZnSe QDs is studied. As discussed, photostable QDs have to be designed in order to use them efficiently as color converters in white light-emitting devices. These parameters strongly depend on the ligands covering their surface. A good passivation of QD surface is required to remove surface trap states that quench luminescence. Within this context, we demonstrate by using NMR, X-ray fluorescence spectroscopy (XRF) and photostability measurements that photostability of InP/ZnSe QDs can be considerably improved by adding thiol molecules to oleylamine-capped InP/ZnSe QDs.

## 1.8 Scientific output

### 1.8.1 Publications in international journals

This work is based on the following publications:

1. Mickaël D. Tessier, **Dorian Dupont**, Kim De Nolf, Jonathan De Roo, Zeger Hens. *Economic and Size-Tunable Synthesis of InP/ZnE (E = S, Se) Colloidal Quantum Dots.* Chemistry of Materials, 27(13):4893-4898, **2015**.

2. Mickaël D. Tessier, Kim De Nolf, **Dorian Dupont**, Davy Sinnaeve, Jonathan De Roo, Zeger Hens. *Aminophosphines: a Double Role in the Synthesis of Colloidal Indium Phosphide Quantum Dots.* Journal of the American Chemical Society, 138(18):5923-5929, **2016**.

3. **Dorian Dupont**, Mickaël D. Tessier, Philippe F. Smet, Zeger Hens. *Shell and Surface Engineering of Indium Phosphide-Based Quantum Dots: Towards White Light-Emitting Devices.* Advanced Materials, 29(29):1700686, **2017**.

Other publications by the author:

1. Louis Biadala, Benjamin Siebers, Yasin Beyazit, Mickaël D. Tessier, **Dorian Dupont**, Zeger Hens, Dmitri R. Yakovlev, and Manfred

Bayer. *Band-Edge Exciton Fine Structure and Recombination Dynamics in InP/ZnS Colloidal Nanocrystals.* ACS Nano, 10(03):3356-3364, **2016**.

2. Valeriia Grigel, **Dorian Dupont**, Kim De Nolf, Zeger Hens, Mickaël D. Tessier. *InAs Colloidal Quantum Dots Synthesis via Aminopnictogen Precursor Chemistry.* Journal of the American Chemical Society, 138(41):13485-13488, **2016**.

3. Vigneshwaran Chandrasekaran, Mickaël D. Tessier, **Dorian Dupont**, Pieter Geiregat, Zeger Hens, Edouard Brainis. *Nearly Blinking-Free, High-Purity Single-Photon Emission by Colloidal InP/ZnSe Quantum Dots.* Nano Letters, **2017 (Article ASAP)**.

4. Jana Ryckaert, António Correia, Kevin Smet, Mickaël D. Tessier, **Dorian Dupont**, Zeger Hens, Peter Hanselaer, and Youri Meuret *Selecting the optimal synthesis parameters of InP/$Cd_xZn_{1-x}$Se quantum dots for a hybrid remote phosphor white LED for general lighting applications*, Optics Express, 25(24):A1009-A1022, **2017 (Article ASAP)**.

5. Mona Rafipoor, Hans Tornatzky, **Dorian Dupont**, Mickaël D. Tessier, Zeger Hens, Janina Maultzsch, Holger Lange. *Strain Engineering in InP/CdZnSe Core/Shell Alloys.* **(Manuscript under preparation)**.

### 1.8.2 Patents

1. WO2016146719A1 - Size-tunable nanoparticle synthesis.

2. EP16206877.9 - Quantum dots with a III-V core and an alloyed II-VI external shell.

### 1.8.3 Conference contributions

1. **Dorian Dupont**, Mickaël D. Tessier, Kim De Nolf, Jonathan De Roo, Zeger Hens. *Economic Synthesis and Size-Tuning of InP/ZnS and InP/ZnSe Colloidal QDs*, 2015 E-MRS Spring Meeting, Lille (France), May 11-15 (Presentation).

2. **Dorian Dupont**, Mickaël D. Tessier, Kim De Nolf, Zeger Hens. *Economic Synthesis of Size-Tunable Indium Phosphide Quantum Dots: Towards White Light-Emitting Device*, ChemCYS 2016, Blankenberge (Belgium), March 16-18 (Presentation).

3. Mickaël D. Tessier, Kim De Nolf, Jonathan De Roo, **Dorian Dupont**, Zeger Hens. *Reaction Chemistry in Innovative Indium Phosphide Quantum Dots Synthesis*, 2016 MRS Spring Meeting, Phoenix (USA), March 28-April 1 (Poster).

4. **Dorian Dupont**, Mickaël D. Tessier, Kim De Nolf, Zeger Hens. *Indium Phosphide-Based Quantum Dots: Towards White Light-Emitting Device*, 2016 MRS Spring Meeting, Phoenix (USA), March 28-April 1 (Presentation).

# References

[1] E Fred Schubert, Jong Kyu Kim, Hong Luo, and J-Q Xi. *Solid-state lighting—a benevolent technology.* Reports on Progress in Physics, 69(12):3069, 2006.

[2] Philippe F. Smet, Anthony B. Parmentier, and Dirk Poelman. *Selecting Conversion Phosphors for White Light-Emitting Diodes.* Journal of The Electrochemical Society, 158(6):R37–R54, 2011.

[3] W. Kondro. *Mercury disposal sole health concern with fluorescent lights.* CMAJ: Canadian Medical Association Journal, 177(2):136–137, 2007.

[4] A. Bergh, G. Craford, A. Duggal, and R. Haitz. *The Promise and Challenge of Solid-State Lighting.* Physics Today, 54(12):42–47, 2001.

[5] S. Pimputkar, J. S. Speck, S. P. DenBaars, and S. Nakamura. *Prospects for LED lighting.* Nature Photonics, 3(4):180–182, 2009.

[6] Shuji Nakamura, Masayuki Senoh, Naruhito Iwasa, Shin ichi Nagahama, Takao Yamada, and Takashi Mukai. *Superbright Green InGaN Single-Quantum-Well-Structure Light-Emitting Diodes.* Japanese Journal of Applied Physics, 34(10B):L1332, 1995.

[7] E. Fred Schubert and Jong Kyu Kim. *Solid-State Light Sources Getting Smart.* Science, 308(5726):1274–1278, 2005.

[8] Takashi Mukai, Motokazu Yamada, and Shuji Nakamura. *Characteristics of InGaN-Based UV/Blue/Green/Amber/Red Light-Emitting Diodes.* Japanese Journal of Applied Physics, 38(7R):3976, 1999.

[9] Y. M. Gu, N. Narendran, T. M. Dong, and H. Y. Wu. *Spectral and Luminous Efficacy Change of High-power LEDs Under Different Dimming Methods.* Sixth International Conference on Solid State Lighting, Proceedings of SPIE, 6337:63370J, 2006.

[10] N. Narendran, Y. Gu, J. P. Freyssinier, H. Yu, and L. Deng. *Solid-state lighting: Failure analysis of white LEDs.* Journal of Crystal Growth, 268(3-4):449–456, 2004.

[11] Volker Bachmann, Cees Ronda, and Andries Meijerink. *Temperature Quenching of Yellow $Ce3^+$ Luminescence in YAG:Ce.* Chemistry of Materials, 21(10):2077–2084, 2009.

[12] S. Ye, F. Xiao, Y.X. Pan, Y.Y. Ma, and Q.Y. Zhang. *Phosphors in phosphor-converted white light-emitting diodes: Recent advances in materials, techniques and properties.* Materials Science and Engineering: R: Reports, 71(1):1–34, 2010.

[13] C. C. Lin, Y. S. Zheng, H. Y. Chen, C. H. Ruan, G. W. Xiao, and R. S. Liu. *Improving Optical Properties of White LED Fabricated by a Blue LED Chip with Yellow/Red Phosphors.* Journal of The Electrochemical Society, 157(9):H900–H903, 2010.

[14] A. P. Alivisatos. *Perspectives on the Physical Chemistry of Semiconductor Nanocrystals.* The Journal of Physical Chemistry, 100(31):13226–13239, 1996.

[15] Tito Trindade, Paul O'Brien, and Nigel L. Pickett. *Nanocrystalline Semiconductors: Synthesis, Properties, and Perspectives.* Chemistry of Materials, 13(11):3843–3858, 2001.

[16] J. Lee, V. C. Sundar, J. R. Heine, M. G. Bawendi, and K. F. Jensen. *Full Color Emission from II–VI Semiconductor Quantum Dot–Polymer Composites.* Advanced Materials, 12(15):1102–1105, 2000.

[17] Ho Seong Jang, Heesun Yang, Sung Wook Kim, Ji Yeon Han, Sang-Geun Lee, and Duk Young Jeon. *White Light-Emitting Diodes with Excellent Color Rendering Based on Organically Capped CdSe Quantum Dots and $Sr_3SiO_5$:$Ce^{3+}$,$Li^+$ Phosphors.* Advanced Materials, 20(14):2696–2702, 2008.

[18] Xiebing Wang, Wanwan Li, and Kang Sun. *Stable efficient CdSe/CdS/ZnS core/multi-shell nanophosphors fabricated through a phosphine-free route for white light-emitting-diodes with high color rendering properties.* Journal of Materials Chemistry, 21(24):8558–8565, 2011.

[19] Eunjoo Jang, Shinae Jun, Hyosook Jang, Jungeun Lim, Byungki Kim, and Younghwan Kim. *White-Light-Emitting Diodes with Quantum Dot Color Converters for Display Backlights.* Advanced Materials, 22(28):3076–3080, 2010.

[20] S. H. Lee, K. H. Lee, J. H. Jo, B. Park, Y. Kwon, H. S. Jang, and H. Yang. *Remote-type, high-color gamut white light-emitting diode based on InP quantum dot color converters.* Optical Materials Express, 4(7):1297–1302, 2014.

[21] Clemens Burda, Xiaobo Chen, Radha Narayanan, and Mostafa A. El-Sayed. *Chemistry and Properties of Nanocrystals of Different Shapes.* Chemical Reviews, 105(4):1025–1102, 2005.

[22] Peter Reiss, Myriam Protière, and Liang Li. *Core/Shell Semiconductor Nanocrystals.* Small, 5(2):154–168, 2009.

[23] Andrew M. Smith and Shuming Nie. *Semiconductor Nanocrystals: Structure, Properties, and Band Gap Engineering.* Accounts of Chemical Research, 43(2):190–200, 2010.

[24] Celso de Mello Donegá. *Synthesis and properties of colloidal heteronanocrystals.* Chemical Society Reviews, 40(3):1512–1546, 2011.

[25] C. B. Murray, D. J. Norris, and M. G. Bawendi. *Synthesis and characterization of nearly monodisperse CdE (E = sulfur, selenium, tellurium) semiconductor nanocrystallites.* Journal of the American Chemical Society, 115(19):8706–8715, 1993.

[26] Y. Yin and A. P. Alivisatos. *Colloidal nanocrystal synthesis and the organic-inorganic interface.* Nature, 437(7059):664–670, 2005.

[27] Nguyen T. K. Thanh, N. Maclean, and S. Mahiddine. *Mechanisms of Nucleation and Growth of Nanoparticles in Solution.* Chemical Reviews, 114(15):7610–7630, 2014.

[28] Victor K. LaMer and Robert H. Dinegar. *Theory, Production and Mechanism of Formation of Monodispersed Hydrosols.* Journal of the American Chemical Society, 72(11):4847–4854, 1950.

[29] Peter W. Dunne, Alexis S. Munn, Chris L. Starkey, Tom A. Huddle, and Ed H. Lester. *Continuous-flow hydrothermal synthesis for the production of inorganic nanomaterials.* Philosophical Transactions of the Royal Society A: Mathematical, Physical and Engineering Sciences, 373(2057), 2015.

[30] Xiaogang Peng, J. Wickham, and A. P. Alivisatos. *Kinetics of II-VI and III-V Colloidal Semiconductor Nanocrystal Growth: "Focusing" of Size Distributions.* Journal of the American Chemical Society, 120(21):5343–5344, 1998.

[31] Celso de Mello Donegá, Peter Liljeroth, and Daniel Vanmaekelbergh. *Physicochemical Evaluation of the Hot-Injection Method, a Synthesis Route for Monodisperse Nanocrystals.* Small, 1(12):1152–1162, 2005.

[32] Jongnam Park, Jin Joo, SoonGu Kwon, Youngjin Jang, and Taeghwan Hyeon. *Synthesis of Monodisperse Spherical Nanocrystals.* Angewandte Chemie International Edition, 46(25):4630–4660, 2007.

[33] P. W. Voorhees. *The theory of Ostwald ripening.* Journal of Statistical Physics, 38(1):231–252, 1985.

[34] B. O. Dabbousi, J. Rodriguez-Viejo, F. V. Mikulec, J. R. Heine, H. Mattoussi, R. Ober, K. F. Jensen, and M. G. Bawendi. *(CdSe)ZnS Core–Shell Quantum Dots: Synthesis and Characterization of a Size Series of Highly Luminescent Nanocrystallites.* The Journal of Physical Chemistry B, 101(46):9463–9475, 1997.

[35] A.L. Rogach, D.V. Talapin, E.V. Shevchenko, A. Kornowski, M. Haase, and H. Weller. *Organization of Matter on Different Size Scales: Monodisperse Nanocrystals and Their Superstructures.* Advanced Functional Materials, 12(10):653–664, 2002.

[36] Jonathan S. Steckel, Brian K. H. Yen, David C. Oertel, and Moungi G. Bawendi. *On the Mechanism of Lead Chalcogenide Nanocrystal Formation.* Journal of the American Chemical Society, 128(40):13032–13033, 2006.

[37] Haitao Liu, Jonathan S. Owen, and A. Paul Alivisatos. *Mechanistic Study of Precursor Evolution in Colloidal Group II–VI Semiconductor Nanocrystal Synthesis.* Journal of the American Chemical Society, 129(2):305–312, 2007.

[38] Sofie Abe, Richard Karel Čapek, Bram De Geyter, and Zeger Hens. *Tuning the Postfocused Size of Colloidal Nanocrystals by the Reaction Rate: From Theory to Application.* ACS Nano, 6(1):42–53, 2012.

[39] Sofie Abe, Richard K. Capek, Bram De Geyter, and Zeger Hens. *Reaction Chemistry/Nanocrystal Property Relations in the Hot Injection Synthesis, the Role of the Solute Solubility.* ACS Nano, 7(2):943–949, 2013.

[40] M.A. Hines and G.D. Scholes. *Colloidal PbS Nanocrystals with Size-Tunable Near-Infrared Emission: Observation of Post-Synthesis Self-Narrowing of the Particle Size Distribution.* Advanced Materials, 15(21):1844–1849, 2003.

[41] Craig R. Bullen and Paul Mulvaney. *Nucleation and Growth Kinetics of CdSe Nanocrystals in Octadecene.* Nano Letters, 4(12):2303–2307, 2004.

[42] W. William Yu and Xiaogang Peng. *Formation of High-Quality CdS and Other II–VI Semiconductor Nanocrystals in Noncoordinating Solvents: Tunable Reactivity of Monomers.* Angewandte Chemie International Edition, 41(13):2368–2371, 2002.

[43] Jacek Jasieniak, Craig Bullen, Joel van Embden, and Paul Mulvaney. *Phosphine-Free Synthesis of CdSe Nanocrystals.* The Journal of Physical Chemistry B, 109(44):20665–20668, 2005.

[44] Jianying Ouyang, Maxime Vincent, David Kingston, Pierre Descours, Thibault Boivineau, Md. Badruz Zaman, Xiaohua Wu, and Kui Yu. *Noninjection, One-Pot Synthesis of Photoluminescent Colloidal Homogeneously Alloyed CdSeS Quantum Dots.* The Journal of Physical Chemistry C, 113(13):5193–5200, 2009.

[45] Liang Li and Peter Reiss. *One-pot Synthesis of Highly Luminescent InP/ZnS Nanocrystals without Precursor Injection.* Journal of the American Chemical Society, 130(35):11588–11589, 2008.

[46] Y. Charles Cao and Jianhui Wang. *One-Pot Synthesis of High-Quality Zinc-Blende CdS Nanocrystals.* Journal of the American Chemical Society, 126(44):14336–14337, 2004.

[47] Jianying Ouyang, Md. Badruz Zaman, Fu Jian Yan, Dennis Johnston, Grace Li, Xiaohua Wu, Don Leek, Christopher I. Ratcliffe, John A. Ripmeester, and Kui Yu. *Multiple Families of Magic-Sized CdSe Nanocrystals with Strong Bandgap Photoluminescence via Noninjection One-Pot Syntheses.* The Journal of Physical Chemistry C, 112(36):13805–13811, 2008.

[48] Kui Yu, Jianying Ouyang, Md. Badruz Zaman, Dennis Johnston, Fu Jian Yan, Grace Li, Christopher I. Ratcliffe, Donald M. Leek, Xiaohua Wu, Jacek Stupak, Zygmunt Jakubek, and Dennis Whitfield. *Single-Sized CdSe Nanocrystals with Bandgap Photoemission via a Noninjection One-Pot Approach.* The Journal of Physical Chemistry C, 113(9):3390–3401, 2009.

[49] Emory M. Chan, Richard A. Mathies, and A. Paul Alivisatos. *Size-Controlled Growth of CdSe Nanocrystals in Microfluidic Reactors.* Nano Letters, 3(2):199–201, 2003.

[50] H. Wang, H. Nakamura, M. Uehara, Y. Yamaguchi, M. Miyazaki, and H. Maeda. *Highly Luminescent CdSe/ZnS Nanocrystals Synthesized Using a Single-Molecular ZnS Source in a Microfluidic Reactor.* Advanced Functional Materials, 15(4):603–608, 2005.

[51] A. D. Yoffe. *Semiconductor quantum dots and related systems: Electronic, optical, luminescence and related properties of low dimensional systems.* Advances in Physics, 50(1):1–208, 2001.

[52] T. J. Liptay, L. F. Marshall, P. S. Rao, R. J. Ram, and M. G. Bawendi. *Anomalous Stokes shift in CdSe nanocrystals.* Physical Review B, 76(15):155314, Oct 2007.

[53] Haizheng Zhong, Michelle Nagy, Marcus Jones, and Gregory D. Scholes. *Electronic States and Exciton Fine Structure in Colloidal CdTe Nanocrystals.* The Journal of Physical Chemistry C, 113(24):10465–10470, 2009.

[54] Bram De Geyter, Yolanda Justo, Iwan Moreels, Karel Lambert, Philippe F. Smet, Dries Van Thourhout, Arjan J. Houtepen, Dominika Grodzinska, Celso de Mello Donega, Andries Meijerink, Daniel Vanmaekelbergh, and Zeger Hens. *The Different Nature of Band Edge Absorption and Emission in Colloidal PbSe/CdSe Core/Shell Quantum Dots.* ACS Nano, 5(1):58–66, 2011.

[55] Anna Rodina and Alexander L. Efros. *Magnetic Properties of Nonmagnetic Nanostructures: Dangling Bond Magnetic Polaron in CdSe Nanocrystals.* Nano Letters, 15(6):4214–4222, 2015.

[56] Ranjani Viswanatha, Sergio Brovelli, Anshu Pandey, Scott A. Crooker, and Victor I. Klimov. *Copper-Doped Inverted Core/Shell Nanocrystals with "Permanent" Optically Active Holes.* Nano Letters, 11(11):4753–4758, 2011.

[57] Justin R. Caram, Sophie N. Bertram, Hendrik Utzat, Whitney R. Hess, Jessica A. Carr, Thomas S. Bischof, Andrew P. Beyler, Mark W. B. Wilson, and Moungi G. Bawendi. *PbS Nanocrystal Emission Is Governed by Multiple Emissive States.* Nano Letters, 16(10):6070–6077, 2016.

[58] Jana Bomm, Andreas Büchtemann, Angela Fiore, Liberato Manna, James H. Nelson, Diana Hill, and Wilfried G. J. H. M. van Sark. *Fabrication and spectroscopic studies on highly luminescent CdSe/CdS nanorod polymer composites.* Beilstein Journal of Nanotechnology, 1:94–100, 2010.

[59] D. J. Norris, Al. L. Efros, M. Rosen, and M. G. Bawendi. *Size dependence of exciton fine structure in CdSe quantum dots.* Physical Review B, 53(24):16347–16354, 1996.

[60] Lianhua Qu and Xiaogang Peng. *Control of Photoluminescence Properties of CdSe Nanocrystals in Growth.* Journal of the American Chemical Society, 124(9):2049–2055, 2002.

[61] Mark Green. *The nature of quantum dot capping ligands.* Journal of Materials Chemistry, 20(28):5797–5809, 2010.

[62] Wilfried G. J. H. M. van Sark, Patrick L. T. M. Frederix, Dave J. Van den Heuvel, Hans C. Gerritsen, Ageeth A. Bol, Joost N. J. van Lingen, Celso de Mello Donegá, and Andries Meijerink. *Photooxidation and Photobleaching of Single CdSe/ZnS Quantum Dots Probed by Room-Temperature Time-Resolved Spectroscopy.* The Journal of Physical Chemistry B, 105(35):8281–8284, 2001.

[63] Margaret A. Hines and Philippe Guyot-Sionnest. *Synthesis and Characterization of Strongly Luminescing ZnS-Capped CdSe Nanocrystals.* The Journal of Physical Chemistry, 100(2):468–471, 1996.

[64] Xiaogang Peng, Michael C. Schlamp, Andreas V. Kadavanich, and A. P. Alivisatos. *Epitaxial Growth of Highly Luminescent CdSe/CdS Core/Shell Nanocrystals with Photostability and Electronic Accessibility.* Journal of the American Chemical Society, 119(30):7019–7029, 1997.

[65] A. B. Greytak, P. M. Allen, W. H. Liu, J. Zhao, E. R. Young, Z. Popović, B. J. Walker, D. G. Nocera, and M. G. Bawendi. *Alternating layer addition approach to CdSe/CdS core/shell quantum dots with near-unity quantum yield and high on-time fractions.* Chemical Science, 3(6):2028–2034, 2012.

[66] Wanzhen Lin, Yuan Niu, Renyang Meng, Lin Huang, Hujia Cao, Zhenxing Zhang, Haiyan Qin, and Xiaogang Peng. *Shell-thickness dependent optical properties of CdSe/CdS core/shell nanocrystals coated with thiol ligands.* Nano Research, 9(1):260–271, 2016.

[67] Xiaobo Chen, Yongbing Lou, Anna C. Samia, and Clemens Burda. *Coherency Strain Effects on the Optical Response of Core/Shell Heteronanostructures.* Nano Letters, 3(6):799–803, 2003.

[68] Markus Grabolle, Jan Ziegler, Alexei Merkulov, Thomas Nann, and Ute Resch-Genger. *Stability and Fluorescence Quantum Yield of CdSe–ZnS Quantum Dots—Influence of the Thickness of the ZnS Shell.* Annals of the New York Academy of Sciences, 1130(1):235–241, 2008.

[69] Lei Chen, Chun-Che Lin, Chiao-Wen Yeh, and Ru-Shi Liu. *Light Converting Inorganic Phosphors for White Light-Emitting Diodes.* Materials, 3(3):2172–2195, 2010.

[70] K. J. Chen, B. C. Lin, H. C. Chen, M. H. Shih, C. H. Wang, H. T. Kuo, H. H. Tsai, M. Y. Kuo, S. H. Chien, P. T. Lee, C. C. Lin, and H. C. Kuo. *Effect of the Thermal Characteristics of Phosphor for the Conformal and Remote Structures in White Light-Emitting Diodes.* IEEE Photonics Journal, 5(5):8200508, 2013.

[71] M. Meneghini, M. Dal Lago, N. Trivellin, G. Meneghesso, and E. Zanoni. *Thermally Activated Degradation of Remote Phosphors for Application in LED Lighting.* IEEE Transactions on Device and Materials Reliability, 13(1):316–318, 2013.

[72] Jong Kyu Kim, Hong Luo, Eric Fred Schubert, Jaehee Cho, Cheolsoo Sone, and Yongjo Park. *Strongly Enhanced Phosphor Efficiency in GaInN White Light-Emitting Diodes Using Remote Phosphor Configuration and Diffuse Reflector Cup.* Japanese Journal of Applied Physics, 44(21):L649–L651, 2005.

[73] N. Narendran, Y. Gu, J. P. Freyssinier-Nova, and Y. Zhu. *Extracting phosphor-scattered photons to improve white LED efficiency.* physica status solidi (a), 202(6):R60–R62, 2005.

[74] B. Fan, H. Wu, Y. Zhao, Y. Xian, and G. Wang. *Study of Phosphor Thermal-Isolated Packaging Technologies for High-Power White Light-Emitting Diodes.* IEEE Photonics Technology Letters, 19(15):1121–1123, 2007.

[75] C. Chartier, C. Barthou, P. Benalloul, and J.M. Frigerio. *Photoluminescence of $Eu^{2+}$ in $SrGa_2S_4$.* Journal of Luminescence, 111(3):147–158, 2005.

[76] Y. Q. Li, A. C. A. Delsing, G. de With, and H. T. Hintzen. *Luminescence Properties of $Eu^{2+}$-Activated Alkaline-Earth Silicon-Oxynitride $MSi_2O_{2-\delta}N_{2+2/3\delta}$ (M = Ca, Sr, Ba): A Promising Class of Novel LED Conversion Phosphors.* Chemistry of Materials, 17(12):3242–3248, 2005.

[77] Xiaojun Wang, Guohong Zhou, Hailong Zhang, Huili Li, Zhejuan Zhang, and Zhuo Sun. *Luminescent properties of yellowish orange $Y_3Al_{5-x}Si_xO_{12-x}N_x$:Ce phosphors and their applications in warm white light-emitting diodes.* Journal of Alloys and Compounds, 519:149–155, 2012.

[78] Heleen F. Sijbom, Reinert Verstraete, Jonas J. Joos, Dirk Poelman, and Philippe F. Smet. *$K_2SiF_6$:$Mn^{4+}$ as a red phosphor for displays*

*and warm-white LEDs: a review of properties and perspectives*. Optical Materials Express, 7(9):3332–3365, 2017.

[79] Jaehoon Lim, Wan Ki Bae, Donggu Lee, Min Ki Nam, Joohyun Jung, Changhee Lee, Kookheon Char, and Seonghoon Lee. *InP@ZnSeS, Core@Composition Gradient Shell Quantum Dots with Enhanced Stability*. Chemistry of Materials, 23(20):4459–4463, 2011.

[80] Bin Xie, Run Hu, and Xiaobing Luo. *Quantum Dots-Converted Light-Emitting Diodes Packaging for Lighting and Display: Status and Perspectives*. Journal of Electronic Packaging, 138(2):020803–020803–13, 2016.

[81] Dmitri V. Talapin and Jonathan Steckel. *Quantum dot light-emitting devices*. MRS Bulletin, 38(9):685–691, 2013.

[82] Chihao Xu, Marc Albrecht, and Tobias Jung. *Dimming of LED LCD Backlights*, pages 567–574. Handbook of Visual Display Technology, Springer Berlin Heidelberg, 2012.

[83] H. S. Jeong, S. W. Woo, S. S. Kim, and B. D. Choi. *Liquid crystal display black light leakage correlation between VA and IPS by curvature*. In 2014 21st International Workshop on Active-Matrix Flatpanel Displays and Devices (AM-FPD), pages 73–76, 2014.

# 2

# Indium Phosphide Quantum Dots Synthesis: State-of-the-Art

*Most studied nanocrystals active at visible wavelengths involve cadmium chalcogenide based materials, which prove relatively easy to synthesize with high quality optical properties. However cadmium is a toxic heavy metal that is banned in packaging applications in several countries. To transfer nanocrystals from the academic field to product applications, there is a need for materials that complies number of important boundary conditions. Apart from a reduced toxicity, this also involves a cost efficient production at an industrial scale and competitive optical properties. To make the use of QDs feasible, interest is therefore shifting from the well-characterized Cd chalcogenide QDs to indium phosphide colloidal quantum dots (InP QDs), a material that combines emission characteristics that come close to cadmium selenide quantum dots (CdSe QDs) with a reduced toxicity.*

## 2.1 Introduction

Over the last 15 years, InP QDs have attracted extensive attention as shown by numerous publications devoted to both the synthesis and the character-

ization of InP QDs.[1;2] With a bulk band gap of ≈ 1.35 eV and a Bohr exciton radius of ≈ 15 nm, InP QDs exhibit stronger size quantization effects as compared to most of the II-VI semiconductors.[3] This enables the emission wavelength of InP QDs to be tuned from the blue to near-infrared by changing the QD size. Therefore, they are of particular interest for applications relying on fluorescent properties such as in vivo imaging,[4] photovoltaics,[5] or lighting.[6–8] In addition, several studies have demonstrated the reduced toxicity of InP-based QDs as compared to CdSe-based QDs, which is of great importance regarding the RoHS (Restriction of Hazardous Substances) directive of the European Commission that restricts the use of Cd and Pb-based materials in product application.[9–12] Hence, InP QDs stands out as an alternative to toxic CdSe-based QDs.

In general, InP QDs have emission linewidths down to ≈ 45 nm, which is considerably larger than QDs based on CdSe. On the other hand, recent optical studies on single InP nanocrystals have shown that single InP QDs have a similar emission linewidth than single CdSe QDs.[13] This implies that the broader emission linewidth obtained by a typical InP QD synthesis is due to inhomogeneous broadening, linked to the distribution in particle sizes, rather than an intrinsic material characteristic. It has been suggested that the more covalent character of the In-P bond makes it more difficult to achieve similar narrow particle size distribution as obtained with II-VI semiconductors NCs[14]. This could arise from a difficult separation of the nucleation and growth stage during the InP QDs formation where high temperatures and reactive precursors are needed because of the covalent bond character of InP QDs. On the other hand, the broader emission lines could also be due to a stronger variation of the InP band gap with size as compared to CdSe, in line with the larger Bohr radius of InP.[15] Even so, numerous research studies have been made to synthesize high quality InP QDs with a narrow size distribution and a high photoluminescence efficiency. The goal of this chapter is to provide an overview of this work, prior to discussing the result obtained as part of this PhD research.

## 2.2 $(TMS)_3P$-based InP quantum dots synthesis

### 2.2.1 Synthesis in coordinating solvents

The Wells' dehalosilylation approach reported in 1989 was used by Healy and coworkers to prepare the first InP NCs.[16;17] This organometallic route involved the reaction between indium(III) chloride ($InCl_3$) and the silylphos-

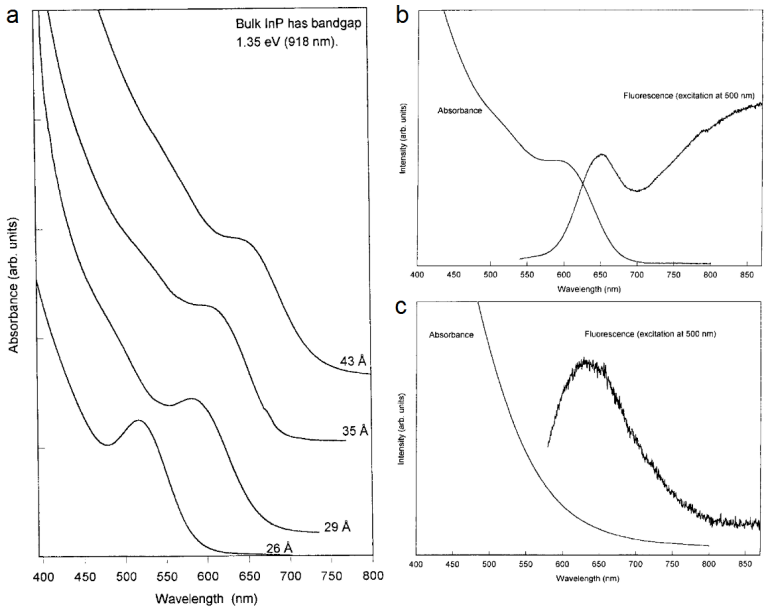


**Figure 2.1: (a)** Absorption spectra of InP QDs with different diameters. Room-temperature photoluminescence and absorption spectra of InP QDs prepared with different ratios of In and P: **(b)** In:P = 1.6 and **(c)** In:P = 0.62. (Reprinted from reference[21]).

phine precursor $(TMS)_3P$. An analysis of the reaction products showed that the resulting InP NCs arised from the room temperature formation of the oligomer $[Cl_2InP(SiMe_3)_2]_x$ followed by elimination of $Me_3SiCl$ groups at high temperatures (650 ℃). In addition, replacing $InCl_3$ by $InBr_3$ or $InI_3$ led to the formation of InP NCs with sizes ranging from 2.5 to 3.7 nm, as estimated by XRD (X-ray powder diffraction) analysis.[18] In 1994, Micic *et al.* proposed a modified approach of the Well's dehalosilylation reaction to produce for the first time colloidal InP QDs.[19] Nanosized InP QDs of approximately 2.5 nm were synthesized by mixing a chloroindium oxalate complex with $(TMS)_3P$ at room temperature. The formed precursor was thermally decomposed by heating for several days at 270 ℃ in the presence of the coordinating trioctylphosphine (TOP) and trioctylphosphine oxide (TOPO) solvent. The introduction of such molecules in the reaction medium was based on previous studies performed on CdSe-based QDs, which demonstrated that a mixture of TOPO/TOP allows for a better control of the particle growth leading to the formation of monodisperse CdSe QDs.[20]

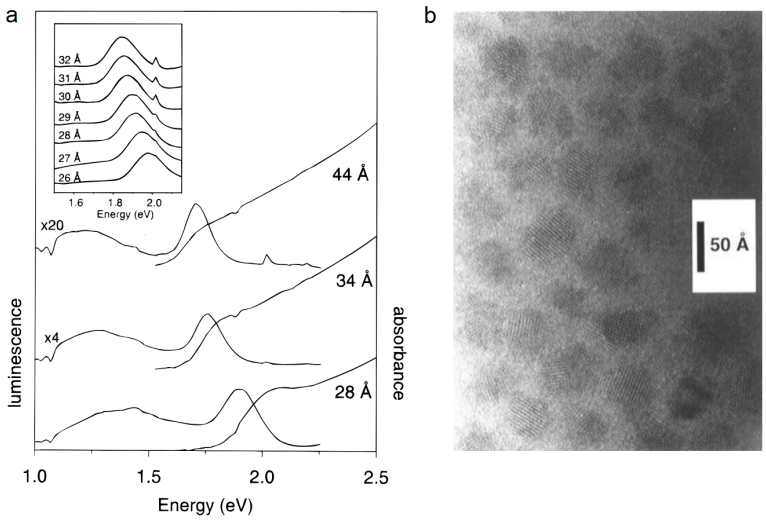


**Figure 2.2:** **(a)** Absorbance and photoluminescence spectra of InP nanocrystals of different sizes. The insert shows additional scaled photoluminescence spectra of InP nanocrystals with sizes decreasing from top to bottom. The samples have been treated with decylamine and were exposed to air. **(b)** Transmission electron micrograph of InP nanocrystals. (Reprinted from reference[23]).

In additional studies, Micic *et al.* proposed the synthesis of zincblende InP QDs with sizes ranging from 2.6 to 4.6 nm by tuning the reaction temperature as well as the In:P or TOPO:TOP ratio.[21;22] The authors obtained the most narrow particle size distributions by using an excess of indium precursor. This result was explained by the idea that TOPO/TOP binds most effectively to indium-rich sites at the QDs surface, which should ensure a homogeneous growth of the particles.[21] This resulted in InP QDs exhibiting a more narrow excitonic feature in their absorption spectrum (see Figure 2.1a), whereas their photoluminescence spectrum showed two emission bands, a narrow band corresponding to the band edge emission of the QDs and a wide tail above 800 nm attributed to trap-related emission (see Figure 2.1b). In contrary, InP QDs synthesized with an excess of phosphorous only displayed band-edge emission whereas no excitonic features could be distinguished in their absorption spectra, which points towards a more polydisperse ensemble (see Figure 2.1c).

Other approaches, extending the work of Micic *et al.* were proposed to synthesize InP QDs of about 2 to 5 nm in diameter.[23;24] In these proto-

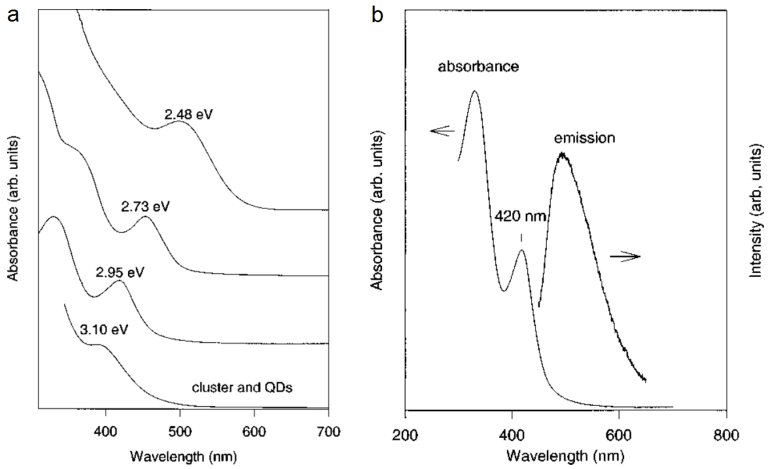


**Figure 2.3: (a)** Absorption spectra for different QD sizes estimated to be 2.3 nm, 1.8 nm, 1.5 nm, and $<$ 1.5 nm from top to bottom curves. **b)** Absorption and emission spectra of $\approx$ 1.5 nm InP QDs prepared in trioctylamine. (Reprinted from reference[27]).

cols, $InCl_3$ is reacted with $(TMS)_3P$ for 7 days in the presence of TOPO at elevated temperature. Despite a size selective precipitation allowing to attain a size distribution of about 20 %, UV-Vis and photoluminescence (PL) studies of the as-formed InP QDs did not show a significant improvement of the optical properties as compared to previously established protocols (see Figure 2.2). Furthermore, a careful study of the nanocrystals surface by X-ray photoelectron spectroscopy (XPS) and nuclear magnetic resonance spectroscopy (NMR) showed that after air exposure, the surface of the QDs was completely passivated by oxidized In and P in combination with TOPO. Interestingly, the authors found that the latter is essential to obtain luminescent InP QDs, which arise from an enhanced surface passivation that eliminate deep trap emissions. Furthermore, the solubility of the resulting InP QDs was tailored by replacing part of the TOPO capping by different ligands. Similar studies on the surface chemistry of InP QDs were performed on TOPO-capped InP QDs.[25;26] In this case, the authors were able to quantify the density of TOPO molecules adsorbed at the surface of the QDs and provided a thermodynamic approach to characterize the QD-capping.

With the aim of improving size dispersion and obtain better defined optical properties in the case of InP QDs, Talapin *et al.* proposed the use of high boiling primary amines in combination with TOP as stabilizing and size-regulating agents.[28] This method allowed to produce small-sized InP QDs,

ranging from 1.5 to 4 nm in diameter, which were difficult to make with the prevailing protocols involving TOPO/TOP. However, the as-prepared InP QDs showed little photoluminescence, with quantum yields remaining well below 1 %. Smaller InP QDs were synthesized with only amine as a substitute for the coordinating solvent TOPO/TOP.[27] The addition of a protic reagent such as amine was believed to hydrolyze $(TMS)_3P$ and accelerate the formation of the nanocrystals.[29] In this way, InP QDs with diameters ranging from 1.5 to 2.3 nm were synthesized with narrow size distribution as indicated by the absorption spectra for different QD sizes (see Figure 2.3a). However, the as-formed InP QDs had a relatively broad emission spectrum as seen in Figure 2.3b.

Despite numerous synthesis methods involving the use of different coordinating solvents, the relatively slow decomposition of the In-P oligomer in such media did not provide a sufficient control over the nucleation and growth stage. As a consequence, these approaches yielded colloids of InP nanocrystals with a rather poor size distribution as compared to typical II-VI synthesis.[28] Furthermore, the formed InP QDs were generally amorphous and long annealing times at high temperatures were required to obtain crystalline particles.

### 2.2.2 Synthesis in non-coordinating solvents

A significantly faster method for the synthesis of InP QDs was proposed in 2002 by the group of Peng.[30] These authors replaced the coordinating solvents such as TOPO/TOP by a the combination of a non-coordinating solvent, 1-octadecene (ODE), and carboxylic acids that act as coordinating ligands. The same combination was introduced by the same authors to improve the size distribution of CdSe QDs.[31] For a typical synthesis of InP QDs, indium(III) acetate was mixed with carboxylic acids and ODE. The mixture was then heated at 100-120 ℃ under vacuum to remove traces of impurities or water, after which a solution of $(TMS)_3P$ in ODE was swiftly injected in the reaction mixture at 300 ℃. The authors explored different possible ligands such as amines, phosphines, phosphine oxides, and phosphonic acids, yet they found that only carboxylic acids with specific chain lengths, such as palmitic acid and myristic acid, led to the formation of high quality InP QDs with narrow size distributions (see Figure 2.4a). The authors hypothesized that such carboxylic acids with an intermediate chain length were most suited to balance nucleation and growth. Moreover, they found that the concentration of the ligands had a dramatic impact on the size distribution of the as-formed InP QDs as it was previously observed in CdSe-QDs syntheses.[32] A molar ratio of 1:3 of In:MA in the solution was

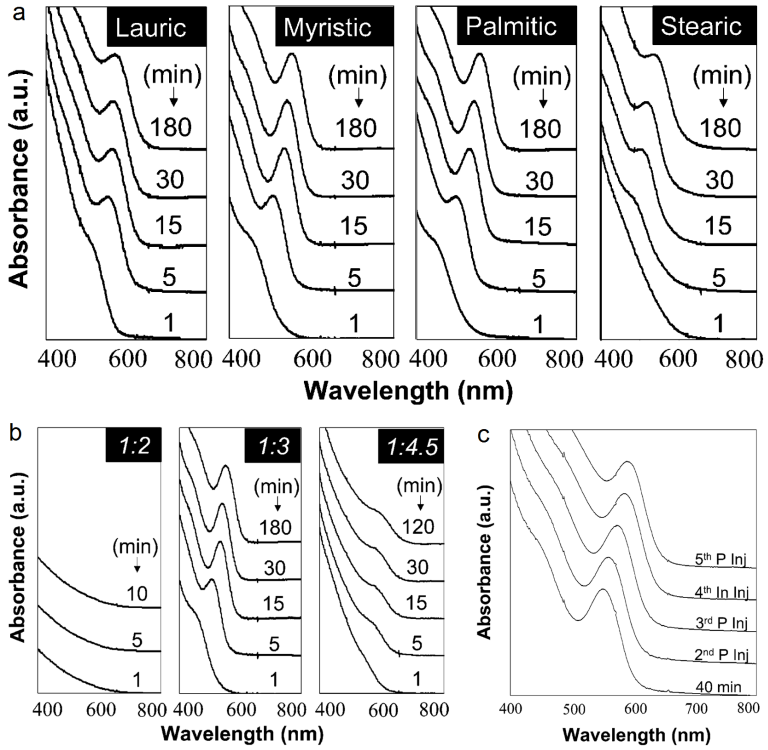


**Figure 2.4: (a)** Temporal evolution of the UV-Vis spectra of InP nanocrystals grown with fatty acids as the ligands. In:acid ratio = 1:3 for all reactions. **(b)** Temporal evolution of the UV-Vis spectra of InP nanocrystals grown at 270 ℃ with different In:MA ratio in ODE. **(c)** UV-Vis spectra of InP nanocrystals grown by multiple injections. (Reprinted from reference[30]).

found to be optimal to generate high quality InP nanocrystals as indicated by the well-distinguished absorption features in the UV-Visible (UV-Vis) spectra (see Figure 2.4b). Furthermore, due to the surface sensitivity of InP QDs after air exposure, a degassing process was considered necessary for the formation of high quality nanocrystals. Secondary injection, a technique also used for the growth of II-VI nanocrystal, was employed to tune the size of the InP QDs, resulting in a narrow first excitonic absorption feature ranging from 550 to 600 nm (see Figure 2.4c).

It should be noted that the absorption spectra of the InP QDs synthesised using a non-coordinating solvent showed more narrow excitonic features than InP QDs synthesised using coordinating solvents such as TOPO/TOP.

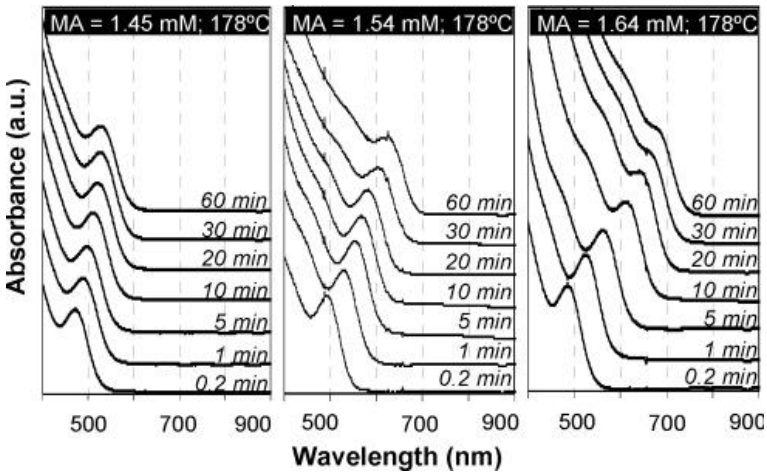


**Figure 2.5:** Temporal evolution of UV-Vis spectrum of InP nanocrystals grown with different myristic acid concentration. (Reprinted from reference[34]).

In addition, the use of ODE allows for a cheaper and greener synthesis in comparison with existing schemes using coordinating solvents. Therefore a large majority of $(TMS)_3P$-based InP QDs synthesis expanded on the use of ODE as a solvent in combination with stabilizing ligands such as fatty acids. For example, the group of Prasad proposed an InP QDs synthesis without using any surfactant or coordinating ligand in the reaction mixture.[33] The synthesis allows to produce InP QDs from indium(III) carboxylate complexes in ODE. According to the authors, a fast nucleation immediately occurs after the $(TMS)_3P$ injection and the growth step can be controlled by varying the growth temperature. Thanks to a fast nucleation followed by a slow growth, relatively monodisperse InP QDs were produced with this method. Moreover, selecting appropriate carboxylic acids or varying the reaction temperature allowed to tune the exciton feature of the InP QDs from 467 to 574 nm. However, the as-formed QDs still exhibited poor band-edge photoluminescence, featuring PL spectra dominated by a broad emission band related to deep-trap recombination.

In 2007, the group of Peng improved on its initial protocol to produce InP QDs with an extended size range at a relatively low temperature (190 ℃).[34] The authors hypothesized that the latter is required to avoid the hydrolysis of the indium carboxylate precursor into non-desired $In_2O_3$ nanoparticles. In that matter, amine was used to make the indium carboxylate precursor more reactive at low temperature in order to prevent the concomitant

formation of $In_2O_3$ NCs. This approach allowed the authors to synthesize InP QDs in a relatively shorter time (60 min) compared to previous reported methods. Furthermore, by changing the synthesis parameters, InP QDs with a narrow absorption feature tunable from 390 to 720 nm were obtained, a range that is considerably larger than what previous protocols could attain (see Figure 2.5).[30] The use of non-coordinating solvent such as ODE led further research to look for alternatives, where for example the group of Nann proposed methyl myristate and dibutyl sebacate as weakly coordinating solvents.[35] These authors hypothesized that a nucleation process similar to that in noncoordinating solvents could also be obtained in weakly coordinating solvents. However, the coordinating effect of the latter had to be much weaker than that of the introduced ligands. In this respect, trimethylindium was used in combination with $(TMS)_3P$, which was injected at high temperature in a mixture of esters and carboxylic acids. The authors also investigated the role of protic reagents, such as amine or alcohol, in the hydrolysis of the $(TMS)_3P$ precursor to accelerate the nucleation process. This approach allowed them to produce InP NCs with a mean diameter of 2.5 nm and a narrow size distribution, as shown by the distinguishable absorption features in the UV-Vis spectra.

### 2.2.3 Optimization of the $(TMS)_3P$ precursor

Despite significant improvements in the synthesis, InP QDs still featured broader emission lines as compared to CdSe QDs. In this respect, the group of Bawendi investigated the molecular mechanism involved in the formation of InP QDs to understand the broader size distributions that characterized InP QD dispersions.[36] The authors found that $(TMS)_3P$ is subjected to a fast depletion at high temperature which leaves no phosphorous monomers for a proper growth of the NCs. Therefore the growth of the InP QDs is mainly achieved by Ostwald ripening, which may explain the broader size distribution of InP QDs as compared to CdSe QDs. The authors also showed that amines can inhibit the precursor decomposition, which is in contradiction with previous reports that claim that amines can activate the $(TMS)_3P$ precursor.[27;34;37].

Because of the rapid precursor depletion, further research has focused on adjusting the phosphorous precursor chemistry itself. For example, a new $(TMS)_3P$-based precursor with different functional groups was designed to have better control over the reaction during the nucleation stage.[39] The authors preserved the P-Si bonds of the $(TMS)_3P$ precursor, yet substituted a methyl group by a tertiary butyl or phenyl group. These newly synthesized phosphorus precursors resulted in larger InP QDs (540-640 nm), while keep-

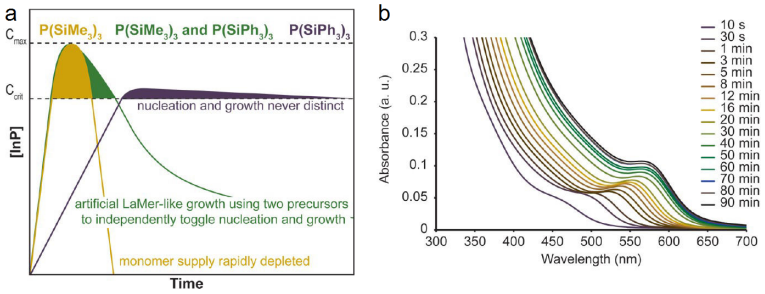


**Figure 2.6:** **(a)** Growth profile of the InP QDs using $(TMS)_3P$ (gold), $P(SiPh_3)_3$ (purple), and the mixture of the two reagents (green). **(b)** Absorption spectra of InP QDs prepared using a mixture of $P(SiMe_3)_3$ and $P(SiPh_3)_3$. (Reprinted from reference[38]).

ing a narrow size distribution with respect to conventional $(TMS)_3P$-based InP synthesis. Gary *et al.* proposed the used of two phosphine precursors with a different reactivity to tune the nucleation and growth stage of $(TMS)_3P$-based InP synthesis.[38] The protocol involved a first injection of $(TMS)_3P$ to initiate a rapid nucleation, followed by the use of a less reactive triarylsilylphosphine $(PSiPh_3)_3$ that acts as a monomer reservoir during the QD growth. Although realizing a LaMer-like nucleation and growth reaction (see Figure 2.6a), this approach could not reduce the size distribution of InP QDs as shown in the UV-Vis absorption spectra of the thus synthesized QDs (see Figure 2.6b). In this respect, this study demonstrated that a separation of nucleation and growth is not the only criterium to produce monodisperse InP QDs, as it was previously considered.[36] Other approaches to adjust the $(TMS)_3P$ precursor were proposed, where for example the Si atom was replace by Ge.[40] Although this new phosphorous precursor was 4 time less reactive than the $(TMS)_3P$, the reaction kinetics study showed that the precursor conversion rate still occurs on a time scale faster than the particle growth. Hence, in spite of all this work, little progress has been made in terms of an improved size distribution by changing the reactivity of the phosphorous precursor.

More recent studies highlighted the presence of magic-sized clusters (MSCs) as reaction intermediates in the synthesis of InP QDs.[41–44] Featuring sizes of $\approx 1$ nm and a well-defined chemical formula, such magic size clusters are a state of matter in between molecules and nanocrystals, which are already characterized by continuously varying properties. Two possible explanations for the formation of InP QDs through MSCs were proposed.[41] The first is that nucleation of InP QDs may proceed via dissolution of MSCs

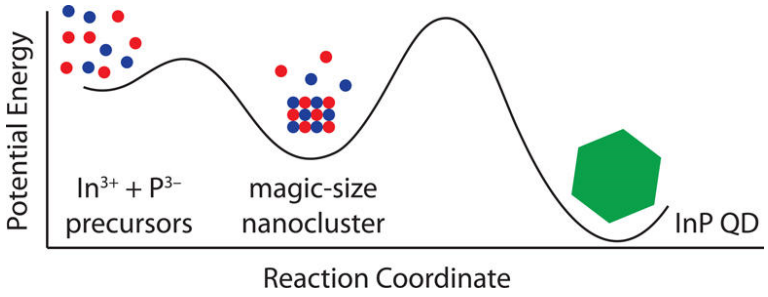


**Figure 2.7:** Schematic representation of the two-step nucleation mechanism for the growth of InP QDs via magic-sized cluster intermediates. (Reprinted from reference [41]).

into monomers followed by a second nucleation that allows the formation of InP QDs. The second explanation is that the MSCs may simply aggregate to produce QDs. Therefore, tuning the phosphorous reactivity to control both nucleation and growth turned out to be ineffective as the QDs formation proceeds via formation of MSCs followed by subsequent heterogeneous growth from the MSCs directly to QDs (see Figure 2.7). Even if such insight could eventually lead to InP QD dispersions with improved properties, $(TMS)_3P$ remains an expensive and pyrophoric precursor for the production of InP QDs. Therefore, these is a clear need for cheaper and safer phosphorous precursors for the synthesis of high quality InP QDs.

## 2.3 Alternative phosphorus precursors

### 2.3.1 $P_4$-based InP quantum dots synthesis

In 1999, yellow phosphorous ($P_4$) has been investigated as an alternative phosphorous to produce InP QDs.[45] The first synthesis involved the reaction of $InCl_3$ with $P_4$ and $KBH_4$ at 80-160 ℃ in ethylenediamine. In this method, $KBH_4$ acts as a reducing agent to produce metallic indium intermediates that react with $P_4$ to form InP QDs with sizes between 11-20 nm. UV-Vis absorption spectrum shows ill-defined excitonic features due to the relatively broad size dispersions of the as-prepared nanocrystals, which exhibit irregular morphologies as observed in transmission electron microscopy (TEM) images. Based on a similar protocol, Li *et al.* proposed an alternative sonochemical approach to produce InP NCs at room temperature.[46] In this case, NCs with an average diameter of $\approx 9$ nm were obtained under ultrasonic irradiation from the reaction of $InCl_3$, $P_4$ and $KBH_4$ in a mixture

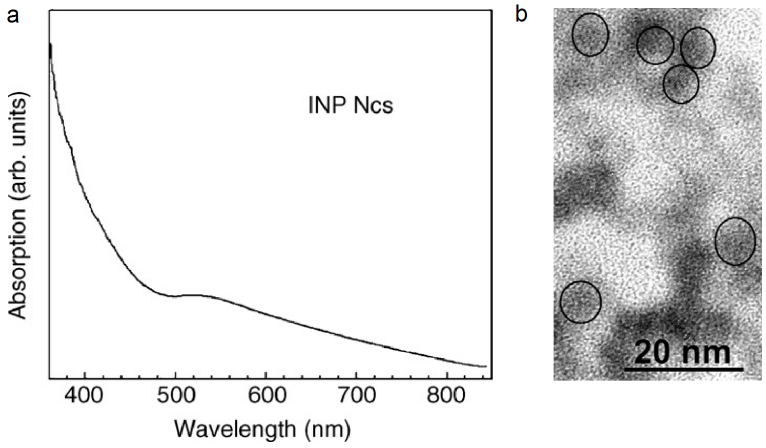


**Figure 2.8: (a)** UV-Vis absorption spectrum and **(b)** TEM image of InP NCs obtained with synthesis protocol of reference[47]. Individual monocrystalline particles are highlighted with circles. (Reprinted from reference[47]).

of ethanol and benzene. In addition, size-tuning was possible by changing the volume ratio of added solvents. This influenced the viscosity of the reaction system, which by itself influenced the balance between nucleation and growth. However, the absorption spectrum of these sonochemically prepared InP nanocrystals exhibited a relatively broad absorption peak as compared to particles produce with $(TMS)_3P$ precursor. A similar approach without the use of ultrasound was proposed by the group of Reiss to synthesize zincblende InP NCs with a mean size of 3 to 4 nm.[47] This reaction had several advantages with respect to previous protocols as InP NCs were produce in shorter reaction time (1-5 h), using lower temperatures ($< 75$ ℃) and at near unity reaction yield. Nevertheless, UV-Vis (see Figure 2.8a) attested to the relative broad size distribution of the as-formed InP NCs, which tend to aggregate according to TEM images (see Figure 2.8b).

Hydrothermal approach for the synthesis of InP NCs were proposed by Wei *et al.*[48;49] In this method, InP NCs were hydrothermally synthesized in aqueous ammonia by reacting $InCl_3$, $P_4$, $NaBH_4$, in the presence of potassium stearate $C_{18}H_{35}KO_2$ as a surfactant. Spherical and rod-like NCs were obtained as confirmed by XRD and TEM analysis. Hence, no excitonic structure is observed in the UV-Vis spectra, which points towards the broad size distribution of the as-prepared InP NCs. A similar hydrothermal procedures was used in 2008 by Yang *et al.* to synthesize InP NCs with In-ethylenediamine tetraacetic acid as the indium source in combination with red phosphorous, and $KBH_4$ in aqueous solution at 160-200 ℃.[50]

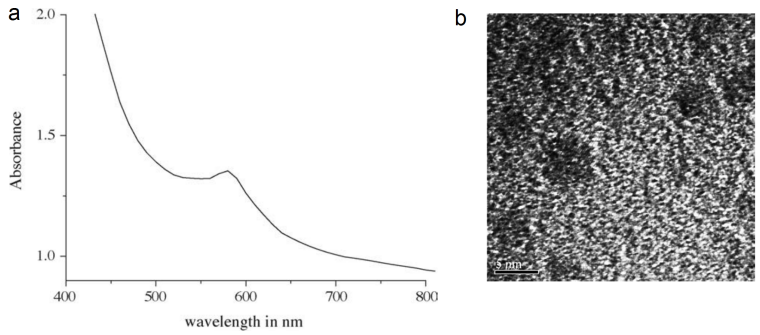


**Figure 2.9: (a)** UV-Vis spectrum and **(b)** TEM images of InP nanocrystals obtained with synthesis protocol of reference[51]. (Reprinted from reference[51]).

In this case, increasing the reaction temperature led to the production of size-tunable InP NCs with diameters ranging from 8.7 to 15.8 nm as determined by XRD and TEM analysis. However, no UV-Vis or PL studies were performed to analysis the particle distributions.

In 2003, Khanna *et al.*, reported the use of sodium phosphide ($Na_3P$) for the synthesis of InP NCs.[52] First, $P_4$ was reacted with sodium metal in N,N-dimethylformamide (DMF) for 2 to 3 days at a temperature of 120-160 ℃ to produce $Na_3P$. Then, indium chloride dissolved in DMF was added and the reaction mixture was heated at 120-160 ℃ during 2-3 days. Amorphous InP NCs with a broad size dispersion were obtained according to XRD and UV-Vis measurements. The authors optimized there synthesis in 2006, where they used TOP and 4-ethylpyridine as solvents and capping agents to control the particle growth.[51] InP nanocrystals with sizes ranging from 3 to 7 nm were obtained, as evidenced by XRD and TEM analysis. Although the UV-Vis absorption spectrum was characterized by a more narrow excitonic peak as compared to previous work (see Figure 2.9), the size distribution remained broader than the $(TMS)_3P$-based approaches. Based on a sonochemical approach developed by Xi *et al*, the group of Casadonte used yellow phosphorous and sodium metal for the synthesis of nano-sized InP.[46;53] The synthesis involved the in situ formation of sodium phosphide and a subsequent reaction with $InCl_3$ using sonication. XRD analysis show that elemental indium is formed concomitantly with amorphous InP particles. TEM images also revealed the amorphous nature of the as-formed InP particles, which required further annealing at high temperature 600 ℃ to obtain crystalline InP NCs.

In 2010, an alternative method to produce InP NCs was proposed by the group of Mezaille, in which $P_4$ was reacted with indium metal nanoparticles.[54] The latter were previously formed by reduction of $InCl_3$ by sodium naphthalenide in the presence trialkyl-phosphine/amine as surface stabilizing agents. A mechanism is envisaged were InP NCs are supposed to be formed by surface assisted phosphorous diffusion into metallic indium particles. However, TEM studies revealed broad size dispersion of the as formed InP NCs and no UV-Vis study were performed to give further insight of the as-formed particles. An alternative method using $P_4$ to produce $PH_3$ as the phosphorous source was first reported in 2002 by Gao *et al.*[55] This reaction was carried out in aqueous solution at 120-160 ℃ and involved the formation of $PH_3$ by either white phosphorous dismutation or reduction of phosphoric acid $H_3PO_4$ into unstable phosphorous acid $H_3PO_3$ by white phosphorous. However, no excitonic features were observed in the absorption spectra, once more indicating that polydisperse samples were obtained.

### 2.3.2 $PH_3$-based InP quantum dots synthesis

Thanks to the work of Gao *et al.*, $PH_3$ has also been intensively studied as a cheap, alternative phosphorous precursor.[55] In 2008, Li *et al.* proposed a rapid method for the synthesis of large, high quality InP NCs via the in situ generation of $PH_3$ gas.[56] The synthesis involved the reaction between calcium phosphide $Ca_3P_2$ and hydrochloric acid HCl to produce $PH_3$ gas. The latter was subsequently carried by a argon flow into a mixture of indium acetate ($In(Ac)_3$), myristic acid and ODE at 250 ℃. Depending on the reaction parameters, absorption spectra of the obtained InP NCs showed well-defined exitonic features, indicative of a narrow size distribution (see Figure 2.10a). Furthermore, by adjusting the reaction conditions, excitonic peaks in the range of 650-700 nm could be obtained without broadening of the size distribution (see Figure 2.10b). The latter is confirmed by TEM images of two differently sized samples, which had mean diameters of 3 and 6.4 nm and size dispersions of $\approx$ 11 % and 9 %, respectively. Therefore, $PH_3$ can be considered as a viable, cost efficient alternative to produce monodisperse InP QDs, comparable to InP QDs made using $(TMS)_3P$. However, despite the preparation of relatively high quality InP QDs with the low cost $PH_3$ gas, this precursor has considerable drawbacks. It is highly toxicity and pyrophoric, two aspects that question its use as a viable phosphorous source for the production of InP QDs.

In this respect, an alternative $PH_3$-based InP NCs route was proposed in 2008 by Vinokurov *et al.*[57] $PH_3$, previously prepared by the reaction of $Zn_3P_2$ and phosphoric acid $H_3PO_4$, is reacted with $InCl_3$ in the solvent and

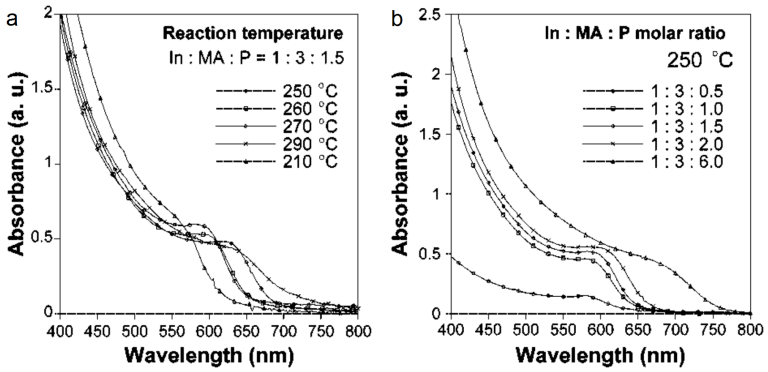


**Figure 2.10:** UV-Vis absorption spectra of InP NCs synthesized after 30 min of reaction with different **(a)** temperature and **(b)** In:P ratio. (Reprinted from reference [56]).

particle stabilizer dodecylamine at 200 ℃. However, the use of dodecylamine made it difficult to separate the as-formed particles, which complicated the further study of the as prepared sample. The authors proposed two purification protocols, where a first resulted in the isolation of InP QDs with a relatively narrow excitonic peak at 497 nm (estimated size 2.2 nm), whereas a second lead to further particle growth that broadened the size distributions as shown by the resulting ill-defined absorption feature. In another study, Ren *et al.* used $Zn_3P_2$ as the phosphorous source to produce $PH_3$, which is reacted with indium myristate in the non-coordinating solvent ODE.[58] $Zn_3P_2$ was preferred over calcium phosphide $Ca_3P_2$ as it has an improved air-stability and a lower reactivity. This results in a slower generation of $PH_3$ gas, which makes the overall reaction more controllable. Although reaction parameters such as the molar ratio of reactants and the reaction temperature were varied, no further improvements of the InP QDs have been reported in comparison with similar methods.

In 2014, Gabka *et al.* used the same reagents and investigated the role of the indium moieties and ligands on the formation of InP QDs.[59] Using only indium-carboxylate as both indium source and ligand allowed to improve the definition of the excitonic transition as compared to previous work in which indium acetate was used in combination with free carboxylic acid.[56;58]. In the same year, Mordvinova *et al.* developed an InP QDs synthesis by using gaseous phosphine $PH_3$ and indium acetate in combination with ODE and either myristic acid or TOP/TOPO as stabilizers.[60] They found that using myristic acid as stabilizer at relatively low temperatures resulted in a contamination with $In(OH)_3$ due to the hydrolysis of indium myristate

by the water contained in the hygroscopic $In(OAc)_3$ precursor. This could be prevented by replacing myristic acid by a TOP/TOPO mixture or by carrying out the reaction at elevated temperature. However, UV-Vis absorption spectra of InP QDs prepared using these different schemes did not show improvements in size distribution with respect to previously reported protocols.

### 2.3.3 Other phosphorus precursors

In 1998, Green *et al.* proposed the thermolysis of a single source molecule precursor $InBu_2P_3$ for the preparation of InP QDs.[61] The synthesis was enabled by the decomposition of $InBu_2P_3$ at 167 ℃ in the polar coordinating solvent 4-ethylpyridine. Single source precursor were developed in order to obtain a better control over the nucleation and growth process. However, absorption spectroscopy as well as transmission electron microscopy attest to the polydispersity of the thus prepared InP QDs. Therefore, this synthesis route did not lead to further study or optimization. In 2006, the group of Fang proposed a wet chemical reduction approach where $P_4$ and lithium triethylborohydride were involved.[62] Again, the resulting QDs showed a broad size distribution and the authors proposed the used of $PCl_3$ as a more efficient phosphorous source. This synthesis involved the co-reduction of indium acetate and $PCl_3$ by lithium triethylborohydride in a mixture of ODE and stearic acid. Due to the low boiling point of $PCl_3$ (76 ℃), this redox reaction was first carried at low temperature (40 ℃) while the subsequent NCs growth occurred at elevated temperature (250 ℃). Based on TEM images, the as-synthesized InP QDs were spherical and monodisperse with an average size of about 3.5 nm. In addition, the particle growth was investigated by UV-Vis absorption spectroscopy, where a well-defined excitonic peak was observed, which confirmed the narrow size distributions as obtained from TEM studies. Furthermore, the sizes of the NCs could be tuned by varying the growth temperature, which led to InP QDs which an excitonic peak ranging from 500 to 600 nm as shown by UV-Vis studies. However, the features were not as well defined as in the case of InP QDs prepared with $(TMS)_3P$, pointing to a somewhat broader size distribution.[30]

In 2013, TOP was introduced as both a phosphorous source and a stabilizing agent for the synthesis of 8 to 9 nm InP QDs.[63] The reaction involved a transmetalation reaction, in which metallic indium particles – first obtained by the reduction of $InF_3$ by butyllithium – were reacted with TOP. This synthesis is based on previous studies that describe a catalytic cleavage of the P-C bond in TOP by elemental iron or indium NCs.[64] Phosphorous is expected to be released and should diffuse into the metallic NCs to form

metallic phosphide NCs. The authors assumed that the same synthesis pathway could lead to the formation of InP QDs. XRD studies confirmed the high crystallinity of the thus prepared particles, with diffraction peaks corresponding to zincblende InP. However, despite size-selective precipitation, UV-Vis absorption spectra of InP QDs prepared with this method did not show any excitonic features.

### 2.3.4 Aminophosphines

Despite the extensive research on alternative phosphorous precursors, InP QDs produced with $(TMS)_3P$ seem to stand out in terms of narrow size distributions. In addition, the large majority of alternative precursors explored are toxic and difficult to handle, which makes that $(TMS)_3P$ remains the preferable precursor for the synthesis of high quality InP QDs. In 2004, Mastumoto *et al.* were the first to report the use of aminophosphine $P(NMe_2)_3$ as a safer and cheaper phosphorous source for the synthesis of InP QDs.[65] In their protocol, InP QDs were synthesized via the pyrolysis of $InCl_3$ and tris(dimethylamino)phosphine $[P(NMe_2)_3]$ in a mixture of TOP/TOPO at 300 ℃. InP QDs with an average diameter of 6.4 nm were obtained according to TEM, yet they featured a size dispersion of about 50 %. The first improvement was achieved in 2008, when Li *et al.* prepared InP NCs through a one pot solvothermal synthesis using the pyrolysis reaction between $InCl_3$ and $P(NMe_2)_3$ in a mixture of dodecylamine and toluene at rather low temperatures.[66] After size selective precipitation, the as-prepared InP QDs displayed a size distribution of about 10 % and showed a distinguishable absorption feature that could be tuned from the green to red region (see Figure 2.11).

In 2013, Song *et al.* proposed a modified approach for the synthesis of high-quality InP QDs by reacting $P(NMe_2)_3$ with $InCl_3$ through a hot-injection route. In this procedure, $InCl_3$ and $ZnCl_2$ were first dissolved in oleylamine that was used as a coordinating solvent, followed by the injection of $P(NMe_2)_3$ at 220 ℃ to initiate the QD formation. Control experiments were performed by injecting $P(NMe_2)_3$ into a mixture of In and Zn precursors (in the form of either chloride or acetate), myristic acid (or palmitic acid) and ODE, in which case no InP QDs were formed. These experiments highlighted the critical role of oleylamine in this synthesis and a reaction mechanism was hypothesized where the amine supposedly activated $P(NMe_2)_3$ to yield highly reactive phosphine ($PH_3$). This would then react with $InCl_3$, leading to QD nucleation and growth. Depending on the reaction parameters, the resulting NCs presents an excitonic peak tunable from $\approx$ 490 to 600 nm, with a size distribution similar to that obtained with

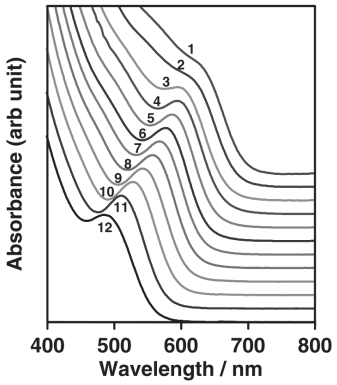


**Figure 2.11:** Absorption spectra of solvothermally synthesized InP NCs after size-selective precipitation. (Reprinted from reference [66]).

$(TMS)_3P$-based approaches (see Figure 2.12b). Hence, at the start of this PhD research, $P(NMe_2)_3$ appeared to be the most promising alternative to $(TMS)_3P$, especially since it is a considerably cheaper chemical that poses no specific safety hazards.

## 2.4 The role of zinc in the synthesis of InP quantum dots

As mentioned in the previous section, Song *et al.* included $ZnCl_2$ next to indium chloride and $P(NMe_2)_3$ in their reaction flask to produce monodisperse InP QDs. Analyzing the role of zinc in their protocol, they found that in absence of zinc chloride, a broader size distribution is obtained with a tail to the lower energy side of the first exciton transition as seen from UV-Vis absorption spectra (see Figure 2.12a). On the other hand, the use of higher Zn:In ratios resulted in a blue shift and more narrow exciton feature as compared to InP QDs synthesized without zinc chloride (see Figure 2.12b-c). Therefore, the authors conclude by XPS analysis that the zinc species could stabilize the particle surface, reduce the size of the nuclei and thus ensure a narrow size distribution.

Several groups have discussed the influence of zinc salts added to the reaction mixture on the optical properties of the InP QDs formed. Depending on the reaction condition, zinc salts were found to act either as a ligand that passivates the outer surface of InP QDs or as precursor leading to (In,Zn)P alloyed nanocrystals. In the case of $(TMS)_3P$-based synthesis, the group of

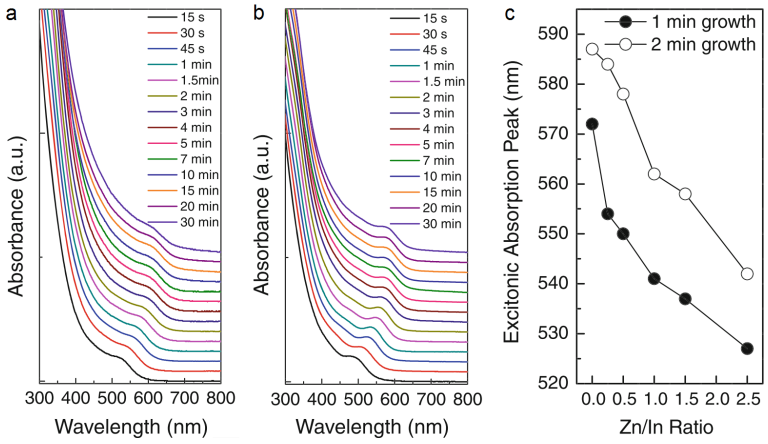


**Figure 2.12:** Temporal evolutions of absorption spectra of InP QDs synthesized with Zn:In molar ratios of **(a)** 0, **(b)** 1.5. **(c)** Changes of excitonic absorption peak wavelengths of 1 and 2 min-grown InP QDs synthesized under different Zn:In ratios from 0 to 2.5. (Reprinted from reference[67]).

Nann was the first to introduce zinc salts as a co-reagent in the initial reaction mixture of InP QDs synthesis.[68] In this method, highly luminescent InP NCs were obtained by reacting $InCl_3$ and $(TMS)_3P$ in octadecene (ODE) in the presence of zinc undecylenate and hexadecylamine. It was expected that the zinc ions could replace the indium ion on the indium rich surface of InP QDs. As a consequence, zinc could play a role in removing surface dangling bonds and improving the PLQY of the InP QDs. In addition, the authors explained that zinc carboxylates show little tendency to react with phosphorous, which could avoid the formation of an (In,Zn)P alloy. In this respect, the strong electron donating properties of hexadecylamine together with zinc carboxylates can account for the enhanced photoluminescence efficiency of InP QDs, that could be as high as 30 %. A confirmation of this surface passivation mechanism was found in the decrease of the PLQY, dropping to a mere 1-5 %, when InP QDs were synthesized with a deficiency of hexadecylamine or zinc carboxylate. In addition, XPS analysis confirmed the presence of zinc at the surface of the InP QDs.

Other groups noticed the beneficial effect of adding zinc salts during the preparation of InP QDs. Without the use of zinc stearate, Li *et al.* obtained InP QDs with a PLQY of only 0.2 %, whereas a reaction performed with an In:Zn ratio of 1:1 resulted in InP QDs with a PLQY of up to 21 %.[69] This was again explained as an effect of the improved surface passivation of the phosphorous dangling bonds by zinc carboxylates, similar to the

work of Xu *et al.*[68] A similar observation was made when zinc acetate was added to a mixture containing InP QDs previously synthesized with indium acetate, $(TMS)_3P$, and palmitic acid.[70] The release of acetic acid by the reaction of zinc acetate and palmitic acid was expected to etch the particle surface and improve the quantum yield of InP QDs. Evidence of this etching occuring was found in the blue-shift of the InP absorption when the Zn:P ratio was increased. This was further confirmed by the slight increase of the PLQY when zinc acetylacetonate was used instead of zinc acetate, which contrasted with the more than two-fold increase in PLQY obtained by additional injections of acetic acid.

Several groups used detailed investigations into the internal structure of InP QDs to explain the possible role of zinc salts in the synthesis of InP QDs.[71–73] Using time-resolved PL spectroscopy and XRD, Thuy *et al.* demonstrated that the improved optical properties of InP QDs synthesized in the presence of Zn where due to the formation of an (In,Zn)P alloy rather than an enhanced surface passivation.[72] Further studies corroborated the ability of zinc to produce (In,Zn)P alloyed nanocrystals.[71] Using a combination of inductively coupled plasma optical emission spectrometry (ICP-OES), XRD and XPS, Pietra *et al.* showed that $Zn^{2+}$ can replace $In^{3+}$ to form an alloyed (In,Zn)P core. In addition, increasing the Zn:In ratio up to 1.5 resulted in a systematic blue shift of the exciton peak (see Figure 2.13a-b). This change is explained, in correlation with TEM ananlysis, by the increased band gap of (In,Zn)P as compared to bulk InP. At the same time, the PLQY of the as-formed QDs increased from less than 1 % for pure InP QDs to about 20 % for (In,Zn)P QDs synthesized with a Zn:In ratio of 1.5 (see Figure 2.13c). In addition, a study on the effect of zinc carboxylates on the structural and optical properties of red-emitting InP QDs was proposed by Xi *et al.*[73] In this case, XPS studies showed that most of the Zn was present in the phosphate layer on the QD surface rather than in the core of the InP QDs. No evidence was found of the formation of (In,Zn)P alloys, although the PLQY of the formed InP QDs in the presence of zinc increased significantly as compared to pure InP QDs.

The beneficial role of zinc salts was also observed in the case of aminophopshine based syntheses. As previously mentioned, Song *et al.* obtained more narrow size distributions when zinc chloride was included in the initial reaction mixture.[67]. Further studies also demonstrated that zinc chloride can influence the shape of the resulting InP NCs.[74] Using a similar synthesis approach as Song *et al.*, the group of Heong synthesized InP QDs with a tetrahedral shape by removing the zinc chloride during an aminophosphine-based InP QDs synthesis. In their protocol, $InCl_3$ was reacted with $P(NMe_2)_3$ in

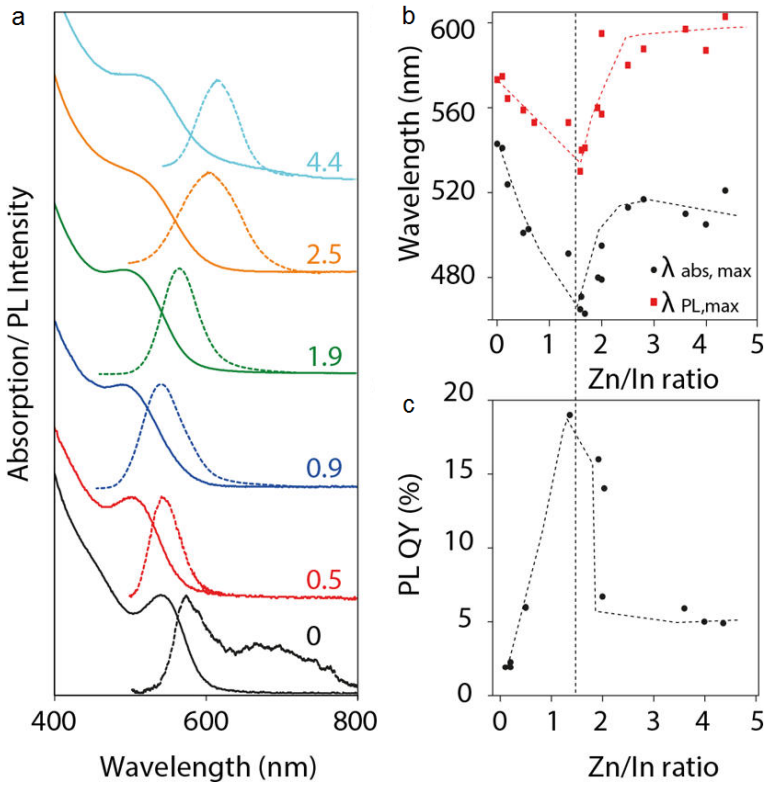


**Figure 2.13:** **(a)** Normalized absorption and PL spectra of $In_xZn_y$ QDs. Except for a variable Zn:In ratio, all other synthesis conditions were identical. **(b)** Plot of $\lambda_{Abs,max}$ (nm) for the absorption (black dots) and PL emission (red squares) wavelengths as a function of the Zn:In molar ratio obtained by ICP(OES) analysis. Dashed lines represent a guide to the eye. **(c)** Plot of the PLQY (%) of $In_xZn_y$ QDs as a function of the Zn:In molar ratio obtained by ICP(OES) elemental analysis. (Reprinted from reference [71]).

the presence of oleylamine at elevated temperature. TEM analysis of the resulting nanocrystals showed that tetrahedrally shaped InP nanocrystals were formed, whereas more spherical nanocrystals were obtained with Song's protocol. Chemical analysis indicated that these tetrahedrally shaped InP nanocrystals were stabilized by both oleylamine and chloride. It thus appears that including zinc salts in the reaction mixture used to form InP QDs can have several beneficial effects, which include a reduction of density of surface traps and an improved particle size distribution. In addition, the

presence of Zn can facilitate the formation of (In,Zn)P alloys, which often show an enhanced PLQY.

## 2.5 Core/shell InP-based quantum dots: towards luminescent particles

Despite the increased PLQY that results from including zinc salts in the reaction mixture, core InP QDs generally exhibit a low PLQY and suffer from pronounced photo-oxidation upon air exposure.[30;33] As seen in the introduction, coating a core nanocrystal with a wider band gap semiconductor to form a core/shell heteronanostructure can improve both the PLQY and the photo and chemical stability of the QDs. Specific semiconductor shell materials can be used, where the optimal choice depends on their band gap, band offsets, crystal structure and lattice parameter with respect to the InP core QDs.[75] A type I structure is generally preferred to increase the PLQY as it results in a better confinement of the charge carriers within the core. This makes that InP/ZnS[34;68;69;76] and InP/ZnSe[77] are the most synthesized core/shell structure, since they have such a type I band alignment in combination with a zincblende crystal structure that has limited mismatch with InP.

The group of Weller was the first to propose a ZnS shell coating on top of InP core QDs.[76] The authors noted that InP/ZnS QDs had a PLQY of up to 23 %, which corresponded in their case to a 73 fold enhancement as compared to the original InP core QDs. Improved protocols were proposed for the production of InP/ZnS QDs with a PLQY of up to 50-70 % and narrow emission linewidth between 40-60 nm.[68;69]. However TEM investigations of the as formed particles suggested that only shallow ZnS shell were formed, often being less than 1 nm thick.[1] This might be due to the relatively high lattice mismatch of 7.7 % between the InP core and the ZnS shell material, which hindered a proper epitaxial growth of ZnS on InP.[75] Other explanations of this limited growth of ZnS could be the formation of an oxide layer at the core/shell interface. Several studies have shown that carboxylic acids or amine used in $(TMS)_3P$-based synthesis can lead to the production of water that form an oxidized layer at the surface of the InP nanocrystals during synthesis.[78;79]

To obtain thicker coatings, materials with a reduced lattice mismatch relative to InP have been explored as possible shell materials. Micic *et al.* investigated the formation of lattice matched InP/$Zn_{50}Cd_{50}Se$ QDs. However, despite a shell thickness of up to 5 nm, the PLQY of these heteronanocrys-

tals remained low, at 5-10 %.[80] Other groups made use of (In,Zn)P alloyed nanocrystals with a tunable lattice constant to reduce strain when growing ZnS or Zn(Se,S) shells that are lattice matched to the (In,Zn)P cores. Such approaches attained PLQYs of up to 70 % with emission line of $\approx$ 50 nm wide.[71;72] Alternative approaches to reduce the lattice mismatch at the core-shell interface were proposed by using ZnSe as an intermediate layer, based on its lower lattice mismatch (3.3 %) with respect to InP.[81–84] This resulted in the formation of InP/ZnSe/ZnS or InP/Zn(Se,S) core/shell QDs with a thick shell, a PLQY as high as 70-80 % and emission linewidths of 45-50 nm.[81;82;84]. Another system involved the growth of a GaP intermediate layer on top of InP core QDs. Despite a lattice mismatch of 7 % with InP, thus formed InP/GaP/ZnS core/shell QDs could attain a PLQY of up to 85 % and display an improved photostability as compared to InP/ZnS QDs.[85]

## 2.6 Conclusion

In the last 20 years, numerous studies have addressed the synthesis of InP QDs as an alternative to CdSe QDs, which are subjected to regulatory constraints owing to the toxicity of cadmium. In particular, great improvements have been achieved in term of synthesis protocols that allow for the production of InP QDs with a narrow size distribution. Researchers still strive to improve synthesis methods since at the time of writing this manuscript, new promising protocols based-on elemental phosphorous and $(TMS)_3P$ have been published. The former enables the synthesis of high-quality InP/ZnS QDs of up to 6 g per one-batch reaction,[86] while the latter reports the synthesis of green-emitting InP/ZnSe/ZnS QDs with a size distribution as low as 36 nm.[87] This has been accomplished by careful studies where various aspects, such as the appropriate precursor or reactions conditions, were analysed in view of attaining the highest quality InP QDs. Moreover, the formation of specific core/shell structures has allowed to obtain InP QDs with a photoluminescence quantum yield that approaches that of CdSe-based QDs. In this respect, industry has started to use InP-based QDs as alternative color converters into QD-enhanced products, in particular in QD-based liquid crystal displays. Still, most reports on the synthesis of InP QDs involve the use of the hazardous and expensive $(TMS)_3P$ phosphorous, which poses several drawbacks in view of large scale production. Recently, promising alternatives, notably $P(NMe_2)_3$ have been proposed as cheaper and less toxic phosphorous precursors for the synthesis of InP QDs. These comounds have been shown to lead to high quality InP QDs, comparable to what is obtained with protocols involving $(TMS)_3P$ precursor. Neverthe-

less, no studies have addressed the basic properties of this reaction, such as its chemical yield, the possibility for effective size tuning, and, probably more challenging, the actual reaction mechanism. This analysis formed the starting point of the work done within the framework of this PhD.

# References

[1] Sudarsan Tamang, Christophe Lincheneau, Yannick Hermans, Sohee Jeong, and Peter Reiss. *Chemistry of InP Nanocrystal Syntheses.* Chemistry of Materials, 28(8):2491–2506, 2016.

[2] S. B. Brichkin. *Synthesis and properties of colloidal indium phosphide quantum dots.* Colloid Journal, 77(4):393–403, Jul 2015.

[3] P. Mushonga, M. O. Onani, A. M. Madiehe, and M. Meyer. *Indium Phosphide-Based Semiconductor Nanocrystals and Their Applications.* Journal of Nanomaterials, 2012, 2012.

[4] Benoit Dubertret, Paris Skourides, David J. Norris, Vincent Noireaux, Ali H. Brivanlou, and Albert Libchaber. *In Vivo Imaging of Quantum Dots Encapsulated in Phospholipid Micelles.* Science, 298(5599):1759–1762, 2002.

[5] S. A. McDonald, G. Konstantatos, S. Zhang, P. W. Cyr, E. J. Klem, L. Levina, and E. H. Sargent. *Solution-processed PbS quantum dot infrared photodetectors and photovoltaics.* Nature Materials, 4(2):138–42, 2005.

[6] S. Coe, W. K. Woo, M. Bawendi, and V. Bulovic. *Electroluminescence from single monolayers of nanocrystals in molecular organic devices.* Nature, 420(6917):800–803, 2002.

[7] Nir Tessler, Vlad Medvedev, Miri Kazes, ShiHai Kan, and Uri Banin. *Efficient Near-Infrared Polymer Nanocrystal Light-Emitting Diodes.* Science, 295(5559):1506–1508, 2002.

[8] Virgilio Brunetti, Hicham Chibli, Roberto Fiammengo, Antonio Galeone, Maria Ada Malvindi, Giuseppe Vecchio, Roberto Cingolani, Jay L. Nadeau, and Pier Paolo Pompa. *InP/ZnS as a safer alternative to CdSe/ZnS core/shell quantum dots: in vitro and in vivo toxicity assessment.* Nanoscale, 5(1):307–317, 2013.

[9] Kenichi Oda. *Toxicity of a Low Level of Indium Phosphide (InP) in Rats after Intratracheal Instillation.* Industrial Health, 35(1):61–68, 1997.

[10] Hicham Chibli, Lina Carlini, Soonhyang Park, Nada M. Dimitrijevic, and Jay L. Nadeau. *Cytotoxicity of InP/ZnS quantum dots related to reactive oxygen species generation.* Nanoscale, 3(6):2552–2559, 2011.

[11] Guimiao Lin, Qingling Ouyang, Rui Hu, Zhangchi Ding, Jinglin Tian, Feng Yin, Gaixia Xu, Qiang Chen, Xiaomei Wang, and Ken-Tye Yong. *In vivo toxicity assessment of non-cadmium quantum dots in BALB/c mice.* Nanomedicine: Nanotechnology, Biology and Medicine, 11(2):341–350, 2015.

[12] Ayabei Kiplagat, Nicole R. S. Sibuyi, Martin O. Onani, Mervin Meyer, and Abram M. Madiehe. *The cytotoxicity studies of water-soluble InP/ZnSe quantum dots.* Journal of Nanoparticle Research, 18(6):147, 2016.

[13] J. Cui, A. P. Beyler, L. F. Marshall, O. Chen, D. K. Harris, D. D. Wanger, X. Brokmann, and M. G. Bawendi. *Direct probe of spectral inhomogeneity reveals synthetic tunability of single-nanocrystal spectral linewidths.* Nature Chemistry, 5(7):602–606, 2013.

[14] James R. Heath. *Covalency in semiconductor quantum dots.* Chemical Society Reviews, 27(1):65–71, 1998.

[15] L. E. Brus. *Electron–electron and electron-hole interactions in small semiconductor crystallites: The size dependence of the lowest excited electronic state.* The Journal of Chemical Physics, 80(9):4403–4409, 1984.

[16] Richard L. Wells, Colin G. Pitt, Andrew T. McPhail, Andrew P. Purdy, Soheila Shafieezad, and Robert B. Hallock. *The use of tris(trimethylsilyl)arsine to prepare gallium arsenide and indium arsenide.* Chemistry of Materials, 1(1):4–6, 1989.

[17] Matthew D. Healy, Paul E. Laibinis, Paul D. Stupik, and Andrew R. Barron. *The reaction of indium(III) chloride with tris(trimethylsilyl)phosphine: a novel route to indium phosphide.* Journal of the Chemical Society, Chemical Communications, (6):359–360, 1989.

[18] Richard L. Wells, Steven R. Aubuchon, Shreyas S. Kher, Michael S. Lube, and Peter S. White. *Synthesis of Nanocrystalline Indium Arsenide and Indium Phosphide from Indium(III) Halides and Tris(trimethylsilyl)pnicogens. Synthesis, Characterization, and Decomposition Behavior of $I_3In{\cdot}P(SiMe_3)_3$.* Chemistry of Materials, 7(4):793–800, 1995.

[19] Olga I. Micic, Calvin J. Curtis, Kim M. Jones, Julian R. Sprague, and Arthur J. Nozik. *Synthesis and Characterization of InP Quantum Dots.* The Journal of Physical Chemistry, 98(19):4966–4969, 1994.

[20] C. B. Murray, D. J. Norris, and M. G. Bawendi. *Synthesis and characterization of nearly monodisperse CdE (E = sulfur, selenium, tellurium) semiconductor nanocrystallites.* Journal of the American Chemical Society, 115(19):8706–8715, 1993.

[21] O. I. Mićić and A. J. Nozik. *Synthesis and characterization of binary and ternary III–V quantum dots.* Journal of Luminescence, 70(1):95–107, 1996.

[22] O. I. Micic, J. R. Sprague, C. J. Curtis, K. M. Jones, J. L Machol, A. J. Nozik, H. Giessen, B. Fluegel, G. Mohs, and N. Peyghambarian. *Synthesis and Characterization of InP, GaP, and $GaInP_2$ Quantum Dots.* The Journal of Physical Chemistry, 99(19):7754–7759, 1995.

[23] A. A. Guzelian, J. E. B. Katari, A. V. Kadavanich, U. Banin, K. Hamad, E. Juban, A. P. Alivisatos, R. H. Wolters, C. C. Arnold, and J. R. Heath. *Synthesis of Size-Selected, Surface-Passivated InP Nanocrystals.* The Journal of Physical Chemistry, 100(17):7212–7219, 1996.

[24] M. Tomaselli, J. L. Yarger, M. Bruchez Jr., R. H. Havlin, D. deGraw, A. Pines, and A. P. Alivisatos. *NMR study of InP quantum dots: Surface structure and size effects.* The Journal of Chemical Physics, 110(18):8861–8864, 1999.

[25] Zeger Hens, Iwan Moreels, and Jose C. Martins. *In Situ $^1H$ NMR Study on the Trioctylphosphine Oxide Capping of Colloidal InP Nanocrystals.* ChemPhysChem, 6(12):2578–2584, 2005.

[26] Iwan Moreels, Jose C. Martins, and Zeger Hens. *Ligand Adsorption/Desorption on Sterically Stabilized InP Colloidal Nanocrystals: Observation and Thermodynamic Analysis.* ChemPhysChem, 7(5):1028–1031, 2006.

[27] Olga I. Mićić, S. P. Ahrenkiel, and Arthur J. Nozik. *Synthesis of extremely small InP quantum dots and electronic coupling in their disordered solid films.* Applied Physics Letters, 78(25):4022–4024, 2001.

[28] Dmitri V Talapin, Andrey L Rogach, Ivo Mekis, Stephan Haubold, Andreas Kornowski, Markus Haase, and Horst Weller. *Synthesis and surface modification of amino-stabilized CdSe, CdTe and InP nanocrystals.* Colloids and Surfaces A: Physicochemical and Engineering Aspects, 202(2):145–154, 2002.

[29] Trevor. Douglas and Klaus H. Theopold. *Molecular precursors for indium phosphide and synthesis of small III-V semiconductor clusters in solution.* Inorganic Chemistry, 30(4):594–596, 1991.

[30] David Battaglia and Xiaogang Peng. *Formation of High Quality InP and InAs Nanocrystals in a Noncoordinating Solvent.* Nano Letters, 2(9):1027–1030, 2002.

[31] Lianhua Qu and Xiaogang Peng. *Control of Photoluminescence Properties of CdSe Nanocrystals in Growth.* Journal of the American Chemical Society, 124(9):2049–2055, 2002.

[32] Xiaogang Peng, J. Wickham, and A. P. Alivisatos. *Kinetics of II-VI and III-V Colloidal Semiconductor Nanocrystal Growth: "Focusing" of Size Distributions.* Journal of the American Chemical Society, 120(21):5343–5344, 1998.

[33] Derrick W. Lucey, David J. MacRae, Madalina Furis, Yudhisthira Sahoo, Alexander N. Cartwright, and Paras N. Prasad. *Monodispersed InP Quantum Dots Prepared by Colloidal Chemistry in a Noncoordinating Solvent.* Chemistry of Materials, 17(14):3754–3762, 2005.

[34] Renguo Xie, David Battaglia, and Xiaogang Peng. *Colloidal InP Nanocrystals as Efficient Emitters Covering Blue to Near-Infrared.* Journal of the American Chemical Society, 129(50):15432–15433, 2007.

[35] Shu Xu, Sandeep Kumar, and Thomas Nann. *Rapid Synthesis of High-Quality InP Nanocrystals.* Journal of the American Chemical Society, 128(4):1054–1055, 2006.

[36] Peter M. Allen, Brian J. Walker, and Moungi G. Bawendi. *Mechanistic Insights into the Formation of InP Quantum Dots.* Angewandte Chemie International Edition, 49(4):760–762, 2010.

[37] Myriam Protiere and Peter Reiss. *Amine-induced growth of an $In_2O_3$ shell on colloidal InP nanocrystals.* Chem. Commun., (23):2417–2419, 2007.

[38] Dylan C. Gary, Benjamin A. Glassy, and Brandi M. Cossairt. *Investigation of Indium Phosphide Quantum Dot Nucleation and Growth Utilizing Triarylsilylphosphine Precursors.* Chemistry of Materials, 26(4):1734–1744, 2014.

[39] S. Joung, S. Yoon, C. S. Han, Y. Kim, and S. Jeong. *Facile synthesis of uniform large-sized InP nanocrystal quantum dots using tris(tert-butyldimethylsilyl)phosphine.* Nanoscale Research Letters, 7(1):93, 2012.

[40] Daniel K. Harris and Moungi G. Bawendi. *Improved Precursor Chemistry for the Synthesis of III–V Quantum Dots.* Journal of the American Chemical Society, 134(50):20211–20213, 2012.

[41] Dylan C. Gary, Maxwell W. Terban, Simon J. L. Billinge, and Brandi M. Cossairt. *Two-Step Nucleation and Growth of InP Quantum Dots via Magic-Sized Cluster Intermediates.* Chemistry of Materials, 27(4):1432–1441, 2015.

[42] Brandi M. Cossairt. *Shining Light on Indium Phosphide Quantum Dots: Understanding the Interplay among Precursor Conversion, Nucleation, and Growth.* Chemistry of Materials, 28(20):7181–7189, 2016.

[43] Dylan C. Gary, Sarah E. Flowers, Werner Kaminsky, Alessio Petrone, Xiaosong Li, and Brandi M. Cossairt. *Single-Crystal and Electronic Structure of a 1.3 nm Indium Phosphide Nanocluster.* Journal of the American Chemical Society, 138(5):1510–1513, 2016.

[44] Lisi Xie, Yi Shen, Daniel Franke, Víctor Sebastián, Moungi G. Bawendi, and Klavs F. Jensen. *Characterization of Indium Phosphide Quantum Dot Growth Intermediates Using MALDI-TOF Mass Spectrometry.* Journal of the American Chemical Society, 138(41):13469–13472, 2016.

[45] Ping Yan, Yi Xie, Wenzhong Wang, Fuyu Liu, and Yitai Qian. *A low-temperature route to InP nanocrystals.* Journal of Materials Chemistry, 9(8):1831–1833, 1999.

[46] Bin Li, Yi Xie, Jiaxing Huang, Yu Liu, and Yitai Qian. *A novel method for the preparation of III–V semiconductors: sonochemical synthesis of InP nanocrystals.* Ultrasonics Sonochemistry, 8(4):331–334, 2001.

[47] Ung Thi Dieu Thuy, Tran Thi Thuong Huyen, Nguyen Quang Liem, and Peter Reiss. *Low temperature synthesis of InP nanocrystals.* Materials Chemistry and Physics, 112(3):1120–1123, 2008.

[48] Shuo Wei, Jun Lu, Liling Zeng, Weichao Yu, and Yitai Qian. *Hydrothermal Synthesis of InP Semiconductor Nanocrystals.* Chemistry Letters, 31(10):1034–1035, 2002.

[49] Shuo Wei, Jun Lu, Weichao Yu, and Yitai Qian. *InP nanocrystals via surfactant-aided hydrothermal synthesis.* Journal of Applied Physics, 95(7):3683–3688, 2004.

[50] Heqing Yang, Wenyan Yin, Hua Zhao, Ruili Yang, and Yuzhe Song. *A complexant-assisted hydrothermal procedure for growing well-dispersed InP nanocrystals.* Journal of Physics and Chemistry of Solids, 69(4):1017–1022, 2008.

[51] Ki-Won Jun, P.K. Khanna, Ki-Bum Hong, Jin-Ook Baeg, and Yung-Doug Suh. *Synthesis of InP nanocrystals from indium chloride and sodium phosphide by solution route.* Materials Chemistry and Physics, 96(2):494–497, 2006.

[52] P.K. Khanna, M.-S. Eum, Ki-Won Jun, Jin-Ook Baeg, and Sang Il Seok. *A novel synthesis of indium phosphide nanoparticles.* Materials Letters, 57(30):4617–4621, 2003.

[53] Zhengrong Li and Dominick J. Casadonte. *Facile sonochemical synthesis of nanosized InP and GaP.* Ultrasonics Sonochemistry, 14(6):757–760, 2007.

[54] Sophie Carenco, Matthieu Demange, Jing Shi, Cedric Boissiere, Clement Sanchez, Pascal Le Floch, and Nicolas Mezailles. *White phosphorus and metal nanoparticles: a versatile route to metal phosphide nanoparticles.* Chemical Communications, 46(30):5578–5580, 2010.

[55] Shanmin Gao, Jun Lu, Nan Chen, Yan Zhao, and Yi Xie. *Aqueous synthesis of III-V semiconductor GaP and InP exhibiting pronounced quantum confinement.* Chemical Communications, (24):3064–3065, 2002.

[56] Liang Li and Peter Reiss. *One-pot Synthesis of Highly Luminescent InP/ZnS Nanocrystals without Precursor Injection.* Journal of the American Chemical Society, 130(35):11588–11589, 2008.

[57] Alexander A. Vinokurov, Sergey G. Dorofeev, Konstantin O. Znamenkov, Anastasia V. Panfilova, and Tatiana A. Kuznetsova. *Synthesis of InP quantum dots in dodecylamine from phosphine and indium(III) chloride.* Mendeleev Communications, 20(1):31–32, 2010.

[58] Feng Zan and Jicun Ren. *Gas-liquid phase synthesis of highly luminescent InP/ZnS core/shell quantum dots using zinc phosphide as a new phosphorus source.* Journal of Materials Chemistry, 22(5):1794–1799, 2012.

[59] Grzegorz Gabka, Klaudyna Leniarska, Andrzej Ostrowski, Karolina Malinowska, Lukasz Skorka, Mikolaj Donten, and Piotr Bujak. *Effect of indium precursor and ligand type on the structure, morphology*

*and surface functionalization of InP nanocrystals prepared by gas–liquid approach.* Synthetic Metals, 187:94–101, 2014.

[60] Natalia Mordvinova, Alexander Vinokurov, Sergey Dorofeev, Tatiana Kuznetsova, and Konstantin Znamenkov. *Phosphine synthetic route features and postsynthetic treatment of InP quantum dots.* Journal of Alloys and Compounds, 582(Supplement C):43 – 49, 2014.

[61] Mark Green and Paul O'Brien. *A novel metalorganic route for the direct and rapid synthesis of monodispersed quantum dots of indium phosphide.* Chemical Communications, pages 2459–2460, 1998.

[62] Zhaoping Liu, Amar Kumbhar, Dan Xu, Jun Zhang, Zhaoyong Sun, and Jiye Fang. *Coreduction Colloidal Synthesis of III–V Nanocrystals: The Case of InP.* Angewandte Chemie, 120(19):3596–3598, 2008.

[63] Jannika Lauth, Tim Strupeit, Andreas Kornowski, and Horst Weller. *A Transmetalation Route for Colloidal GaAs Nanocrystals and Additional III–V Semiconductor Materials.* Chemistry of Materials, 25(8):1377–1383, 2013.

[64] P.K. Khanna, Ki-Won Jun, Ki Bum Hong, Jin-Ook Baeg, and G.K. Mehrotra. *Synthesis of indium phosphide nanoparticles via catalytic cleavage of phosphorus carbon bond in n-trioctylphosphine by indium.* Materials Chemistry and Physics, 92(1):54–58, 2005.

[65] Taichi Matsumoto, Shinya Maenosono, and Yukio Yamaguchi. *Organometallic Synthesis of InP Quantum Dots Using Tris(dimethylamino)phosphine as a Phosphorus Source.* Chemistry Letters, 33(11):1492–1493, 2004.

[66] Liang Li, Myriam Protière, and Peter Reiss. *Economic Synthesis of High Quality InP Nanocrystals Using Calcium Phosphide as the Phosphorus Precursor.* Chemistry of Materials, 20(8):2621–2623, 2008.

[67] Woo-Seuk Song, Hye-Seung Lee, Ju Chul Lee, Dong Seon Jang, Yoonyoung Choi, Moongoo Choi, and Heesun Yang. *Amine-derived synthetic approach to color-tunable InP/ZnS quantum dots with high fluorescent qualities.* Journal of Nanoparticle Research, 15(6):1750, 2013.

[68] Shu Xu, Jan Ziegler, and Thomas Nann. *Rapid synthesis of highly luminescent InP and InP/ZnS nanocrystals.* Journal of Materials Chemistry, 18(23):2653–2656, 2008.

[69] Chunliang Li, Masanori Ando, and Norio Murase. *Facile Preparation of Highly Luminescent InP Nanocrystals by a Solvothermal Route.* Chemistry Letters, 37(8):856–857, 2008.

[70] Euidock Ryu, Sungwoo Kim, Eunjoo Jang, Shinae Jun, Hyosook Jang, Byungki Kim, and Sang-Wook Kim. *Step-Wise Synthesis of InP/ZnS Core–Shell Quantum Dots and the Role of Zinc Acetate.* Chemistry of Materials, 21(4):573–575, 2009.

[71] Francesca Pietra, Luca De Trizio, Anne W. Hoekstra, Nicolas Renaud, Mirko Prato, Ferdinand C. Grozema, Patrick J. Baesjou, Rolf Koole, Liberato Manna, and Arjan J. Houtepen. *Tuning the Lattice Parameter of $In_xZn_yP$ for Highly Luminescent Lattice-Matched Core/Shell Quantum Dots.* ACS Nano, 10(4):4754–4762, 2016.

[72] Ung Thi Dieu Thuy, Peter Reiss, and Nguyen Quang Liem. *Luminescence properties of In(Zn)P alloy core/ZnS shell quantum dots.* Applied Physics Letters, 97(19):193104, 2010.

[73] Lifei Xi, Deok-Yong Cho, Astrid Besmehn, Martial Duchamp, Detlev Grützmacher, Yeng Ming Lam, and Beata E. Kardynał. *Effect of Zinc Incorporation on the Performance of Red Light Emitting InP Core Nanocrystals.* Inorganic Chemistry, 55(17):8381–8386, 2016.

[74] Kyungnam Kim, Dongsuk Yoo, Hyekyoung Choi, Sudarsan Tamang, Jae-Hyeon Ko, Sungwoo Kim, Yong-Hyun Kim, and Sohee Jeong. *Halide–Amine Co-Passivated Indium Phosphide Colloidal Quantum Dots in Tetrahedral Shape.* Angewandte Chemie International Edition, 55(11):3714–3718, 2016.

[75] Peter Reiss, Myriam Protière, and Liang Li. *Core/Shell Semiconductor Nanocrystals.* Small, 5(2):154–168, 2009.

[76] Stephan Haubold, Markus Haase, Andreas Kornowski, and Horst Weller. *Strongly Luminescent InP/ZnS Core–Shell Nanoparticles.* ChemPhysChem, 2(5):331–334, 2001.

[77] Mee Rahn Kim, Jae Hun Chung, Mihee Lee, Seonghoon Lee, and Du-Jeon Jang. *Fabrication, spectroscopy, and dynamics of highly luminescent core–shell InP@ZnSe quantum dots.* Journal of Colloid and Interface Science, 350(1):5–9, 2010.

[78] Arnaud Cros-Gagneux, Fabien Delpech, Céline Nayral, Alfonso Cornejo, Yannick Coppel, and Bruno Chaudret. *Surface Chemistry of InP Quantum Dots: A Comprehensive Study.* Journal of the American Chemical Society, 132(51):18147–18157, 2010.

[79] Héloïse Virieux, Marianne Le Troedec, Arnaud Cros-Gagneux, Wilfried-Solo Ojo, Fabien Delpech, Céline Nayral, Hervé Martinez, and Bruno Chaudret. *InP/ZnS Nanocrystals: Coupling NMR and XPS for Fine Surface and Interface Description.* Journal of the American Chemical Society, 134(48):19701–19708, 2012.

[80] Olga I. Mićić, Barton B. Smith, and Arthur J. Nozik. *Core–Shell Quantum Dots of Lattice-Matched $ZnCdSe_2$ Shells on InP Cores: Experiment and Theory.* The Journal of Physical Chemistry B, 104(51):12149–12156, 2000.

[81] Jaehoon Lim, Wan Ki Bae, Donggu Lee, Min Ki Nam, Joohyun Jung, Changhee Lee, Kookheon Char, and Seonghoon Lee. *InP@ZnSeS, Core@Composition Gradient Shell Quantum Dots with Enhanced Stability.* Chemistry of Materials, 23(20):4459–4463, 2011.

[82] Christian Ippen, Tonino Greco, and Armin Wedel. *InP/ZnSe/ZnS: A Novel Multishell System for InP Quantum Dots for Improved Luminescence Efficiency and Its application in a Light-Emitting Device.* Journal of Information Display, 13(2):91–95, 2012.

[83] Kyungnam Kim, Hangyeoul Lee, Jaewook Ahn, and Sohee Jeong. *Highly luminescing multi-shell semiconductor nanocrystals InP/ZnSe/ZnS.* Applied Physics Letters, 101(7):073107, 2012.

[84] Jaehoon Lim, Myeongjin Park, Wan Ki Bae, Donggu Lee, Seonghoon Lee, Changhee Lee, and Kookheon Char. *Highly Efficient Cadmium-Free Quantum Dot Light-Emitting Diodes Enabled by the Direct Formation of Excitons within InP@ZnSeS Quantum Dots.* ACS Nano, 7(10):9019–9026, 2013.

[85] Sungwoo Kim, Taehoon Kim, Meejae Kang, Seong Kwon Kwak, Tae Wook Yoo, Lee Soon Park, Ilseung Yang, Sunjin Hwang, Jung Eun Lee, Seong Keun Kim, and Sang-Wook Kim. *Highly Luminescent InP/GaP/ZnS Nanocrystals and Their Application to White Light-Emitting Diodes.* Journal of the American Chemical Society, 134(8):3804–3809, 2012.

[86] Eunbyul Bang, Yonghoon Choi, Jinhee Cho, Yo-Han Suh, Hyeong Woo Ban, Jae Sung Son, and Jongnam Park. *Large-Scale Synthesis of Highly Luminescent InP@ZnS Quantum Dots Using Elemental Phosphorus Precursor.* Chemistry of Materials, 29(10):4236–4243, 2017.

[87] Parthiban Ramasamy, Nayeon Kim, Yeon-Su Kang, Omar Ramirez, and Jong-Soo Lee. *Tunable, Bright, and Narrow-Band Luminescence*

*from Colloidal Indium Phosphide Quantum Dots.* Chemistry of Materials, 29(16):6893–6899, 2017.

# 3

# Mechanistic Insight into Economical Synthesis of Indium Phosphide-Based Quantum Dots[1,2]

*We present synthesis protocols, based on indium chloride and aminophosphine precusors, that allow for the economic, up-scaled production of indium phosphide quantum dots (InP QDs). The reactions attain a close to full yield conversion with respect to the indium precursor. In addition, investigation of the chemical reactions leading to InP formation starting from $InCl_3$ and tris(dialkylamino)phosphines, is presented. Nuclear magnetic resonance spectroscopy, mass spectrometry and single crystal X-ray diffraction are used to demonstrate that the aminophosphine is both precursor and reducing agent.*

[1] *Adapted from:* Mickaël D. Tessier, **Dorian Dupont**, Kim De Nolf, Jonathan De Roo, Zeger Hens. *Economic and Size-Tunable Synthesis of InP/ZnE (E = S, Se) Colloidal Quantum Dots.* Chemistry of Materials, 27(13):4893-4898, **2015**.

[2] *Adapted from:* Mickaël D. Tessier, Kim De Nolf, **Dorian Dupont**, Davy Sinnaeve, Jonathan De Roo, Zeger Hens. *Aminophosphines: a Double Role in the Synthesis of Colloidal Indium Phosphide Quantum Dots.* Journal of the American Chemical Society, 138(18):5923-5929, **2016**.

## 3.1 Introduction

As mentioned in chapter 2, an innovative and potentially efficient alternative to make InP QDs was proposed by Song *et al.* in 2013.[1] These authors use $P(NEt_2)_3$ as a phosphorous precursor. As compared to $(TMS)_3P$, aminophosphines are inexpensive precursors that are safe-to-use under ambient conditions and proved to lead to InP QDs of comparable quality as the best samples obtained with $(TMS)_3P$.[2;3] To further improve on the result of a given QD synthesis, achieve size control and minimize size dispersions, insights in the reaction mechanism were used since the early days of Cd-based QD syntheses.[4] By now, several QD synthesis methods have been shown to follow a two-step process where the injected precursors first react to form the solute or monomer whose increasing concentration subsequently gives rise to nucleation and growth of nanocrystals.[5–7] In this respect, mechanistic studies have addressed both the chemical reactions involved in monomer formation and the relation between the monomer formation rate and the size of the resulting nanocrystals.[8–11] Especially in the case of CdSe QDs synthesized using trioctylphosphine selenide (TOP-Se), precursor conversion was investigated in great detail and found to consist of two essential steps, *i.e.*, a coordination of TOP-Se to the Cd center, followed by the cleavage of the Se=P bond. Moreover, this precursor conversion was found to be limiting the overall rate of CdSe formation.[11] This finding not only resulted in several size tuning strategies,[8–10] it also indicates that a controlled synthesis of nanocrystals will only be possible if the precursor conversion is slow as compared to the nucleation and growth of the nanocrystals proper.

Importantly, such studies are shifting synthesis development from a semiemperical trial-and-error approach to a more rational design of synthesis protocols that allows for optimal control of the QD size and size dispersion. A recent and most striking example involves the formation of lead sulfide QDs from thiourea precursors where insight in the relation between reaction rate and nanocrystal size was implemented to achieve size control at full reaction yield over a broad range of nanocrystal diameters.[12] In the case of $(TMS)_3P$-based synthesis protocols for InP QDs, different mechanistic studies showed that precursor conversion is complete upon injection,[13;14] resulting in ripening-driven nanocrystal growth. Although this was linked to the difficulty of synthesizing monodisperse InP QDs, the use of substituted silylphosphines with a lower reactivity did not overcome this problem.[15] In the case of aminophosphine precursors on the other hand, the chemistry of the conversion reaction is not yet understood. This, however, is crucial to further optimize the reaction and extend it to the synthesis of other metal phosphide and metal arsenide nanocrystals.

In this chapter, we take the method published by Song *et al.* as a starting point to develop an InP synthesis protocol that combines economic feasibility with state-of-the art optical properties.[1] We confirm that InP can be formed by combination of $InCl_3$ and P(amino)$_3$ (amino = dimethylamino [$NMe_2$], diethylamino [$NEt_2$]) as the respective indium and phosphorous precursor. In addition, we find that the conversion yield depends on the P:In molar ratio of the precursors. About full conversion of the indium precursor is achieved for P:In ratios exceeding 4. Several key aspects that govern the formation of InP from aminophosphine precursors and indium chloride in the presence of primary amines are identified. First, it is shown that the reaction involves the substitution of the original amino groups by amines present in the reaction mixture, where only transamination with primary amines leads to InP formation. Furthermore, it was found that the substituted aminophosphine has a double role in the reaction, both serving as the phosphorous precursor and the reducing agent by the formation of $P^V$ phosphonium salt. These findings are summarized in a chemical reaction mechanism that may help using this unique precursor chemistry for the formation of, *e.g.*, GaP, InAs or GaAs nancrystals. These have proven even more challenging than InP to synthesize as nanocrystals, with synthesis methods suffering from poor size dispersions[16] or requiring extremely hazardous precursors.[17;18]

## 3.2 Experimental section

**Chemicals:** Indium(III) chloride (99.999 %), zinc(II) chloride ($\geq$ 98 %), dodecylamine (99 %), P($NMe_2$)$_3$ (97 %), P($NEt_2$)$_3$ (97 %) were purchased from Sigma Aldrich. Oleylamine (80-90 %) was purchased from Acros Organics (NB: Oleylamine is stored under inert atmosphere).

**Full chemical yield synthesis of 3.2 nm InP QDs (first excitonic absorption peak at 560 nm):** 100 mg (0.45 mmol) of indium(III) chloride, as indium raw materials and 300 mg (2.2 mmol) of zinc(II) chloride, as zinc raw materials are mixed in 5.0 mL (15 mmol) of technical oleylamine which is a coordinating solvent. The reaction mixture is stirred and degassed at 120 ℃ for an hour and then heated to 180 ℃ under inert atmosphere. Upon reaching 180 ℃, a volume of 0.45 mL (1.6 mmol) of P($NMe_2$)$_3$ (phosphorous:indium ratio = 3.6:1) are quickly injected in the above mixture. After the phosphorous precursor injection, the InP nanocrystals synthesis proceeded. The reaction occurs during 20 min. At the end of the reaction, the temperature is cooled down. InP nanocrystals are then precipitated in ethanol and suspended in tolune.

**Mass spectrometry:** InP core QDs are synthesized and precipitated with methanol. The supernatant is analyzed using a 6230 TOF-MS with ESI-source mass spectrometer of Agilent Technologies in a range from 55 to 1160 g.mol$^{-1}$.

**NMR spectroscopy:** Aliquots of 40-100 $\mu$L are taken from a synthesis and put into vials containing inert atmosphere (Argon). It is crucial to prevent contact between aliquots and air. Oxidation of the aminophosphine species into aminophosphine oxide species leads to the appearance of extra resonances in the NMR spectra that complicate the interpretation. A fixed volume of the aliquots is dissolved in 500 $\mu$L toluene-$d_8$ (99,50 % D, purchased at Euriso-top) and transferred to an NMR tube (5 mm). NMR measurements were recorded on a Bruker Avance III Spectrometer operating at a $^1$H frequency of 500.13 MHz and equipped with a BBI-Z probe or on a Bruker Avance II Spectrometer operating at a $^1$H frequency of 500.13 MHz and equipped with a TXI-Z probe (channels are $^1$H, $^{13}$C, $^{31}$P ). The sample temperature was set to 298.15 K. Quantitative $^1$H spectra were recorded with a 20s delay between scans to allow full relaxation of all NMR signals. The quantification was done by using the Digital ERETIC method. $^{31}$P spectra were recorded with a 20 s delay between scans to allow full relaxation of all NMR signals as well. Diffusion measurements (2D $^{31}$P DOSY) were performed using a double stimulated echo sequence for convection compensation and with monopolar gradient pulses.[19] Smoothed rectangle gradient pulse shapes were used throughout.

**Single crystal X-ray diffraction:** X-ray intensity data were collected on a Agilent Supernova Dual Source (Cu at zero) diffractometer equipped with an Atlas CCD detector using CuK$\alpha$ radiation ($\lambda$ = 1.54184 Å) and $\omega$ scans. The images were interpreted and integrated with the program CrysAlisPro (Agilent Technologies, Agilent (2013). CrysAlis PRO. Agilent Technologies UK Ltd, Yarnton, England.). Using Olex2,[20] the structures were solved by direct methods using the ShelXS structure solution program and refined by full-matrix least-squares on F2 using the ShelXL program package.[21] Non-hydrogen atoms were anisotropically refined and the hydrogen atoms in the riding mode and isotropic temperature factors fixed at 1.2 times U(eq) of the parent atoms (1.5 times U(eq) for methyl groups).

**Crystal data for [$C_2H_6NH_2Cl$]:** M = 81.54, orthorhombic, space group Ibam (No. 72), a = 7.2377(5) Å, b = 14.3892(11) Å, c = 9.8897(9) Å, V = 1029.96(14) Å,[22] Z = 8, T = 100 K, $\rho_{calc}$ = 1.052 g.$cm^{-3}$, $\mu$(Cu-K$\alpha$) = 0.564 $mm^{-1}$, F(000) = 352.0, 2992 reflections measured, 558 unique ($R_{int}$

= 0.0545) which were used in all calculations. The final R1 was 0.0320 (I> $2\sigma$(I)) and wR2 was 0.0676 (all data).

The structure of [$C_2H_6NH_2Cl$], has been previously determined and deposited with the Cambridge Structural Database (CSD, Version 5.37),[22] with CCDC-numbers 204844, 661061 and 721889.

**Chemical yield evaluation method:** The chemical yield (C.Y.) is estimated by measuring the absorbance of a known dilution of the reaction mixture in the short wavelength range. The dilution is estimated by first measuring the mass of the aliquot withdrawn from the mixture. Then a known volume of toluene is added to the aliquot. The absorbance of the provided solution is then measured. It is well-known that the intrinsic absorption coefficient ($\mu_{(i)}$) of differently sized colloidal nanocrystals coincide at short wavelengths.[23–26] This trend was observed for differently sized InP QDs at wavelength of 413 nm where the average value of $\mu_{(i)}$ was smaller (relative standard deviation 8.08 %) suggesting a lack of quantum confinement effects at this wavelength.[27] Therefore, a good match between $\mu_{(i)}$ of InP QDs and of the bulk InP material is expected at this wavelenght.[27] Knowing the intrinsic absorption coefficient of bulk InP at 413 nm, we can then use these values to calculate the chemical yield of InP nanocrystals solution.

As an example, we take an aliquot with a measured mass $m_{aliquots}$ = 20 mg that was taken from a reaction mixture that had a total mass $m_{total}$ of 4.5 g. Then, 3.0 mL of toluene is added to the aliquot and it is loaded in an absorbance cuvette. An absorbance $A$ of 0.45 is measured at $\lambda = 413$ nm for the aliquot in toluene. According to literature,[25] the intrinsic absorption coefficient is given by:

$$\mu_{(i,th)} = \frac{4\pi nk|f_{LF}|^2}{n_s\lambda} \tag{3.1}$$

Here, $n$ and $k$ are the real and imaginary part of the refractive index of bulk zincblende InP and $n_s$ is the refractive index of toluene. The local field factor $f_{LF}$ is given by:[25]

$$|f_{LF}|^2 = \frac{9n_s^4}{(n^2 - k^2 + 2n_s^2)^2 + (nk)^2} \tag{3.2}$$

We can have access to $n$, $k$ and $n_s$ from the literature,[28] which yields at $\lambda = 413$ nm: $n = 4.395$, $k = 1.247$, $n_s = 1.52$. Then $|f_{LF}|^2 = 0.078$ and $\mu_{(i,th)} = 8.5 \cdot 10^6 m^{-1}$.

We can then deduce the volume fraction $f$ of InP in the aliquot with the measured absorbance A and the theoretical intrinsic absorption coefficient $\mu_{(i,th)}$:[25]

$$f = \frac{A \cdot ln(10)}{\mu_{(i,th)} \cdot L} = 1.2 \cdot 10^{-5} \tag{3.3}$$

Where $L$ is the cuvette length (m). The amounts of InP units can then be deduced from $f$ and the InP molar volume $V_M$.

$$n_{cuvette} = f \cdot \frac{V_{cuvette}(m^3)}{V_M(\frac{m^3}{mol})} = 1.2 \cdot 10^{-5} \cdot \frac{3.0 \cdot 10^{-6}}{3.0 \cdot 10^{-5}} = 1.2 \cdot 10^{-6}\, mol \tag{3.4}$$

The total amount of InP units in the reaction mixture can be calculated with the ratio between the mass of the aliquot $m_{aliquots}$ and the mass $m_{total}$ of the reaction mixture.

$$n_{total} = n_{cuvette} \cdot \frac{m_{total}}{m_{aliquots}} = 1.2 \cdot 10^{-6} \frac{4.5}{20 \cdot 10^{-3}} = 0.27\, mmol \tag{3.5}$$

We have defined the chemical yield $C.Y.$ as a percentage between InP units in the reaction mixture $n_{total}$ and the In quantity $n_{In}$ that we have initially put in the reaction mixture.

$$C.Y. = \frac{n_{total}}{n_{In}} \cdot 100 = \frac{0.27}{0.45} \cdot 100 = 60\,\% \tag{3.6}$$

For this particular example we have measured a chemical yield of 60 %. It means that 60 % of the initially used indium precursor has been effectively converted into InP nanocrystals at the moment of the reaction we have taken the aliquot.

**Concentration evaluation method:** Since the $\mu_i$ values at 413 nm are size-independent we can calculate the molar extinction coefficient at 413 nm $\epsilon_{413}$ (in $cm^{-1}mol^{-1}L$) for InP QDs with a given diameter $d_{QD}$:[27]

$$\epsilon_{413} = \frac{\pi d_{QD}^3 N_A}{6ln10} \mu_{(413)} = 1.29 \cdot 10^4 d_{QD}^3 \tag{3.7}$$

Where $N_A$ is the Avogadro's number.

Using the Lambert-Beer law together with the sizing curve of Inp QDs, the $\epsilon_{413}$ value enables the direct determination of the concentration of InP QDs from the absorption spectrum at 413 nm:[27]

$$c = \frac{A_{413}}{\epsilon_{413} l} = \frac{A_{413}}{1.29 \cdot 10^4 d_{QD}^3 l} \tag{3.8}$$

Where $l$ (cm) is the path length of the sample which corresponds to the path length of the cuvette.

## 3.3 InP quantum dot synthesis

As outlined in the Experimental Section, the first precursor used for the synthesis of InP synthesis is a solution of $InCl_3$ and $ZnCl_2$ in a primary amine. The latter acts both as solvent and ligand and may also have a chemical role in the synthesis. Using specifically oleylamine (OLA) as primary amine allows us to perform reactions at relatively high temperatures – up to 340 ℃ – which is important for the eventual shell growth. In this mixture, $InCl_3$ is the actual indium precursor and $ZnCl_2$ is added to facilitate the shell growth and it also proves to reduce the size dispersion of the InP QDs (see Figure 3.1). As already mentioned by other authors,[1;29] adding Zn at the beginning of an InP nanocrystal synthesis does not automatically produce In(Zn)P alloys. Nevertheless, the formation of Zn-doped InP core nanocrystals by this approach cannot be excluded. To form InP QDs, the $(amino)_3P$ is injected at high temperature, where we prefer tris(diethylamino)phosphine $P(NEt_2)_3$ because of its low price and its boiling point (240 ℃) being higher than the reaction temperature (180 ℃). After injection, the initially colorless reaction mixture turns dark red within 20min. This is reflected by the progressive shift to longer wavelengths of the absorption spectra of aliquots taken at different times after the injection (see Figure 3.2).

A TEM study of the InP QDs obtained from a 20 min reaction using the reference conditions outlined in the Experimental Section showed that the formed QDs have an average diameter of 3.2 nm (see Figure 4.1c Chapter 4) and XRD revealed that these InP QDs have a zincblende structure (Figure 4.2a in Chapter 4). Two excitonic features, separated by 0.3 eV, can be distinguished in the absorption spectrum. These could correspond to transitions from the upper hole states to the first and second electron state, respectively, as this energy difference corresponds to the calculated splitting between these electron states.[30] It should be noted that the resulting InP core QDs are not luminescent. This could be due the use of oxygen-free precursors. Indeed in the case of $(TMS)_3P$-based synthesis, the

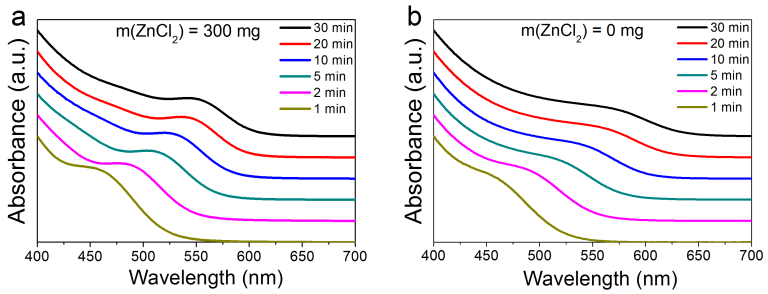


**Figure 3.1:** Influence of the $ZnCl_2$ on the size-dispersion. **(a)** Absorbance spectra of aliquots using the synthesis protocol outlined in the Experimental Section with 300 mg of $ZnCl_2$. **(b)** Absorbance spectra of aliquots using the same protocol without $ZnCl_2$.

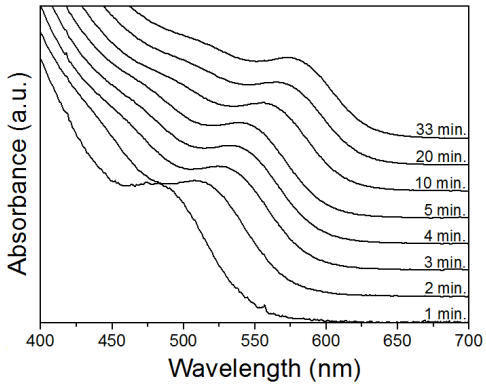


**Figure 3.2:** Absorbance spectra of aliquots taken during the synthesis outlined in the Experimental Section.

formation of an oxide layer arises from the presence of carboxylate ligands that transform into ketones thereby providing oxidative conditions.[31] This oxide layer could act as an inorganic shell that passivates surface traps and consequently enhance the PLQY of the core InP QDs.

Next to precursor cost, a key element of an economical QD synthesis is the chemical yield, *i.e.*, the fraction of the precursors eventually incorporated in the QDs. Since the InP synthesis presented here is typically run using a phosphorous excess, the reaction yield is defined as the amount (moles) of indium in the InP QDs relative to the amount of indium precursor used. We calculate the yield by comparing the absorbance of quantitative aliquots at 413 nm with the intrinsic absorption coefficient of InP QDs at the same

**Table 3.1:** Cost estimation of InP QDs syntheses.

**$(TMS)_3P$-based synthesis:**

| Chemical Yield : 80 % assumed | unit cost | unit | units/g InP | cost/g InP |
|---|---|---|---|---|
| $(TMS)_3P$ | 232.5 | G | 1,8 | 502 |
| Indium Acetate | 5,15 | G | 2 | 12 |
| Octadecene | 42.8 | L | 0,1 | 5 |
| Methanol | 50 | L | 0,3 | 18 |
| Total Cost | | | | €537 |

**$(DEA)_3P$-based synthesis (P:In = 1):**

| Chemical Yield : 20% measured | unit cost | unit | units/g InP | cost/g InP |
|---|---|---|---|---|
| P(DEA)3 | 6 | G | 8,5 | 51 |
| Indium Chloride | 12,36 | G | 7,6 | 94 |
| Oleylamine | 0,16 | mL | 382,6 | 61 |
| Ethanol | 0,023 | mL | 765,3 | 18 |
| Total Cost | | | | € 224 |

**$(DEA)_3P$-based synthesis (P:In = 3.6):**

| Chemical Yield : 80% measured | unit cost | unit | units/g InP | cost/g InP |
|---|---|---|---|---|
| $P(DEA)_3$ | 6 | G | 7.7 | 46 |
| Indium Chloride | 12,36 | G | 1,9 | 23 |
| Oleylamine | 0.16 | mL | 94.8 | 15 |
| Ethanol | 0.023 | mL | 189.5 | 4 |
| Total Cost | | | | €88 |

wavelength (see Experimental Section for details). Most importantly, we find that the chemical yield depends on the $(amino)_3P$:$InCl_3$ ratio. Using a 1:1 $(amino)_3P$:$InCl_3$ ratio, a chemical yield of 10-30 % is typically obtained. However, the yield increases to 75-85 % when the $(amino)_3P$:$InCl_3$ ratio is increased to 3.6:1 or more. In this respect, it is instructive to take a look at the total synthesis cost. Counting only the cost of the chemicals, we find that in a classical $(TMS)_3P$ based InP QDs synthesis, about 95 % of the total synthesis cost is due to the phosphorous precursor (see Table 3.1). Using $P(NEt_2)_3$ in a 1:1 ratio to the In precursor reduces the synthesis cost by at least a factor of 2.5 as compared to a $(TMS)_3P$ based synthesis. The increase in chemical yield with a $(amino)_3P$:$InCl_3$ ratio of 3.6 further reduces this cost by a factor of 2 since the most expensive precursor – $InCl_3$ – is used more effectively. Hence, even without considering the further cost

benefits of having a more stable, less hazardous precursor, it should be clear that opposite from $(TMS)_3P$, the use of $(amino)_3P$ under close to full yield conditions may result in affordable InP QDs.

## 3.4 Reaction mechanism

Although aminophosphines prove most useful precursors for synthesizing InP QDs, they are not the most obvious. In $(TMS)_3P$, the phosphorus atom has an oxidation state of -III, rendering a reaction with an $In^{III}$ precursor such as indium chloride or indium acetate most likely. Aminophosphines on the other hand are $P^{III}$ compounds, such that intermediate reduction steps are needed to form InP in a reaction with an $In^{III}$ precursor. Two-step methods in which at least the indium precursor is reduced before reacting with the phosphorus precursor have already been described in the literature. $InCl_3$ for example can be reduced by $KBH_4$ to form $In^0$ which then reacts with white phosphorus ($P_4$).[32] Another example is the reduction of $InCl_3$ by an organolithium reagent, followed by the reaction of the resulting $In^0$ with trioctylphosphine by a catalytic cleavage at high temperature.[33] Opposite from aminophosphine-based syntheses, however, such two-step strategies lead to rather polydisperse InP QDs. Alternatively, Song *et al.* hypothesized that InP formation starting from aminophosphine could involve the *in-situ* formation of phosphine ($PH_3$) due to the presence of labile hydrogen in the primary amine solvent.[1] However, amines being poor Brønsted acids, such a mechanism seems unlikely.

### 3.4.1 Transamination reaction

To investigate possible intermediate reaction steps involved in the formation of InP out of aminophosphine and $InCl_3$, the exhaust of an InP QD synthesis was scrubbed using a chemical gas trap (Figure 3.3a). Most notably, the formation of a copper hydroxide precipitate was observed upon scrubbing with a saturated aqueous $CuSO_4$ solution, a strong indication that the exhaust contains a basic gas (Figure 3.3b). Scrubbing with a methanolic solution of hydrogen chloride enabled us to trap the base as a salt. After rotary evaporation, a solid residue was obtained and after recrystallization in ethyl acetate, this salt was identified by single crystal X-ray diffraction as dimethylammonium chloride for a reaction where $P(NMe_2)_3$ was used as the phosphorus precursor (see Experimental Section for details). This points towards an exchange between the amines used as a solvent in the synthesis and the amino groups coordinating to phosphorus in the original

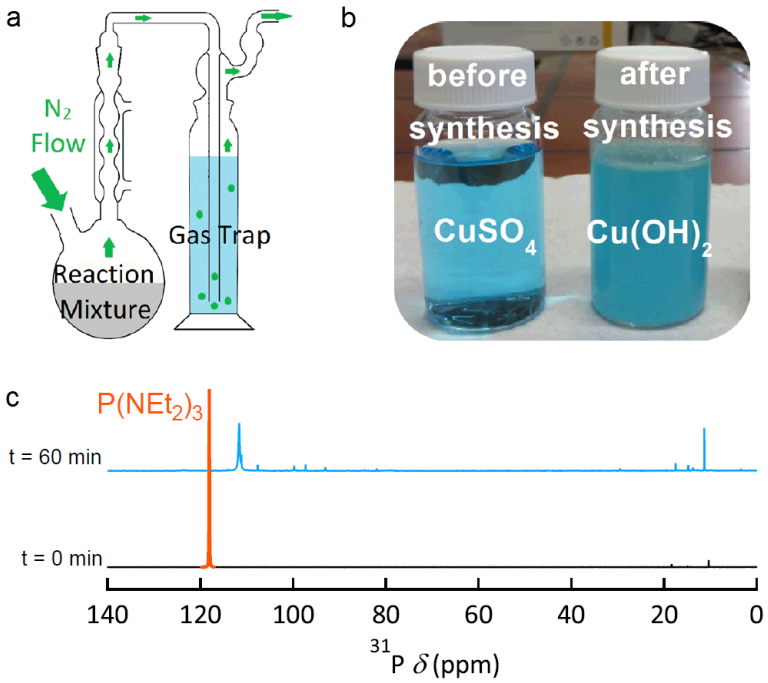


**Figure 3.3:** **(a)** Scheme of the gas trap mounting. **(b)** Picture of the $CuSO_4$ gas trap aqueous solution before and after an InP synthesis. **(c)** $^{31}P$ NMR spectra of aliquots taken during the reaction of $P(NEt_2)_3$ and dodecylamine.

precursor. This exchange is also observed using $P(NEt_2)_3$ as the phosphorus precursor.

Simply mixing $P(NEt_2)_3$ and dodecylamine (ratio 1:3) in a vial under an inert atmosphere confirms this transamination. Indeed, when the temperature is raised above 100 °C, gas bubbles evolve, which we attribute to $Et_2NH$ rather than $P(NEt_2)_3$, as the latter has a boiling point of 245 °C. This is further corroborated by the two $^{31}P$ NMR spectra shown in Figure 3.3c, recorded on a mixture of $P(NEt_2)_3$ and dodecylamine prior to and 1 h after reaction. The initial solution features a single resonance of $P(NEt_2)_3$ at 118 ppm. This has almost completely vanished after 1 h of reaction due to transamination. Diethylamine is formed and has evaporated from the mixture (boiling point = 55 °C). Moreover, a new, somewhat shifted dominant resonance appears at 111 ppm, most likely a transaminated aminophosphine, next to several less intense resonances especially at around 11 ppm.

**Table 3.2:** Reaction results as a function of the solvent used

| Class | Example | Result |
|---|---|---|
| Primary amines | Butylamine | InP QDs |
| | Octylamine | |
| | Dodecylamine | |
| | Oleylamine | |
| Secundary amines | Dioctylamine | No reaction |
| Tertiary amines | Trioctylamine | |
| Other | Trioctylphosphine | |

Denoting an alkyl moiety in general as R, this transamination can be written as a sequence of three successive reactions:

$$P(NEt_2)_3 + RNH_2 \rightleftharpoons P(NEt_2)_2(NHR) + Et_2NH \tag{3.9}$$

$$P(NEt_2)_2(NHR) + RNH_2 \rightleftharpoons P(NEt_2)(NHR)_2 + Et_2NH \tag{3.10}$$

$$P(NEt_2)(NHR)_2 + RNH_2 \rightleftharpoons P(NHR)_3 + Et_2NH \tag{3.11}$$

Transamination reactions for $P(NMe_2)_3$ and $P(NEt_2)_3$ have been described before.[34;35] Burgada for example argues that an exchange between the dimethylamino group of $P(NMe_2)_3$ and a heavier second amino group can occur if the hydrogen of this second amino group is sufficiently labile.[34] As the boiling point of dimethylamine is 7.4 ℃, this compound is eliminated from the reaction mixture after its formation, shifting the equilibrium of the reaction to the formation of a fully transaminated aminophosphine where the amino group has a higher boiling point than dimethylamine. Even if the author mentioned exchange between secondary amines only, it underlines our observation that a similar exchange involving a primary amine, such as dodecylamine or oleylamine, and a more volatile amino group, such as dimethylamino or diethylamino, occurs in the aminophosphine-based synthesis of InP.

The occurrence of transamination provides an important perspective on the role of the amino group in a particular aminophosphine precursor. First of all, it implies that adjusting this group to tune the precursor reactivity and thus the outcome of an InP synthesis risks to be an inefficient strategy if – as seems necessary – high boiling point amines are used as the solvent for the reaction. Indeed, in that case it will be the solvent that dictates what amino groups make up the true aminophosphine precursor. This explains for one

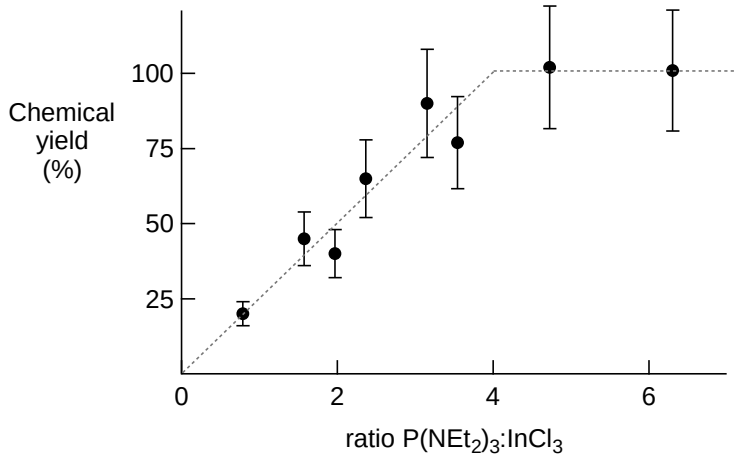


**Figure 3.4:** Yield conversion – amount of InP formed as fraction of the amount of $InCl_3$ used – of a tris(diethylamino)phosphine-based InP QDs synthesis plotted as a function of the $P(NEt_2)_3$:$InCl_3$ ratio used in the synthesis. The trend line is a straight line through the origin reaching full yield at a $P(NEt_2)_3$:$InCl_3$ ratio of 4, followed by a horizontal at 100 % for higher $P(NEt_2)_3P$:$InCl_3$ ratios.

thing why we do not observe significant differences in reactivity between, *e.g.*, $P(NMe_2)_3$ and $P(NEt_2)_3$. On the other hand, the amino exchange highlights the role of the primary amine used as the solvent. By screening several amines, we find that InP is only formed when a primary amine is used. No reaction takes place in the case of secondary or tertiary amines (see Table 3.2). This clearly indicates that primary amines are not just the solvent or the ligand in an aminophosphine-based InP synthesis. Rather, they must play a central role in the whole precursor chemistry.

### 3.4.2 Reaction yield development

Focusing on syntheses using $P(NEt_2)_3$ and $InCl_3$ in oleylamine, a key point to get further insight in the precursor conversion is the observation we already made before that the conversion yield of the indium precursor into InP, *i.e.*, the chemical yield, depends on the aminophosphine *vs.* indium(III) chloride equivalence. Here, the chemical yield is calculated by comparing the absorbance of quantitative aliquots with the intrinsic absorption coefficient of InP QDs at the same short wavelength (see Experimental Section for details). As shown in Figure 3.4, we find that the chemical yield increases

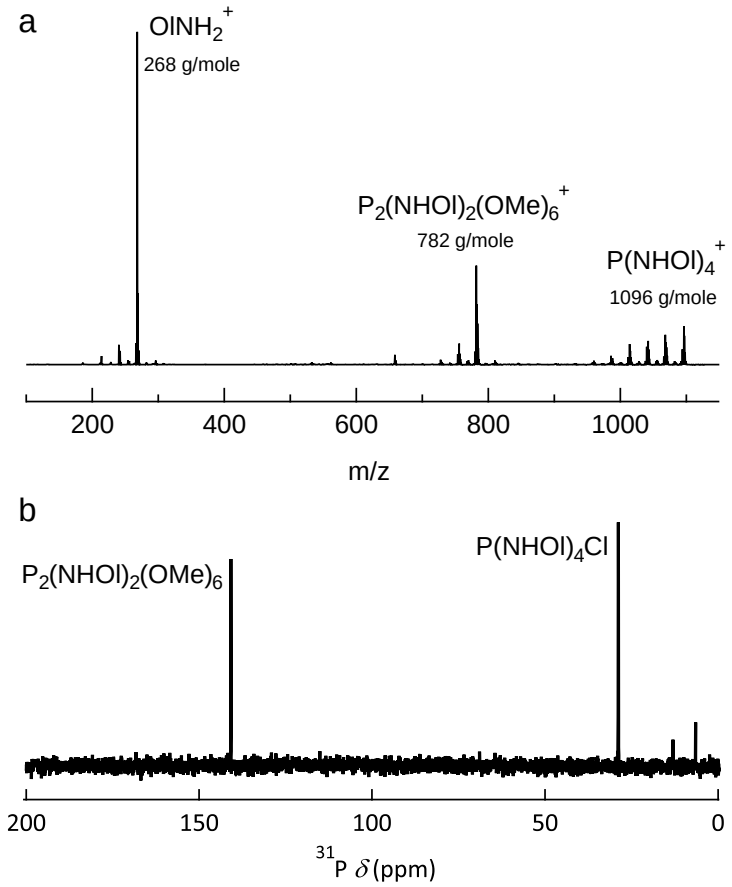


**Figure 3.5: (a)** Mass-spectrum of the supernatant obtained after purification by methanol addition of a full yield diethylaminophosphine-based InP QDs synthesis **(b)** $^{31}$P NMR spectrum of the supernatant used for mass spectrometry diluted using toluene-$d_8$.

proportionally to the $P(NEt_2)_3$:$InCl_3$ molar ratio to reach 100 % for ratios of $\approx 4$ or more. At this point, we hypothesize that a phosphorus precursor excess is needed to obtain full chemical yield because the aminophosphine plays more than one role in the synthesis. As discussed before, formation of an InP unit from $P(NEt_2)_3$ comes with a reduction of $P^{III}$ to $P^{-III}$. One way to achieve this – and that accounts for the observed phosphorous excess needed to reach full conversion of the indium – is that one equivalent of phosphorous is reduced to $P^{-III}$ by the oxidation of 3 equivalents of phos-

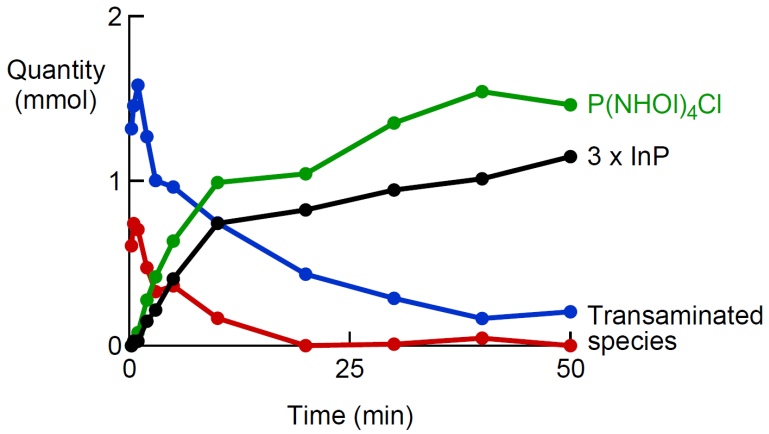


**Figure 3.6:** (colored) Concentration development of the prevailing species during a diethylaminophosphine based InP synthesis run at 170°C with $ZnCl_2$ present as estimated from $^{31}P$ NMR resonance intensities and (black) the concomitant amount of InP formed.

phorous to $P^V$. We have already demonstrated that injected $P(NEt_2)_3$ is modified during the synthesis by transamination. To continue this line of thought, we therefore propose an overall redox reaction in which 1 equivalent of InP is formed by the oxidation of 3 equivalents of the substituted aminophosphine to a phosphonium salt:

$$InCl_3 + 4\,P(NHR)_3 \rightleftharpoons InP + 3\,P(NHR)_4Cl \qquad (3.12)$$

In this chemical equation, R represents an alkyl moiety of a primary amine.

First evidence that Equation 3.12 indeed describes the overall reaction leading to InP comes from the mass spectrum of the reaction mixture after removal of the InP QDs by methanol addition. As shown in Figure 3.5a, it contains three main compounds. A first has a molar mass of 268 g/mol, most likely corresponding to oleylamine, which is the solvent of the reaction and thus present in large amounts. The second compound has a molar mass of 782 g/mole, which corresponds to $P_2(NHOl)_2(OMe)_6$. Probably, this has been produced during the purification in a reaction between aminophosphine compounds and methanol (see Experimental Section). The third compound has a measured molar mass of 1096 g/mol which is close to the 1097 g/mol expected for $P(NHOl)_4^+$, *i.e.*, the oleylamino phosphonium cation generated by the reaction according to Equation 3.12.

By identifying the transaminated species and $P(NHOl)_4Cl$ as the main reaction byproduct, the development of these different phosphorus species can be monitored during a reaction by analyzing successive aliquots (see Figure 3.6). Here, we derived the concentration of each species from the integrated intensity of its $^{31}P$ resonance. By taking a reaction carried out at 190 ℃ as an example, Figure 3.6 show that 15 s after injection the phosphorous precursor has disappeared and the transaminated compounds are already the prevailing species. Next, Figure 3.6 shows that, during the reaction, the concentration of $P(NHOl)_4Cl$ gradually increases at a rate concurring with the formation of InP with an estimated equivalence somewhat exceeding 3:1. Clearly, this observation confirms the overall chemical reaction equation 3.12, where indeed one InP equivalent is formed together with 3 equivalents of $P(NHOl)_4Cl$ and it agrees with the MS analysis showing $P(NHOl)_4Cl$ to be the dominant reaction byproduct. The decrease in concentration of both transaminated aminophosphines follows the formation of InP, confirming their role as the actual phosphorus precursor in this reaction. More specifically, the absence of partially substituted phosphonium salts suggests that the actual precursor is most likely $P(NHOl)_3$, the fully transaminated compound. Note that the concentration of the tautomeric form, on the other hand, stays largely constant during the reaction, suggesting that this $P^V$ compound is unreactive and only formed in the initial stage of the reaction.

## 3.5 Conclusion

In conclusion, we have presented an economic method to make InP QDs that do not require the expensive and inconvenient $(TMS)_3P$ precursor. Using an excess of $(amino)_3P$ type precursors enables the production of InP QDs at full chemical yield with a quality that is at least comparable to the best obtained in literature. We have also shown that upon injection, dimethyl- and diethylaminophosphine undergo rapid transamination with the amine used as the solvent. This leads to the release of dimethyl or diethylamine and an effective aminophosphine precursor that is most likely the fully transaminated compound. Only in the case that primary amines are used, this leads to the eventual formation of InP, where a quaternary aminophosphonium salt is formed as the major reaction byproduct. This finding enables the overall InP formation reaction to be written as a redox reaction where three equivalents of the transaminated aminophosphine reduce a fourth equivalent to form one equivalent of InP. Importantly, this double role of the aminophosphine explains why full conversion of the In precursor into InP is only attained with a 4-fold excess of the aminophosphine.

This picture is confirmed by monitoring the reaction development using $^{31}$P NMR spectroscopy. We believe that the new chemistry introduced here for the formation of InP QDs may be extended to the formation of other III-V quantum dots, such as GaP, InAs or GaAs, using similar aminophosphine or aminoarsine precursors.

# References

[1] Woo-Seuk Song, Hye-Seung Lee, Ju Chul Lee, Dong Seon Jang, Yoonyoung Choi, Moongoo Choi, and Heesun Yang. *Amine-derived synthetic approach to color-tunable InP/ZnS quantum dots with high fluorescent qualities.* Journal of Nanoparticle Research, 15(6):1750, 2013.

[2] Renguo Xie, David Battaglia, and Xiaogang Peng. *Colloidal InP Nanocrystals as Efficient Emitters Covering Blue to Near-Infrared.* Journal of the American Chemical Society, 129(50):15432–15433, 2007.

[3] Liang Li, Myriam Protière, and Peter Reiss. *Economic Synthesis of High Quality InP Nanocrystals Using Calcium Phosphide as the Phosphorus Precursor.* Chemistry of Materials, 20(8):2621–2623, 2008.

[4] C. B. Murray, D. J. Norris, and M. G. Bawendi. *Synthesis and characterization of nearly monodisperse CdE (E = sulfur, selenium, tellurium) semiconductor nanocrystallites.* Journal of the American Chemical Society, 115(19):8706–8715, 1993.

[5] Zhengtao Deng, Li Cao, Fangqiong Tang, and Bingsuo Zou. *A New Route to Zinc-Blende CdSe Nanocrystals: Mechanism and Synthesis.* The Journal of Physical Chemistry B, 109(35):16671–16675, 2005.

[6] Jonathan S. Steckel, Brian K. H. Yen, David C. Oertel, and Moungi G. Bawendi. *On the Mechanism of Lead Chalcogenide Nanocrystal Formation.* Journal of the American Chemical Society, 128(40):13032–13033, 2006.

[7] Haitao Liu, Jonathan S. Owen, and A. Paul Alivisatos. *Mechanistic Study of Precursor Evolution in Colloidal Group II–VI Semiconductor Nanocrystal Synthesis.* Journal of the American Chemical Society, 129(2):305–312, 2007.

[8] Sofie Abe, Richard Karel Čapek, Bram De Geyter, and Zeger Hens. *Tuning the Postfocused Size of Colloidal Nanocrystals by the Reaction Rate: From Theory to Application.* ACS Nano, 6(1):42–53, 2012.

[9] Sofie Abe, Richard K. Capek, Bram De Geyter, and Zeger Hens. *Reaction Chemistry/Nanocrystal Property Relations in the Hot Injection Synthesis, the Role of the Solute Solubility.* ACS Nano, 7(2):943–949, 2013.

[10] Kim De Nolf, Richard K. Capek, Sofie Abe, Michael Sluydts, Youngjin Jang, José C. Martins, Stefaan Cottenier, Efrat Lifshitz, and Zeger

Hens. *Controlling the Size of Hot Injection Made Nanocrystals by Manipulating the Diffusion Coefficient of the Solute.* Journal of the American Chemical Society, 137(7):2495–2505, 2015.

[11] Jonathan S. Owen, Emory M. Chan, Haitao Liu, and A. Paul Alivisatos. *Precursor Conversion Kinetics and the Nucleation of Cadmium Selenide Nanocrystals.* Journal of the American Chemical Society, 132(51):18206–18213, 2010.

[12] Mark P. Hendricks, Michael P. Campos, Gregory T. Cleveland, Ilan Jen-La Plante, and Jonathan S. Owen. *A tunable library of substituted thiourea precursors to metal sulfide nanocrystals.* Science, 348(6240):1226–1230, 2015.

[13] Peter M. Allen, Brian J. Walker, and Moungi G. Bawendi. *Mechanistic Insights into the Formation of InP Quantum Dots.* Angewandte Chemie International Edition, 49(4):760–762, 2010.

[14] Dylan C. Gary and Brandi M. Cossairt. *Role of Acid in Precursor Conversion During InP Quantum Dot Synthesis.* Chemistry of Materials, 25(12):2463–2469, 2013.

[15] Dylan C. Gary, Benjamin A. Glassy, and Brandi M. Cossairt. *Investigation of Indium Phosphide Quantum Dot Nucleation and Growth Utilizing Triarylsilylphosphine Precursors.* Chemistry of Materials, 26(4):1734–1744, 2014.

[16] O. I. Micic, J. R. Sprague, C. J. Curtis, K. M. Jones, J. L Machol, A. J. Nozik, H. Giessen, B. Fluegel, G. Mohs, and N. Peyghambarian. *Synthesis and Characterization of InP, GaP, and $GaInP_2$ Quantum Dots.* The Journal of Physical Chemistry, 99(19):7754–7759, 1995.

[17] A. A. Guzelian, U. Banin, A. V. Kadavanich, X. Peng, and A. P. Alivisatos. *Colloidal chemical synthesis and characterization of InAs nanocrystal quantum dots.* Applied Physics Letters, 69(10):1432–1434, 1996.

[18] YunWei Cao and Uri Banin. *Growth and Properties of Semiconductor Core/Shell Nanocrystals with InAs Cores.* Journal of the American Chemical Society, 122(40):9692–9702, 2000.

[19] Mark A. Connell, Paul J. Bowyer, P. Adam Bone, Adrian L. Davis, Alistair G. Swanson, Mathias Nilsson, and Gareth A. Morris. *Improving the accuracy of pulsed field gradient NMR diffusion experiments: Correction for gradient non-uniformity.* Journal of Magnetic Resonance, 198(1):121–131, 2009.

[20] Oleg V. Dolomanov, Luc J. Bourhis, Richard J. Gildea, Judith A. K. Howard, and Horst Puschmann. *OLEX2: a complete structure solution, refinement and analysis program.* Journal of Applied Crystallography, 42(2):339–341, 2009.

[21] George M. Sheldrick. *A short history of SHELX.* Acta Crystallographica Section A, 64(1):112–122, 2008.

[22] Frank H. Allen. *The Cambridge Structural Database: a quarter of a million crystal structures and rising.* Acta Crystallographica Section B, 58(Part 3):380–388, 2002.

[23] C. A. Leatherdale, W.-K. Woo, F. V. Mikulec, and M. G. Bawendi. *On the Absorption Cross Section of CdSe Nanocrystal Quantum Dots.* The Journal of Physical Chemistry B, 106(31):7619–7622, 2002.

[24] John Sundar Kamal, Abdoulghafar Omari, Karen Van Hoecke, Qiang Zhao, André Vantomme, Frank Vanhaecke, Richard Karel Capek, and Zeger Hens. *Size-Dependent Optical Properties of Zinc Blende Cadmium Telluride Quantum Dots.* The Journal of Physical Chemistry C, 116(8):5049–5054, 2012.

[25] Richard Karel Čapek, Iwan Moreels, Karel Lambert, David De Muynck, Qiang Zhao, André Van Tomme, Frank Vanhaecke, and Zeger Hens. *Optical Properties of Zincblende Cadmium Selenide Quantum Dots.* The Journal of Physical Chemistry C, 114(14):6371–6376, 2010.

[26] Iwan Moreels, Karel Lambert, Dries Smeets, David De Muynck, Tom Nollet, José C. Martins, Frank Vanhaecke, André Vantomme, Christophe Delerue, Guy Allan, and Zeger Hens. *Size-Dependent Optical Properties of Colloidal PbS Quantum Dots.* ACS Nano, 3(10):3023–3030, 2009.

[27] J Ministro and Z. Hens. *A study on the synthesis and the optical properties of InP-based quantum dots.* 2014.

[28] D. E. Aspnes and A. A. Studna. *Dielectric functions and optical parameters of Si, Ge, GaP, GaAs, GaSb, InP, InAs, and InSb from 1.5 to 6.0 eV.* Physical Review B, 27(2):985–1009, 1983.

[29] Kai Huang, Renaud Demadrille, Mathieu G. Silly, Fausto Sirotti, Peter Reiss, and Olivier Renault. *Internal Structure of InP/ZnS Nanocrystals Unraveled by High-Resolution Soft X-ray Photoelectron Spectroscopy.* ACS Nano, 4(8):4799–4805, 2010.

[30] A. Franceschetti, H. Fu, L. W. Wang, and A. Zunger. *Many-body pseudopotential theory of excitons in InP and CdSe quantum dots.* Physical Review B, 60(3):1819–1829, 1999.

[31] Arnaud Cros-Gagneux, Fabien Delpech, Céline Nayral, Alfonso Cornejo, Yannick Coppel, and Bruno Chaudret. *Surface Chemistry of InP Quantum Dots: A Comprehensive Study.* Journal of the American Chemical Society, 132(51):18147–18157, 2010.

[32] Ping Yan, Yi Xie, Wenzhong Wang, Fuyu Liu, and Yitai Qian. *A low-temperature route to InP nanocrystals.* Journal of Materials Chemistry, 9(8):1831–1833, 1999.

[33] Jannika Lauth, Tim Strupeit, Andreas Kornowski, and Horst Weller. *A Transmetalation Route for Colloidal GaAs Nanocrystals and Additional III–V Semiconductor Materials.* Chemistry of Materials, 25(8):1377–1383, 2013.

[34] R. Burgada. Bull. Soc. Chim. Fr., 10:2335, 1963.

[35] Janarthanan Gopalakrishnan. *Aminophosphines: their chemistry and role as ligands and synthons.* Applied Organometallic Chemistry, 23(8):291–318, 2009.

# 4

# Size-Tunable Synthesis of Luminescent InP/ZnE (E = Se, S) Core/Shell Quantum Dots[1]

*We demonstrate that size tuning of InP QDs at full chemical yield is possible by changing the nature of the indium halide salt. In addition, we present ZnS and ZnSe shell growth procedures that lead to InP/ZnS and InP/ZnSe core/shell QDs that emit from 510 nm to 630 nm with an emission linewidth between 46 nm and 63 nm. This synthetic method is an important step towards performing Cd-free QDs, and it could help the transfer of colloidal QDs from the academic field to product applications.*

[1] *Adapted from:* Mickaël D. Tessier, **Dorian Dupont**, Kim De Nolf, Jonathan De Roo, Zeger Hens. *Economic and Size-Tunable Synthesis of InP/ZnE (E = S, Se) Colloidal Quantum Dots.* Chemistry of Materials, 27(13):4893-4898, **2015**.

## 4.1 Introduction

In chapter 3, we established efficient protocols based on aminophosphines to synthesize InP QDs.[1] This compound is safe to use under ambient conditions and its cost is only a fraction of that of $(TMS)_3P$. In this chapter, we show that replacing $InCl_3$ by $InBr_3$ or $InI_3$ leaves the conversion yield and the reaction rate unchanged, yet leads to InP QDs with systematically smaller diameters at the end of the reaction. In addition, we introduce ZnS and ZnSe shell growth strategies that result in InP/ZnE (E = S, Se) batches with state-of-the-art emission linewidths (FWHM: 46-63 nm) and photoluminescence quantum yields (PLQY: 20-60 %). We thus conclude that $P(amino)_3$-based protocols may open a gateway to the large scale production of InP QDs.

## 4.2 Experimental section

**Chemicals:** Indium(III) chloride (99.999 %), indium(III) bromide (99.999 %), indium(III) iodide (99.999 %), zinc(II) chloride ($\geq$ 98 %), zinc(II) bromide ($\geq$ 98 %), zinc(II) iodide ($\geq$ 98 %), $P(NEt_2)_3$ (97 %), selenium powder 100 mesh (99,99 %) and zinc stearate (technical grade, 65 %) were purchased from Sigma Aldrich. Trioctylphosphine (> 97%) and sulfur powder were purchased from Strem Chemicals. Oleylamine (80-90 %) was purchased from Acros Organics (NB: Oleylamine is stored under inert atmosphere). 1-octadecene (technical 90 %) was purchased from Alfa Aesar.

**Full chemical yield synthesis of 3.2 nm InP QDs (first excitonic absorption peak at 560 nm):** 100 mg (0.45 mmol) of indium(III) chloride, as indium raw materials and 300 mg (2.2 mmol) of zinc(II) chloride, as zinc raw materials are mixed in 5.0 mL (15 mmol) of technical oleylamine which is a coordinating solvent. The reaction mixture is stirred and degassed at 120 ℃ for an hour and then heated to 180 ℃ under inert atmosphere. Upon reaching 180 ℃, a volume of 0.45 mL (1.6 mmol) of $P(NEt_2)_3$ (phosphorous:indium ratio = 3.6:1) are quickly injected in the above mixture. After the phosphorous precursor injection, the InP nanocrystals synthesis proceeded. The reaction occurs during 20 min. At the end of the reaction, the temperature is cooled down. InP nanocrystals are then precipitated in ethanol and suspended in tolune.

**Full chemical yield synthesis of 3.0 nm InP QDs (first excitonic absorption peak at 540 nm):** Same protocol as outlined above but indium chloride is replaced by 160 mg (0.45 mmol) of indium(III) bromide.

**Full chemical yield synthesis of 2.8 nm InP QDs (first excitonic absorption peak at 520 nm):** Same protocol as outlined above but indium chloride is replaced by 224 mg (0.45 mmol) of indium(III) iodide.

**Core/shell InP/ZnS QDs synthesis:** An InP QDs synthesis is performed at 180 ℃. Instead of cooling down the temperature, at 20 min: slow injection of 1 mL of saturated TOP-S (2.2 M). At 60 min: temperature is increased from 180 ℃ to 200 ℃. At 120 min: slow injection of 1 g of $Zn(stearate)_2$ in 4 mL of octadecene (ODE). Temperature is increased from 200 ℃ to 220 ℃. At 150 min: injection of 0.7 mL of stoichiometric TOP-S (2.2 M). Temperature is increased from 220 ℃ to 240 ℃. At 180 min: slow injection of 0.5 g of $Zn(stearate)_2$ in 2 mL of ODE. Temperature is increased from 240 ℃ to 260 ℃. At 210 min: end of reaction. At the end of the reaction, the temperature is cooled down. InP/ZnS nanocrystals are then precipitated in ethanol and suspended in toleune.

**Core/shell InP/ZnSe QDs synthesis:** An InP QDs synthesis is performed at 180 ℃. Instead of cooling down the temperature, after 20 min: slow injection of 1 mL of stoichiometric TOP-Se (2.2 M). At 60 min: temperature is increased from 180 ℃ to 200 ℃. At 120 min: slow injection of 1 g of $Zn(stearate)_2$ in 4 mL of ODE. Temperature is increased from 200 ℃ to 220 ℃. At 150 min: injection of 0.7 mL of saturated TOP-Se (2.2 M). Temperature is increased from 220 ℃ to 240 ℃. At 180 min: slow injection of 1 g of $Zn(stearate)_2$ in 4 mL of ODE. Temperature is increased from 240 ℃ to 280 ℃. At 210 min: slow injection of 0.7 mL of saturated TOP-Se (2.2 M). Temperature is increased from 280 ℃ to 320 ℃. After 240 min: slow injection of 1 g of $Zn(stearate)_2$ in 4 mL of ODE. 300 min: end of reaction. At the end of the reaction, the temperature is cooled down. InP/ZnSe nanocrystals are then precipitated in ethanol and suspended in toluene.

**Full width at half maximum (FWHM) estimation:** Generally, the exciton linewidth is estimated by fitting the absorption spectrum to a sum of Gaussians and a background that accounts for the systematic increase of the absorbance at shorter wavelengths.

However, as the first exciton transition in the InP spectra are not well pronounced, this method is not easy to implement and the final result may strongly depend on the particular functional form of the background correction. Hence, instead of fitting the absorbance spectrum to a sum of Gaussians and a background, we choose to plot the first derivative of the absorption spectrum. Then, the two extrema can be used to estimate the

width of the first exciton transition by using the known relation between these extrema and the FWHM of a Gaussian:

$$FWHM = \sqrt{2ln2}(\lambda_{max} - \lambda_{min}) \tag{4.1}$$

Here, $\lambda_{max}$ and $\lambda_{min}$ refer to the wavelength where the derivative of the absorption spectrum attains a maximum and a minimum, respectively. This method is not perfect as it will only be accurate if the absorption background depends linearly on wavelength, yet it is easier to implement than a Gaussian and it does not require one to assume a particular functional form for the background.

**Calculation of the molar amount of Zn/S precursor present in the shell of InP/ZnS QDs:** The molar amount of Zn/S precursor incorporated into the shell ($n_{Zn/S}$) at the end of a InP/ZnS core/shell QDs synthesis can be calculated from the density of the ZnS zincblende bulk material ($D_{ZnS}$) and on the assumption that both InP and InP/ZnS QDs exhibit spherical shapes.[2] $n_{Zn/S}$ is given by:

$$n_{Zn/S} = \frac{\left(\frac{4\pi({R_1}^3 - {R_0}^3)}{3}\right) D_{ZnS}}{M_{ZnS}} N_A n_{InP_{QD}} \tag{4.2}$$

Where $R_0$ (m) is the radius of the InP core QD, $R_1$ (m) the radius of the InP/ZnS core/shell QD, $D_{ZnS} = 4.10{\cdot}10^6$ g/m$^3$ the density of zincblende ZnS, $M_{ZnS} = 97.474$ g/mol the molecular weight of zincblende ZnS, $N_A = 6.025{\cdot}10^{23}$ mol$^{-1}$ the Avogadro constant and $n_{InP_{QD}}$ the molar amount of InP nanocrystals. The latter can be calculated from the molar extinction coefficien at 413 nm ($\epsilon_{413}$) and Beer–Lambert law (see Equation (3.8) in the Experimental Section of Chapter 3). It thus follows that $n_{InP_{QD}} = 9.55{\cdot}10^{-7}$ mol for a full chemical yield synthesis of 3.2 nm InP QDs.

As outlined in this chapter, the QD radius increase from 1.6 nm (core diameter) to $\approx$ 3.1 nm (core/shell diameter) at the end of a core/shell InP/ZnS QDs synthesis. Using (4.2) we find $n_{Zn/S} = 2.6$ mmol.

**X-Ray Fluorescence Spectroscopy:** InP QDs were washed three times with ethanol and re-suspended in toluene then drop-casted on paper filter. The X-ray fluorescence spectrum were measured using a Rigaku NEX CG.

**Growth rate for surface-reaction controlled growth:** A comprehensive expression for the nanocrystal growth rate comprising both the effects of solute supply by diffusion and the surface reaction was derived by Talapin *et al.*:[3]

$$\mathrm{j}_G = \frac{dr}{dt} = DV_m[M]_0 \left( \frac{S - \exp\left(\frac{2\gamma V_m}{rRT}\right)}{r + \left(\frac{D}{k_g(r)}\right)} \right) \approx V_m k_g(r)[M]_0 \left( S - \exp\left(\frac{2\gamma V_m}{rRT}\right) \right) \tag{4.3}$$

Here, $r$ denotes the nanocrystal radius, $D$ is diffusion coefficient of the solute, $V_m$ the molar volume of the material formed, $[M]_0$ the solute solubility, S the supersaturation, $\gamma$ the surface tension of the material formed, $R$ the gas constant, $T$ the absolute temperature and $k_g(r)$ the rate constant for solute adsorption at a nanocrystal with radius $r$. The last expression holds for surface reaction controlled growth, *i.e.*, when $D/k_g(r) \gg r$. It thus follows that the growth rate will increase if the product $k_g(r)[M]_0$ goes up.

## 4.3 InP core/shell quantum dots synthesis

In a typical aminophosphine-based synthesis of InP QDs, indium(III) chloride and zinc(II) chloride are dissolved in a primary amine as solvent (*e.g.*, $\mathrm{OlNH_2}$, where Ol = $\mathrm{C_{18}H_{35}}$).[1] The reaction mixture is subsequently degassed and heated to 150-220 ℃, followed by the injection of $\mathrm{P(NMe_2)_3}$, or $\mathrm{P(NEt_2)_3}$. Figure 2 in Chapter 3 depicts the UV-Vis absorption spectra of different aliquots taken at various reaction times for the case of an InP QD synthesis at 180 ℃ (see Experimental Section for details). Already after 1 min of reaction, the first excitonic feature is clearly visible and its red-shift with time points towards an increase of the QD diameter during the reaction.

Around these InP cores, ZnS and ZnSe shells can be grown using the respective chalcogen precursor; sulfur or selenium dissolved in trioctylphosphine until saturation (2.2 M), denoted as TOP-S or TOP-Se. Opposite from dodecanethiol – an alternative sulfur precursor for ZnS shell growth – we find that TOP-S does not induce a blue shift of the exciton transition upon ZnS shell growth, a phenomenon that could indicate surface etching.[1] As described in the Experimental Section, the shell growth procedure involves the addition of saturated TOP-S(e) together with zinc-stearate (the reaction would be Zn-limited with just the initial amount of $\mathrm{ZnCl_2}$) to the reaction mixture after the InP core formation yet before any purification. Subsequently, the temperature is increased in several steps along with additional

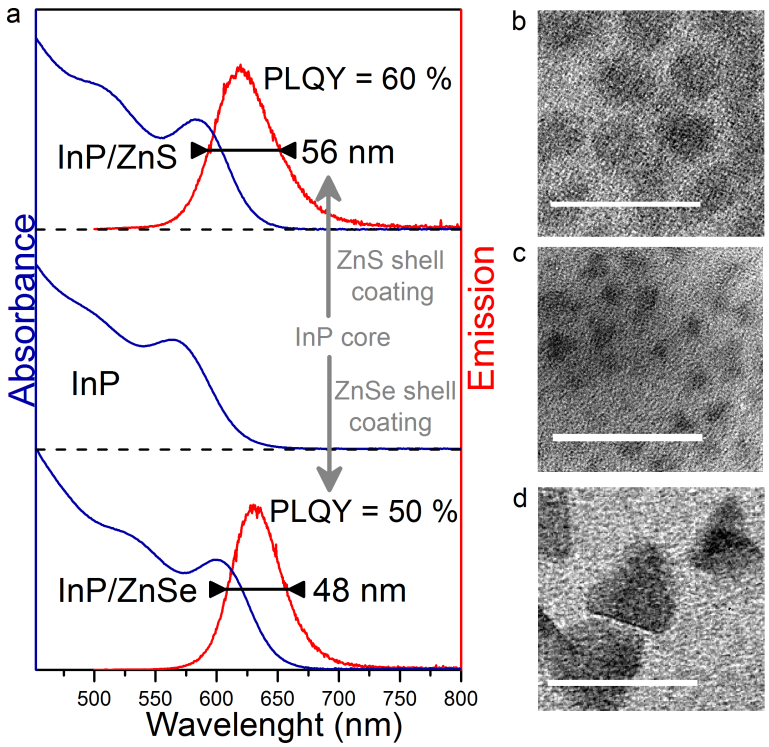


**Figure 4.1:** (**a**) Overview of (blue lines) absorption and (red lines) emission spectra of InP, InP/ZnS and InP/ZnSe QDs synthesized following the reference protocols described in the Experimental Section. b-g. TEM pictures (scale bar 20 nm) of (**b**) InP/ZnS QDs (diameter of ≈ 6.2 nm), (**c**) InP QDs (diameter of ≈ 3.2 nm) and (**d**) InP/ZnSe QDs (diameter of ≈ 10 nm).

precursor injections. It should be noted that adding zinc-stearate only after the first shell layers have formed allows for avoiding a possible oxidation of the InP core surface.[4]

In the case of ZnS coating, the QD diameter initially 3.2 nm increases to ≈ 6.2 nm (see Figure 4.1b), indicating that a 1.5 nm shell has been grown. This indicate that the shell reaction is not completed since 2.6 mmol of Zn- and S-precursors are actually incorporated into the shell whereas 3.8 mmol of S and 4.5 mmol of Zn were added during the synthesis (see Equation (4.2) in the Experimental Section). In XRD (see Figure 4.2c), this leads to a further broadening of the diffraction peaks which shift to a position in between the expected for InP and ZnS. Probably, this is due to the pronounced lattice

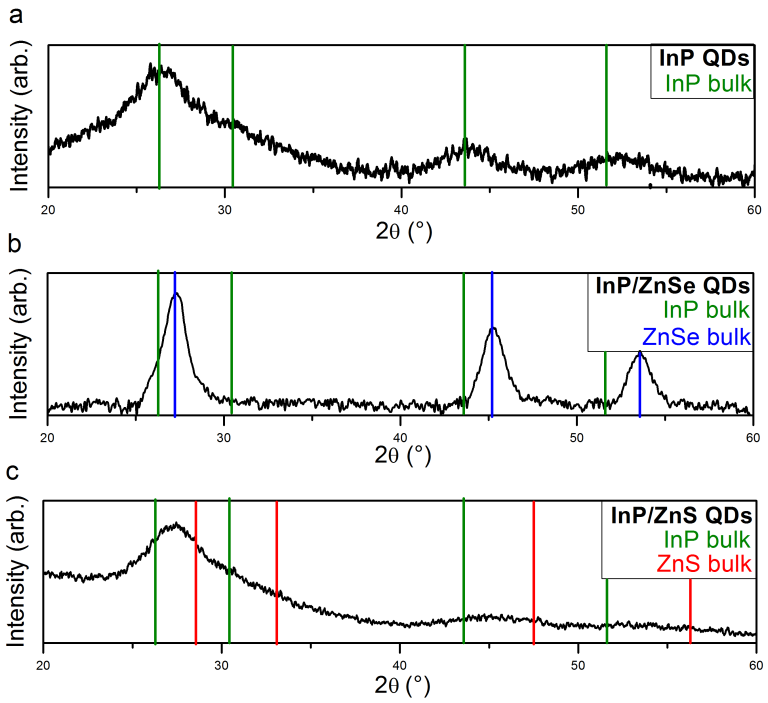


**Figure 4.2:** XRD diagrams of (**a**) InP QDs, (**b**) InP/ZnSe QDs and (**c**) InP/ZnS QDs. Peaks position: InP QDs: 26.3°, 44.0°, 52.3°. InP/ZnSe QDs: 27.3°, 45.3°, 53.6°. InP/ZnS QDs: 27.3°, 45.9°. InP zincblende bulk: 26.28°, 30.44°, 43.58°, 51.61°. ZnSe zincblende bulk: 27.22°, 45.19°, 53.57°. ZnS zincblende bulk: 28.56°, 33.09°, 47.51°, 56.29°.

mismatch between InP and ZnS (7.7 %) as described before for CdSe/CdS QDs.[5] After ZnS coating, the first exciton transition shifts to the red by ≈ 60 meV (see Figure 4.1a). Moreover, photo-excitation now leads to a marked exciton emission with a linewidth of 56 nm and a PLQY of up to 60 %. These values are close to the best obtained in literature with a $(TMS)_3P$ precursor and at a similar emission wavelength.[6]

The ZnSe shell growth procedure results in pyramidal QDs that are considerably larger than the InP/ZnS QDs (4.1d). This enhanced growth may be linked to the smaller lattice mismatch between InP and ZnSe (3.2 %). In line with this, InP/ZnSe QDs have narrow X-ray diffraction peaks, corresponding to those of bulk ZnSe (see Figure 4.2b). As compared to ZnS, ZnSe coating leads to a more considerable redshift (≈ 120 meV) of the first exciton. This can be due to its smaller band gap (2.7 eV vs. 3.6 eV

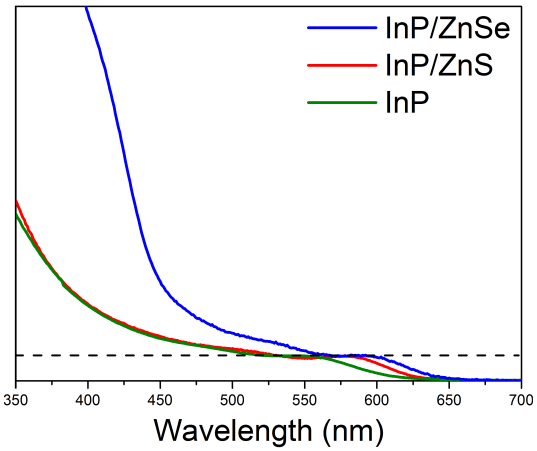


**Figure 4.3:** Absorbance spectra normalized at the first exciton of InP, InP/ZnS and InP/ZnSe QDs.

for zincblende ZnS) and its smaller conduction band offset.[7] As a result, especially the electron may be less confined in the InP core for InP/ZnSe as compared to InP/ZnS. The growth of ZnSe also results in a marked increase of the absorbance at wavelengths below 450 nm (see Figure 4.3), a wavelength that corresponds to the band gap transition of bulk ZnSe. An enhanced absorption at these wavelengths is an important advantage for white light LED application where green and red QDs are excited by a blue LED, or to reduce self-absorption in solar concentrator applications.[8] The InP/ZnSe emission linewidth is 48 nm and the PLQY is 50 %. To the best of our knowledge, it is the first time that InP/ZnSe QDs have been synthesized with such a color-pure and efficient photoluminescence. However, the emission linewidth is still almost twice the width of the CdSe QDs emission, a difference that is most likely due to a worse size-dispersion as the intrinsic emission linewidth of InP and CdSe QDs are about the same.[9]

## 4.4 Size-tunable synthesis of InP quantum dots at full chemical yield

As QD sizes govern their optical and electronic properties, a full yield synthesis is best combined with a strategy to tune the QD size at the end of the reaction rather than stopping QD growth during the synthesis. Size-tuning at full yield has been demonstrated in syntheses for CdSe and CdS QDs by varying the reaction rate, *e.g.*, through a change of the precursor concen-

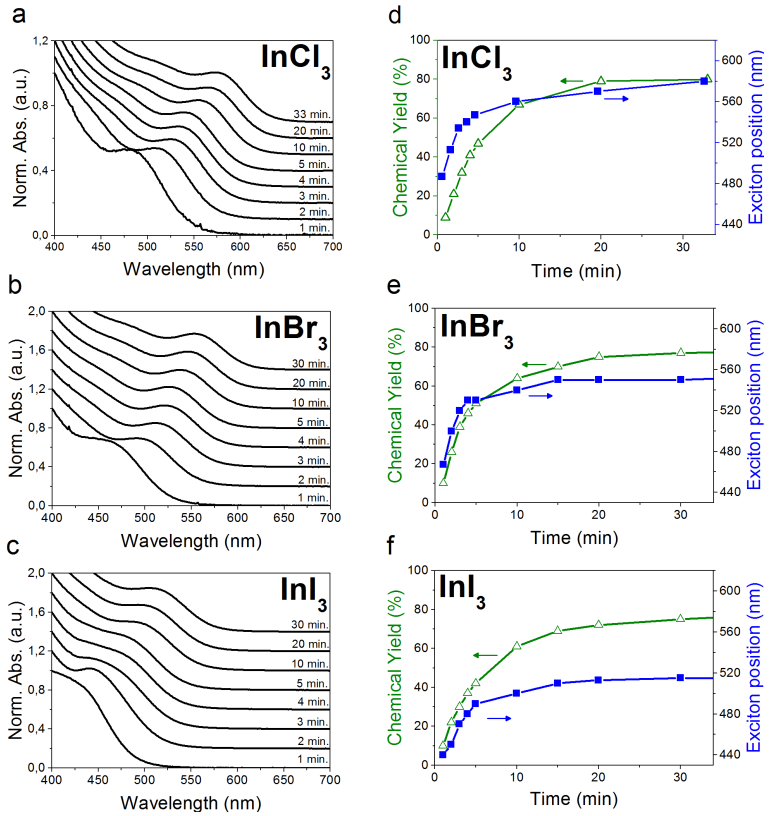


**Figure 4.4:** Development of the absorption spectrum of InP QDs using different indium precursors in combination with $ZnCl_2$ (spectra have been shifted for clarity): (**a**) $InCl_3$ (**b**) $InBr_3$ (**c**) $InI_3$. Chemical yield and exciton energy development using different indium precursors in combination with $ZnCl_2$: (**d**) $InCl_3$ (**e**) $InBr_3$ (**f**) $InI_3$.

tration.[10;11] This size-tuning strategy works with this InP QDs synthesis as well, where higher precursor concentrations indeed result in smaller QDs. However, we found that higher precursor concentrations make it harder to dissolve the solid precursors whereas decreasing the precursor concentration appears to deteriorate the size dispersion. Alternatively, size tuning at full yield and constant reaction rate proved possible with CdSe QDs, either by changing the free ligand concentration or the ligand chain length.[12;13]

A similar phenomenon is observed by changing the nature of the indium salt halide in this InP QDs synthesis. Figure 4.4a-c shows absorption spectra of aliquots taken during three InP QD syntheses that use different indium

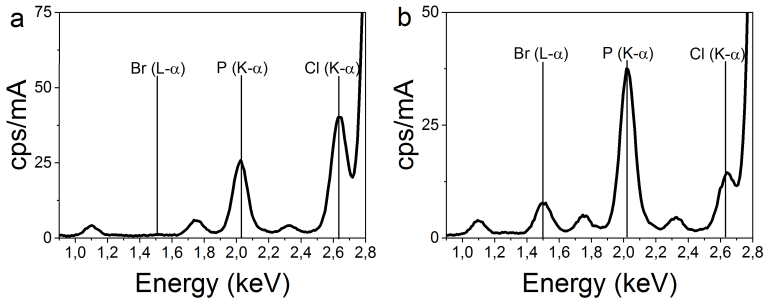


**Figure 4.5:** (**a**) XRF analysis of InP QDs made using $InCl_3$ as the indium precursor, with a zoom an the spectral region containing P, Cl and Br signals. Deduced atomic percentages: In (72 %), P (15 %), Cl (13 %), Br (0 %). (**b**) XRF analysis of InP QDs made using $InBr_3$ as the indium precursor, with a zoom on the spectral region containing P, Cl and Br signals. Deduced atomic percentages: In (77 %), P (16 %), Cl (1 %), Br (6 %). It should be noted that the XRF spectrometer has not been calibrated. Consequently the ratio between In and P is not accurate. The goal of this measurement is only to reveal the presence or absence of bromide.

halides while all other reaction conditions, *i.e.* type of phosphorous and zinc precursor, concentrations, solvent, solvent volume, temperature, etc., are kept constant. It follows that replacing Cl by Br and I leads to a systematic blueshift of the first exciton after a given reaction time, as shown more explicitly in Figure 4.4d-f. Moreover, Figure 4.4d-f also indicates that in all three cases the rate and the eventual yield (75-80 %) of InP formation are identical, irrespective of the halide used. In this way, the first exciton attained after 20 min of reaction can be changed from 560 to 540 or 520 nm by replacing $InCl_3$ by $InBr_3$ or $InI_3$, respectively. We thus conclude that the InP synthesis protocols proposed here allow for an efficient size tuning at close to full chemical yield by a mere change of the indium halide precursor, where higher atomic number halides yield smaller QDs. To the best of our knowledge, this is the first report of size-tuning at constant reaction rate through the inorganic metal salt anion.

For the initially present anion to influence the outcome of a QD synthesis, it should remain bound to the dissolved metal complex and, possibly, adsorbed at the QD surface. Although such observations have been made before for PbS QDs synthesized in oleylamine using $PbCl_2$ as a precursor,[14] it remains atypical. Indeed either Cd, Pb, Zn or In salts are most often dissolved using carboxylic or phosphonic acids as complexing agents, where the original anion is released and replaced by either a carboxylate or a phosphonate.

**Table 4.1:** InP QDs obtained at full chemical yield with different indium and zinc halides.

| | zinc dihalides | | |
|---|---|---|---|
| indium trihalides | $ZnCl_2$ (2.2 mmol) | $ZnBr_2$ (2.2 mmol) | $ZnI_2$ (2.2 mmol) |
| $InCl_3$ (0.45 mmol) | 570 (48) | 515 (51) | 420 (>80) |
| $InBr_3$ (0.45 mmol) | 550 (50) | 450 (>80) | 410 (>80) |
| $InI_3$ (0.45 mmol) | 520 (54) | 440 (>80) | 400 (>80) |

In the case of indium halides and a carboxylic acid or a phosphonic acid, this would result for example in the formation of either HCl, HBr or HI and indium(carboxylate)$_3$ or indium(phosphonate)$_3$ respectively.[15] In this case, the release of the halide anion in the reaction mixture can affect the shape of the nanocrystals.[16;17] Here however, $InX_3$ (X:halide) is dissolved in amines, which are bases that do not favor HX formation. As a result, at least part of the original anions may be retrieved in the precursor and, eventually, on the QD surface. These ideas are confirmed by the fact that the halide is detected in dried, purified InP QDs by X-ray fluorescence (see Figure 4.5) and by the finding that replacing $ZnCl_2$ for $ZnBr_2$ or $ZnI_2$ has a similar effect on the QD size (Table 4.1). For instance using $InCl_3$ with $ZnBr_2$ instead of $ZnCl_2$ leads to InP QDs with a first exciton at 515 nm instead of 560 nm after 20 min of reaction. The smallest sizes are obtained with a mixture of $InI_3$ and $ZnI_2$. As in the case of indium halides, higher atomic number halides yield smaller sizes. Unfortunately, changing the zinc halides deteriorates the size dispersion and is therefore not seen as the most effective size tuning strategy (see Table 4.1).

As mentioned before, size-tuning at constant reaction rate, as seen here with InP QDs through a change of the indium halide, has already been demonstrated for CdSe QDs.[12;13] It was shown to be due to a change in the moment that the increasing solute consumption by nanocrystal growth suppresses the nucleation of new nanocrystals. In this respect, the observation that an increase of the free acid concentration leads to larger CdSe nanocrystals could be explained by assuming that nanocrystal growth is limited by solute diffusion and that the solute solubility increases with the free acid concentration.[12] This explanation, however, is not satisfactory for this InP QDs synthesis. In the case of CdSe QDs, larger nanocrystals were only obtained at the expense of an increased size dispersion, an observation that could be explained by the above mentioned assumptions of diffusion-limited growth. With the InP synthesis studied here however, size tuning

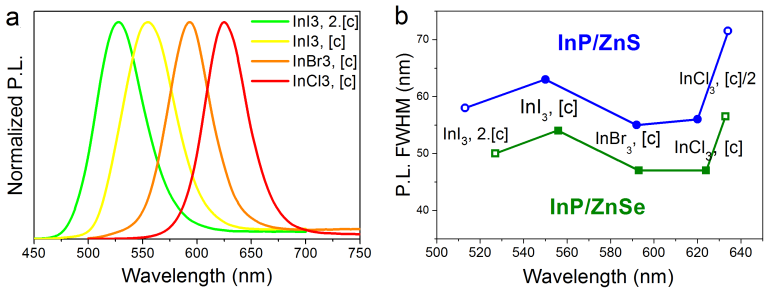


**Figure 4.6:** (**a**) Emission spectra of InP/ZnSe QDs. (**b**) Emission linewidth of InP/ZnS and InP/ZnSe made at full chemical yield using different indium halides and different precursors' concentration ([c] corresponds to 0.45 mmol of indium precursor in 5 mL of OLA).

has no noticeable effect on size dispersion, which could imply that nanocrystal growth is controlled by the rate of the surface reaction rather than solute diffusion. As argued in the Equation (4.3) in the Experimental Section, this will lead to smaller nanocrystals if the rate constant of the surface reaction is reduced and/or the solute solubility goes down when replacing $InCl_3$ by $InBr_3$ and $InI_3$. Although an understanding of such effects requires a detailed description of the nanocrystal surface termination and the composition of the actual solute, the underlying trends may not be unlikely. As amines are described as hard bases, they may coordinate more strongly complexes involving $InCl_3$ than $InI_3$, thus rendering the former more soluble. On the other hand, as the halides adsorb at the InP surface, either a different binding strength or changing steric effects may lead to systematic variations of the surface reaction rate constants. In particular the more voluminous iodide ion may render adsorption sites less accessible and thus reduce surface-reaction rates.

## 4.5 Size-tunable synthesis of InP/ZnE (E = Se, S) core/shell quantum dots at full chemical yield

We combined the full yield size-tuning with the developed shell growth strategy to obtain luminescent InP/ZnE (E = S, Se) QDs, emitting at different wavelengths. The emission spectra of different InP/ZnSe batches, shown in Figure 4.6a, indicate that a large part of the visible region can be addressed. In Figure 4.6b, the emission linewidth of several InP/ZnSe and

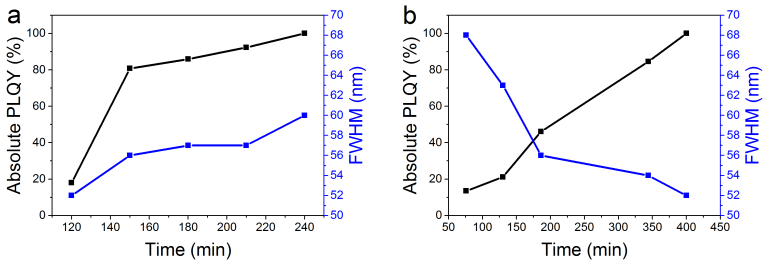


**Figure 4.7:** Evolution of the absolute photoluminescence and emission linewidth during the shell growth procedure of (**a**) InP/ZnS and (**b**) InP/ZnSe QDs

InP/ZnS samples is plotted as a function of the emission maximum. In both cases, the three central samples (filled markers) have been synthesized by changing the indium halide precursor. This gives access to emission wavelengths between roughly 550 and 630 nm for the reference conditions used. Shorter and longer wavelength of the emission maximum can be achieved by increasing the concentration of indium iodide or reducing the concentration of indium chloride respectively (Figure 4.6b, open markers). Unfortunately, a further increase of the precursor concentration is problematic due to the limited solubility of the solid precursors in oleylamine.

Figure 4.6b shows that ZnSe coating systematically leads to a more narrow emission than ZnS coating. Importantly, this is not due to a change in size dispersion of the initial cores, as the width of the first exciton transition is similar for each respective set of core syntheses. Possibly, this larger emission linewidth may originate from the higher lattice mismatch between InP and ZnS (7.7 %) than between InP and ZnSe (3.2 %). Indeed, if we measure the linewidth evolution during ZnS shell growth, we observe that the emission line progressively broadens as a function of reaction time and thus shell thickness, whereas the PLQY concomitantly increases (see Figure 4.7). This is in line with the idea that a type-I core/shell system is formed, where the increasing strain induced by the core/shell lattice mismatch leads to additional heterogeneous broadening. In this way, we managed to push the PLQY up to 80 %, at the expense however of a larger (70 nm) linewidth. Opposite from this, ZnSe shell growth leads to an increase of the photoluminescence PLQY, without the increasing linewidth during shell growth. These findings underline that in the case of InP QDs, the shell growth procedure can modify the emission linewidth without changing the size dispersion of the core QDs as it has already been observed on other colloidal nanoparticles.[18] Whereas a ZnSe shell has the advantage to exhibit more

narrow emission lines, we have observed that the PLQY of InP/ZnSe QDs dispersed in toluene decreases with time. A reduction from 50 to 15 % was for example measured after 6 months of storage in the dark and at room temperature. On the other hand, InP/ZnS QDs proof much more resistant to aging and their PLQY remains unchanged even after one year of storage in the same conditions. This indicates that an alternate solution to combine the more narrow emission lines of ZnSe shells and the enhanced stability of ZnS shell could be to make InP/ZnSe/ZnS multishell as it has been done recently for InP QDs obtained with $(TMS)_3P$.[19]

## 4.6 Conclusion

In conclusion, we have presented an economic method to size-tune the InP QDs core size at full chemical yield by playing with the inorganic moieties, linked to the metallic precursors. This full chemical yield size-tuning method combined with our shell growth procedure allows obtaining InP/ZnS and InP/ZnSe core/shell QDs with an emission that covers a large part of the visible spectrum

# References

[1] Woo-Seuk Song, Hye-Seung Lee, Ju Chul Lee, Dong Seon Jang, Yoonyoung Choi, Moongoo Choi, and Heesun Yang. *Amine-derived synthetic approach to color-tunable InP/ZnS quantum dots with high fluorescent qualities.* Journal of Nanoparticle Research, 15(6):1750, 2013.

[2] Dingan Chen, Fei Zhao, Hang Qi, Michael Rutherford, and Xiaogang Peng. *Bright and Stable Purple/Blue Emitting CdS/ZnS Core/Shell Nanocrystals Grown by Thermal Cycling Using a Single-Source Precursor.* Chemistry of Materials, 22(4):1437–1444, 2010.

[3] Dmitri V. Talapin, Andrey L. Rogach, Markus Haase, and Horst Weller. *Evolution of an Ensemble of Nanoparticles in a Colloidal Solution: Theoretical Study.* The Journal of Physical Chemistry B, 105(49):12278–12285, 2001.

[4] Arnaud Cros-Gagneux, Fabien Delpech, Céline Nayral, Alfonso Cornejo, Yannick Coppel, and Bruno Chaudret. *Surface Chemistry of InP Quantum Dots: A Comprehensive Study.* Journal of the American Chemical Society, 132(51):18147–18157, 2010.

[5] Jiaming Zhang, Xuke Zhang, and J. Y. Zhang. *Dependence of Microstructure and Luminescence on Shell Layers in Colloidal CdSe/CdS Core/Shell Nanocrystals.* The Journal of Physical Chemistry C, 114(9):3904–3908, 2010.

[6] Liang Li, Myriam Protière, and Peter Reiss. *Economic Synthesis of High Quality InP Nanocrystals Using Calcium Phosphide as the Phosphorus Precursor.* Chemistry of Materials, 20(8):2621–2623, 2008.

[7] Yoyo Hinuma, Andreas Grüneis, Georg Kresse, and Fumiyasu Oba. *Band alignment of semiconductors from density-functional theory and many-body perturbation theory.* Physical Review B, 90(15):155405, 2014.

[8] F. Meinardi, A. Colombo, K. A. Velizhanin, R. Simonutti, M. Lorenzon, L. Beverina, R. Viswanatha, V. I. Klimov, and S. Brovelli. *Large-area luminescent solar concentrators based on 'Stokes-shift-engineered' nanocrystals in a mass-polymerized PMMA matrix.* Nature Photonics, 8(5):392–399, 2014.

[9] J. Cui, A. P. Beyler, L. F. Marshall, O. Chen, D. K. Harris, D. D. Wanger, X. Brokmann, and M. G. Bawendi. *Direct probe of spectral*

*inhomogeneity reveals synthetic tunability of single-nanocrystal spectral linewidths.* Nature Chemistry, 5(7):602–606, 2013.

[10] Sofie Abe, Richard Karel Čapek, Bram De Geyter, and Zeger Hens. *Tuning the Postfocused Size of Colloidal Nanocrystals by the Reaction Rate: From Theory to Application.* ACS Nano, 6(1):42–53, 2012.

[11] Jonathan S. Owen, Emory M. Chan, Haitao Liu, and A. Paul Alivisatos. *Precursor Conversion Kinetics and the Nucleation of Cadmium Selenide Nanocrystals.* Journal of the American Chemical Society, 132(51):18206–18213, 2010.

[12] Sofie Abe, Richard K. Capek, Bram De Geyter, and Zeger Hens. *Reaction Chemistry/Nanocrystal Property Relations in the Hot Injection Synthesis, the Role of the Solute Solubility.* ACS Nano, 7(2):943–949, 2013.

[13] Stijn Flamee, Marco Cirillo, Sofie Abe, Kim De Nolf, Raquel Gomes, Tangi Aubert, and Zeger Hens. *Fast, High Yield, and High Solid Loading Synthesis of Metal Selenide Nanocrystals.* Chemistry of Materials, 25(12):2476–2483, 2013.

[14] Iwan Moreels, Yolanda Justo, Bram De Geyter, Katrien Haustraete, José C. Martins, and Zeger Hens. *Size-Tunable, Bright, and Stable PbS Quantum Dots: A Surface Chemistry Study.* ACS Nano, 5(3):2004–2012, 2011.

[15] Shu Xu, Jan Ziegler, and Thomas Nann. *Rapid synthesis of highly luminescent InP and InP/ZnS nanocrystals.* Journal of Materials Chemistry, 18(23):2653–2656, 2008.

[16] Mee Rahn Kim, Karol Miszta, Mauro Povia, Rosaria Brescia, Sotirios Christodoulou, Mirko Prato, Sergio Marras, and Liberato Manna. *Influence of Chloride Ions on the Synthesis of Colloidal Branched CdSe/CdS Nanocrystals by Seeded Growth.* ACS Nano, 6(12):11088–11096, 2012.

[17] Cristina Palencia, Koen Lauwaet, Leonor de la Cueva, Maria Acebron, Julio J. Conde, Michaela Meyns, Christian Klinke, Jose M. Gallego, Roberto Otero, and Beatriz H. Juarez. *Cl-capped CdSe nanocrystals via in situ generation of chloride anions.* Nanoscale, 6(12):6812–6818, 2014.

[18] M. D. Tessier, B. Mahler, B. Nadal, H. Heuclin, S. Pedetti, and B. Dubertret. *Spectroscopy of Colloidal Semiconductor Core/Shell*

*Nanoplatelets with High Quantum Yield.* Nano Letters, 13(7):3321–3328, 2013.

[19] Christian Ippen, Tonino Greco, and Armin Wedel. *InP/ZnSe/ZnS: A Novel Multishell System for InP Quantum Dots for Improved Luminescence Efficiency and Its application in a Light-Emitting Device.* Journal of Information Display, 13(2):91–95, 2012.

# 5

# Indium Phosphide-Based Quantum Dots with Shell-Enhanced Absorption for Luminescent Down-Conversion[1]

*InP-based QDs with shell-enhanced absorption for more efficient luminescent down-conversion are proposed. Synthetic methods to coat InP QDs with a ZnSe shell containing small amounts of Cd are developed. This allows to enhance the QD absorption at 450 nm, the typical pump wavelength for optical down-conversion, and concomitantly suppress self-absorption and reduce QD loading in QD-in-polymer based luminescent down-convertor coatings.*

## 5.1 Introduction

Displays, LEDs, or solar concentrators all make use of the efficient and spectrally narrow QD photoluminescence to convert short wavelength incident

[1] *Adapted from:* **Dorian Dupont**, Mickaël D. Tessier, Philippe F. Smet, Zeger Hens. *Shell and Surface Engineering of Indium Phosphide-Based Quantum Dots: Towards White Light-Emitting Devices.* Advanced Materials, 29(29):1700686, **2017**.

light to nearly monochromatic emitted light at a longer wavelength of choice, as determined by the dimensions and shape of the QDs.[1–7] In this respect, CdSe/CdS core/shell QDs stand out. Having a band gap of 2.42 eV (512 nm), a CdS shell can enhance both the photoluminescence quantum yield (PLQY), by passivating the CdSe outer surface, and the absorption cross section of the QDs at blue, violet and UV wavelengths.[8–12] This combination makes for high performing and economical QD down-convertors, where suppressed self-absorption translates the high PLQY of the QDs into a high internal and external PLQY of the down-convertor, while using a minimal amount of QDs.[13–15] A major drawback of this approach, however, is its reliance on compounds rich in Cd, which is a toxic heavy metal that is restricted in several countries. Hence the rise of InP-based QDs as an alternative.[16] Like Cd-based QDs, InP QDs feature a photoluminescence tunable across the visible spectrum with a high PLQY following shelling by ZnS or ZnSe.[17–22] Unfortunately, neither of these materials contributes much to the absorbance of $\approx$ 450 nm blue light, the typical LED pump wavelength in display or lighting applications. This raises the amount of QDs InP-based down-convertors need and deteriorates their conversion efficiency; a double setback in performance and cost.

Here, we address these issues by introducing InP QDs shelled by (Zn,Cd)Se alloys since admixing of Cd is known to reduce the band gap of ZnSe.[23;24] As QDs typically have higher absorption coefficients the more the photon energy exceeds the band-gap energy,[25] we expect that adding even small amounts of Cd can boost the absorbance at 450 nm and suppress self-absorption in remote phosphor films. In the case of ZnSe core QDs, band-gap tuning by addition of Cd has been achieved before via hot injection methods[26–28] or cation exchange reactions.[29;30] In addition, shells of $Zn_{0.5}Cd_{0.5}Se$ alloys have been grown around InP QDs by Micic and coworkers,[31] where this particular composition was chosen to match the core and shell lattice parameter. In spite of this lattice-matched configuration, their approach resulted in rather polydisperse samples with a broad and moderately efficient photoluminescence. We therefore first propose a new method to form InP/(Zn,Cd)Se core/shell QDs, in which an intermediate ZnSe layer is grown between the InP core and the (Zn,Cd)Se shell. We show that such core/shell QDs feature an efficient photoluminescence in combination with a considerably enhanced absorption at 450 nm, similar to CdSe/CdS QDs. Comparing nanocomposites made of InP/ZnSe and InP/(Zn,Cd)Se QDs with a 6 % Cd content, we demonstrate that the latter overcomes the issues with conversion efficiency and material economy that arise when using QDs with shells that are transparent at the pump wavelength for optical down-conversion, as is the case for ZnS or ZnSe at 450 nm.

## 5.2 Experimental section

**Chemicals:** Selenium powder 100 mesh (99.99 %) and zinc stearate (technical grade, 65 %) and cadmium acetate dihydrate (reagent grade, 98 %) were purchased from Sigma Aldrich. Trioctylphosphine (TOP; >97 %) were purchased from Strem Chemicals. Oleylamine (OLA; 80-90 %) was purchased from Acros Organics (NB: Oleylamine is stored under inert atmosphere). 1-octadecene (ODE; technical 90 %) was purchased from Alfa Aesar.

**Full chemical yield synthesis of 3.2 nm InP QDs (first excitonic absorption peak at 560 nm):** See the full chemical yield synthesis protocol of 3.2 nm InP QDs in the Experimental Section of Chapter 4. Here the quantity of chemicals have been divided by two.

**Full chemical yield synthesis of 3.0 nm InP QDs (first excitonic absorption peak at 540 nm):** See the full chemical yield synthesis protocol of 3.0 nm InP QDs in the Experimental Section of Chapter 4. Here the quantity of chemicals have been divided by two.

**Synthesis of 629 nm emitting core/shell InP/ZnSe QDs:** A 3.2 nm InP QD synthesis is performed at 180 ℃. After the InP core formation, instead of cooling down the temperature, at 20 min, 0.45 mL of stoichiometric TOP-Se (2.24 M) is injected at 180 ℃. At 140 min, a mixture of 2 g (3 mmol) of $Zn(stearate)_2$, 8 mL of ODE and 2 mL of OLA is injected. Then temperature is increased from 180 ℃ to 320 ℃ and 1.4 mL of TOP-Se is injected drop by drop during the rise of temperature. At 240 min the reaction is stopped and the temperature is lowered. InP/ZnSe QDs are then precipitated once in ethanol and suspended in toluene.

**Synthesis of 631 nm emitting core/shell InP/$Cd_{0.06}Zn_{0.94}Se$ QDs:** A 3.0 nm InP QDs synthesis is performed at 180 ℃. After the InP core formation, instead of cooling down the temperature, at 20 min, 0.45 mL of stoichiometric TOP-Se (2.24 M) is injected at 180℃. At 140 min, a mixture of 0.08 g (0.3 mmol) of $Cd(acetate)_2$ dihydrate and 1.71 g (2.71 mmol) of $Zn(stearate)_2$, (Cd to Cd+Zn molar ratio = 0.073) mixed with 8 mL of ODE and 2 mL of OLA is injected. Then temperature is increased from 180 ℃ to 320 ℃ and 1.4 mL of TOP-Se is injected drop by drop during the rise of temperature. At 240 min the reaction is stopped and the temperature is lowered. InP/$Cd_{0\cdot06}Zn_{0\cdot94}Se$ QDs are then precipitated once in ethanol and suspended in toluene.

**Synthesis of 634 nm emitting core/shell InP/$Cd_{0.025}Zn_{0.975}Se$ QDs:** A 3.2 nm InP QDs synthesis is performed at 180 ℃. After the InP core formation, instead of cooling down the temperature, at 20 min, 0.45 mL of stoichiometric TOP-Se (2.24 M) is injected at 180 ℃. At 140 min, a mixture of 0.035 g (0.13 mmol) of $Cd(acetate)_2$ and 1.794 g (2.84 mmol) of $Zn(stearate)_2$, (Cd to Cd+Zn molar ratio = 0.032) mixed with 8 mL of ODE and 2 mL of OLA is injected. Then temperature is increased from 180 ℃ to 320 ℃ and 1.4 mL of TOP-Se is injected drop by drop during the rise of temperature. At 240 min the reaction is stopped and the temperature is cooled down. InP/$Cd_{0.025}Zn_{0.975}Se$ QDs are then precipitated once in ethanol and suspended in toluene.

**Synthesis of 644 nm emitting core/shell InP/$Cd_{0.05}Zn_{0.95}Se$ QDs:** The synthesis of InP/$Cd_{0.05}Zn_{0.95}Se$ QDs follows the same protocol as outlined above but 0.035 g (0.13 mmol) of $Cd(acetate)_2$ dihydrate and 1.794 g (2.84 mmol) of $Zn(stearate)_2$ are replaced by 0.069 g (0.26 mmol) of $Cd(acetate)_2$ dihydrate and 1.706 g (2.70 mmol) of $Zn(stearate)_2$, (Cd to Cd+Zn fraction = 0.064).

**Synthesis of 664 nm emitting core/shell InP/$Cd_{0.13}Zn_{0.87}Se$ QDs:** The synthesis of InP/$Cd_{0.13}Zn_{0.87}Se$ QDs follows the same protocol as outlined above but 0.035 g (0.13 mmol) of $Cd(acetate)_2$ dihydrate and 1.794 g (2.84 mmol) of $Zn(stearate)_2$ are replaced by 0.150 g (0.56 mmol) of $Cd(acetate)_2$ dihydrate and 1.52 g (2.4 mmol) of $Zn(stearate)_2$, (Cd to Cd+Zn fraction = 0.138).

**QD-doped remote phosphor layers - formation:** Remote phosphor layers containing either InP/ZnSe or InP/$Cd_{0.06}Zn_{0.94}Se$ QDs were prepared by mixing an appropriate amount of these materials with 80 mg of Kraton FG1901X in 0.5 mL of toluene, stirring, and drop casting on a circular glass substrate with a diameter of 1.8 cm and a corresponding area of 2.54 $cm^2$. After evaporation of the solvents, transparent QD phosphor layers are obtained.

**QD-doped remote phosphor layers - characterization:** Layer efficiency measurements were performed inside an integrating sphere (152 mm, Spectralon coated). Excitation of the samples was done with a blue LED ($\lambda_{max}$ of 446.5 nm, FWHM of 19.2 nm and LER of 37 lm/W) and detection of outgoing light by a CCD camera (Princeton Instruments ProEM 16002), attached to a spectrograph (Princeton Instruments Acton SP2358).

A baffle is mounted between the sample and the detection port of the integrating sphere. Internal and external quantum efficiency were determined by the two measurement approach.[32] The external quantum yield is defined as the ratio between the numbers of photons emitted by and incident on the phosphor layer, whereas the internal quantum yield is the ratio between the number of photons emitted and photons absorbed by the remote phosphor layer.[33] In this work, always the internal PLQY is reported. QDs layers were analyzed by introducing the circular layer in a cylindrical, white teflon mixing chamber with a height of 20 mm, which contains the blue LED in the bottom center for excitation. The measurements were operated at a constant current of 20 mA, which translates in a luminous efficacy of the blue LED of 7.26 lm/W.

**Calculation of the experimental interplanar spacing $d_{(exp)}$:** The experimental interplanar distance $d_{(exp)}$ can be calculated from the Bragg's law:

$$d_{(exp)} = \frac{\lambda}{2sin\theta} \tag{5.1}$$

Here $\lambda = 1{,}5418$ Å which correspond to the wavelength of the incident CuK$\alpha$ radiation and $\theta$ the scattering angle expressed in radians (See Experimental Section in Chapter 3).

**Calculation of $d_{(220)}$ values for zincblende $Cd_xZn_{1-x}Se$ (see red line in Figure 5.4b):**

$$d_{(hkl)ZB} = \frac{a_{(Cd_xZn_{1-x}Se)ZB}}{\sqrt{h^2+k^2+l^2}} = \frac{xa_{(CdSe)ZB} + (1-x)a_{(ZnSe)ZB}}{\sqrt{h^2+k^2+l^2}} \tag{5.2}$$

Here $h$, $k$, and $l$ are the Miller indices of the Bragg plane and $a_{(Cd_xZn_{1-x}Se)ZB}$ is the lattice spacing of zincblende $Cd_xZn_{1-x}Se$ material which is expressed according to the Vegard's law.[34] Since $a_{(CdSe)ZB} = 6.08$ Å and $a_{(ZnSe)ZB} = 5.67$ Å, the $d_{(220)}$ values of zincblende $Cd_xZn_{1-x}Se$ is given by:

$$d_{(220)ZB} = \frac{x6.08 + (1-x)5.67}{2\sqrt{2}} \tag{5.3}$$

**Calculation of $d_{(110)}$ values for wurtzite $Cd_xZn_{1-x}Se$ (see blue line in Figure 5.4b):**

$$d_{(hkl)WZ} = \frac{\sqrt{3}}{2}\frac{a_{(Cd_xZn_{1-x}Se)WZ}}{\sqrt{h^2+hk+k^2}} + \frac{c_{(Cd_xZn_{1-x}Se)WZ}}{l} \tag{5.4}$$

Here $h$, $k$, and $l$ are the Miller indices of the Bragg plane and $a_{(Cd_xZn_{1-x}Se)WZ}$ and $c_{(Cd_xZn_{1-x}Se)WZ}$ the lattice constants of wurtzite $Cd_xZn_{1-x}Se$ material which can be expressed according to the Vegard's law. [34] According to Equation (5.4), the $d_{(hkl)}$ values of wurtzite $Cd_xZn_{1-x}Se$ material for $h = 1$, $k = 1$ and $l = 0$ is:

$$d_{(110)WZ} = \frac{a_{(Cd_xZn_{1-x}Se)WZ}}{2} = \frac{xa_{(CdSe)WZ} + (1-x)a_{(ZnSe)WZ}}{2} \quad (5.5)$$

Since $a_{(CdSe)WZ} = 4.30$ Å and $a_{(ZnSe)WZ} = 3.98$ Å, the $d_{(110)}$ values of wurtzite $Cd_xZn_{1-x}Se$ is given by:

$$d_{(110)WZ} = \frac{x4.30 + (1-x)3.98}{2} \quad (5.6)$$

**Theoretical peak positions $2\theta$ of bulk zincblende ZnSe and wurtzite ZnSe and CdSe (see vertical lines in Figure 5.4a):**

ZnSe ZB (red lines): 27.22°, 45.2°, 53.56°.
ZnSe WZ (blue lines): 25.72°, 26.89°, 29.09°, 37.55°, 45.35°, 48.88°, 53.51°.
CdSe WZ (green lines): 23.89°, 25.39°, 27.10°, 35.14°, 42.00°, 45.81°, 49.72°.

**Experimental peak positions $2\theta_{(exp)}$ of InP/$Cd_xZn_{1-x}Se$ QDs (see Figure 5.4a):**

InP/ZnSe QDs: 27.19°, **45.20°**, 53.52°.
InP/$Cd_{0.025}Zn_{0.975}Se$ QDs: 27.17°, **45.10°**, 52.38°.
InP/$Cd_{0.05}Zn_{0.95}Se$ QDs: 27.06°, **44.89°**, 53.11°.
InP/$Cd_{0.13}Zn_{0.87}Se$ QDs: 26.85°, **44.55°**, 52.68°.

Focusing on the zincblende (220) / wurtzite (110) peak positions of InP/$Cd_xZn_{1-x}Se$ QDs (indicated in bold above) and according to Equation (5.1) we can calculate the $d_{(exp)}$ for x = 0, 0.025, 0.05, 0.13 (see black markers in Figure 5.4b). We found:

$d_{(exp)}$ = 2,006009323 Å for x = 0.
$d_{(exp)}$ = 2,010224407 Å for x = 0.025.
$d_{(exp)}$ = 2,019992511 Å for x = 0.05.
$d_{(exp)}$ = 2,033755624 Å for x = 0.13.

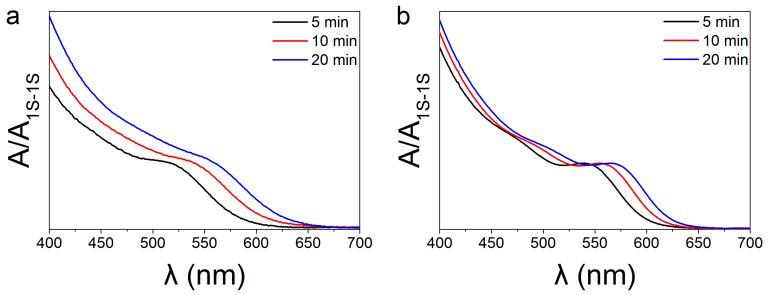


**Figure 5.1:** (**a**) Absorbance spectra of aliquots using the synthesis protocol of 3.2 nm InP QDs (see Experimental Section) but the 150 mg (1.1 mmol) of $ZnCl_2$ are replaced by 22 mg (0.11 mmol) of $CdCl_2$ and 135 mg (0.99 mmol) of $ZnCl_2$. (**b**) Absorbance spectra of aliquots using the synthesis protocol of 3.2 nm InP QDs (see Experimental Section). Admixing $CdCl_2$ during the initial InP core synthesis induces an undesired redshift and a broadening of the first exciton transition. All spectra have been normalized relative to the absorbance maximum $A_{1S\text{-}1S}$ of the band-edge feature.

## 5.3 Synthesis of $InP/Zn_{1-x}Cd_xSe$ quantum dots

Core InP QDs were synthesized according to the protocols outlined in the Experimental Section where tris(diethylamino)phosphine reacts with indium chloride or indium bromide dissolved in oleylamine in the presence of zinc chloride.[35–39] Whereas this reaction mixture readily lends itself to ZnSe shelling, where the trioctylphosphine selenide (TOP-Se) added reacts with the $ZnCl_2$ already present, the formation of alloyed (Zn,Cd)Se shells requires more care. A mere partial replacement of $ZnCl_2$ by $CdCl_2$ results in a redshift and a broadening of the first exciton transition (see Figure 5.1a-b), especially during the shell growth stage through TOP-Se addition (see Figure 5.2). Whereas such changes are in line with reported effects of Cd carboxylate adsorption to InP QDs[40] - indicating that CdSe shell growth is feasible with the same procedure - this is better avoided here. Indeed, also during the formation of (Zn,Cd)Se QDs,[41;42] it is typically seen that the Cd precursor reacts more easily with Se than the Zn precursor and the ensuing InP/CdSe interface will exhibit a staggered, type-II band alignment that comes with an undesired redshift and broadening of the emission.[43] We therefore developed an alternative approach where first an initial ZnSe layer is grown around the InP core QDs at relatively low temperature. Next, a mixture of Zn and Cd carboxylates is injected, the temperature is set to

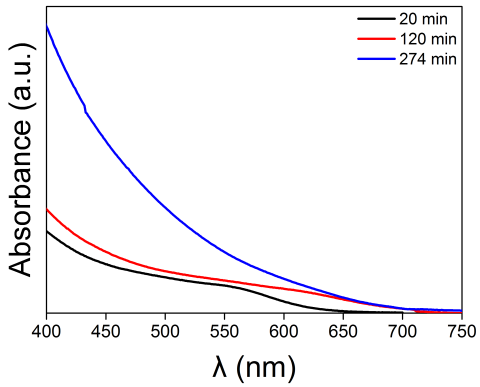


**Figure 5.2:** Absorption spectra during shell growth using the synthesis protocol of 631 nm emitting InP/$Cd_{0.06}Zn_{0.94}Se$ QDs (see Experimental Section) but 150 mg (1.1 mmol) of $ZnCl_2$ is replaced by 22 mg (0.11 mmol) of $CdCl_2$ and 135 mg (0.99 mmol) of $ZnCl_2$. Admixing $CdCl_2$ during the initial InP core synthesis induces an undesired redshift and a broadening of the first exciton transition.

increase and TOP-Se is added dropwise to form an alloyed (Zn,Cd)Se shell. Eventually, the reaction mixture is kept for three hours at 320 ℃.

## 5.4 Characterization of InP/$Zn_{1-x}Cd_xSe$ quantum dots

In the case of a reaction that uses a molar fraction of Cd to Cd+Zn precursors of 3.2 % this protocol results in a 50 nm redshift of the band-edge absorption, which hardly broadens, and a strong enhancement of the absorbance at shorter wavelengths, see Figure 5.3a. Transmission electron microscopy (TEM) images indicate that the thus formed QDs have an average projected diameter of 13.5 nm as compared to the 10.2 nm found for core/shell QDs grown using a Zn-only procedure (see Figure 5.3b-c and Table 5.1). Similar results are obtained upon increasing the Cd precursor fraction to 6.4 % and 13.8 % (Figure 5.3d-e and Table 5.1). Moreover, according to TEM-based energy dispersive X-ray spectroscopy, the Cd to Cd+Zn ratio ($x_{Cd}$) of these core/shell QDs largely corresponds to what is used in the synthesis (see Table 5.2). X-ray diffraction patterns of InP/(Zn,Cd)Se with different Cd composition are shown in Figure 5.4. The patterns indicate a progressive transition from zincblende to wurtzite upon increasing the Cd content, yet the gradual shift of the zincblende (220) / wurtzite (110)

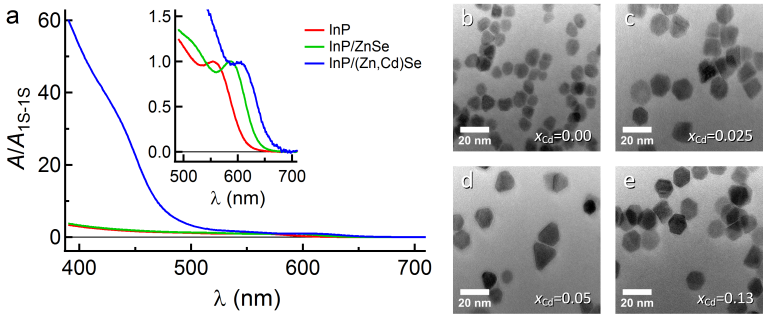


**Figure 5.3:** (**a**) Absorption spectra recorded on aliquots taken during different stages of an InP/(Zn,Cd)Se synthesis with $x_{Cd}$=0.025. (red) InP QDs before the injection of TOP-Se to start the growth of an initial ZnSe shell. (green) InP/ZnSe QDs before the addition of the Zn/Cd carboxylates mixture to grow the (Zn,Cd)Se shell. (blue) InP/(Zn,Cd)Se QDs three hours after starting the (Zn,Cd)Se shell growth. All spectra have been normalized relative to the absorbance maximum $A_{1S-1S}$ of the band-edge feature. The inset shows a zoom on the band-edge transition. (**b-e**) Bright field TEM micrographs of InP/(Zn,Cd)Se QDs with $x_{Cd}$ as indicated. The scale bar always corresponds to 20 nm.

diffraction peak towards a larger lattice spacing is in line with the supposed formation of an alloyed (Zn,Cd)Se shell with increasing Cd content. The structural transformation from zincblende to wurtzite could arise from the polytypism in ZnSe and CdSe materials. Indeed, zincblende CdSe can transform into wurtzite at temperature above 95 °C,[44] whereas the low difference in the total energy between the zincblende and the wurtzite structure of ZnSe (5,3 meV/atom) make possible such structural change.[45] In addition, it was reported in the literature that primary amines could promote a zincblende to wurtzite CdSe crystalline transition and induce a subsequent wurtzite shell growth in the case of CdSe/CdS nanocrystals.[46] We thus conclude that the implemented synthesis protocol results in InP/(Zn,Cd)Se core/shell QDs, where the composition of the shell can be readily tuned by varying the Cd precursor fraction in the synthesis.

Figure 5.5a shows absorbance spectra, normalized to the maximum absorbance at the band-edge transition and photoluminescence (PL) spectra of InP/$Cd_xZn_{1-x}Se$ core/shell QDs with $x_{Cd}$ increasing from 0 to 0.025, 0.05, and 0.13. It follows that the increase of $x_{Cd}$ concurs with a marked enhancement of the absorbance in the blue part of the visible spectrum. In addition, it leads to a progressive redshift of the band-edge PL, which

**Table 5.1:** Diameter statistics of InP/(Zn,Cd)Se QDs for $x_{Cd}$=0, 0.025, 0.05, 0.13 (referred to as InP/$Cd_xZn_{1-x}Se$) as derived from the bright field TEM images.

| QDs | Mean Diameter (nm) | Standard Deviation (nm) | Minimum Diameter (nm) | Median Diameter (nm) | Maximum Diameter (nm) |
|---|---|---|---|---|---|
| **InP/ZnSe** | **10.2** | 0.88 | 8.22 | 10.29 | 12.12 |
| **InP/$Zn_{0.975}Cd_{0.025}Se$** | **13.5** | 1.13 | 10.31 | 13.89 | 15.19 |
| **InP/$Zn_{0.95}Cd_{0.05}Se$** | **13.2** | 1.43 | 10.01 | 13.38 | 16.43 |
| **InP/$Zn_{0.87}Cd_{0.13}Se$** | **13.3** | 1.22 | 10.23 | 13.45 | 15.44 |

**Table 5.2:** Overview of the outcome of EDX analyses on InP/(Zn,Cd)Se QDs synthesized using the synthesis protocols outlined in the Experimental Section, focusing on the Zn, Cd and Se content. One sees that the Cd/(Cd+Zn) atom ratio closely follows the molar ratio of the Cd and Zn precursors used during synthesis.

| Element | Atom% QDs Reference 2 Protocol | Atom% QDs Reference 3 Protocol | Atom% QDs Reference 4 Protocol |
|---|---|---|---|
| **Zn K** | **48.3** | **49.4** | **42.1** |
| Se L | 50.5 | 48.0 | 51.4 |
| **Cd L** | **1.2** | **2.6** | **6.5** |
| **Cd/(Cd+Zn)** | **0.025** | **0.050** | **0.13** |

only shows some notable broadening at the highest molar fraction of Cd ($x_{Cd}$=0.13). Both trends are in line with what can be expected for InP core QDs shelled with (Zn,Cd)Se alloys. Indeed, a simple linear interpolation of semiconductor properties[47] already suggests that admixing Cd into a ZnSe shell will reduce the band gap of the shell and lower the core/shell conduction band offset, see Figure 5.5b. Moreover, both effects will be enhanced by the positive band-gap bowing of (Zn,Cd)Se alloys.[48] With the (Zn,Cd)Se band gap shifting from 2.72 (456 nm) to 1.74 eV (710 nm), the band-gap reduction accounts for the enhanced absorption at short wavelengths. Moreover, the reduced conduction-band offset will promote the spreading of the electron wavefunction in the shell. This leads to an enhanced red shift with increasing shell thickness – an effect also seen in CdSe/CdS QDs[9] – and increasing Cd content.

With a bulk band gap of about 2.72 eV (456 nm), the InP/ZnSe shells will not benefit from an enhanced shell absorbance at around 450 nm, the typical wavelength range of blue LEDs used in lighting and display applications. This has several drawbacks. With only the InP cores contributing to the absorption of the blue pump light, a larger mass or volume of QDs is needed to reach a preset absorptance at 450 nm. Moreover, as the absorption

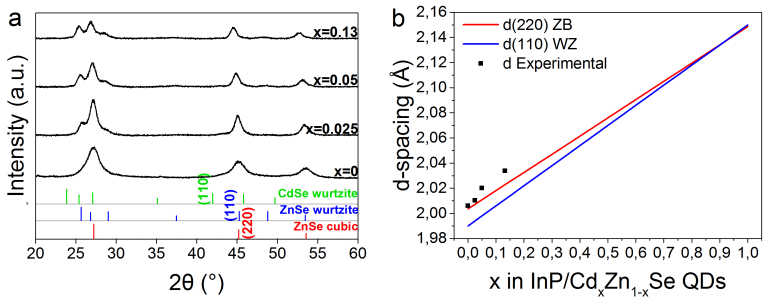


**Figure 5.4:** (**a**) XRD patterns of InP/$Cd_xZn_{1-x}Se$ QDs for x=0, 0.025, 0.05, 0.13. Whereas the InP/ZnSe diffractogram (x=0) points towards a zincblende structure, typical wurtzite diffraction peaks appear with increasing Cd content. To assess the influence of Cd admixing, we therefore focus on the zincblende (220) / wurtzite (110) diffraction peak. Measuring the cation-cation distance, these coincide for zincblende and wurtzite CdSe and are only slightly shifted for zinblende and wurtzite ZnSe. (**b**) (black markers) experimental $d_{(exp)}$ as derived from the zincblende (220) / wurtzite (110) diffraction peak (see Experimental Section); (red line) linear interpolation between the zincblende (220) lattice spacing for ZnSe and CdSe (see Equation 5.3 Experimental Section); (blue line) linear interpolation between the wurtzite (110) lattice spacing for ZnSe and CdSe (see Equation 5.6 Experimental Section). Although the experimental lattice plane spacing does not fully coincide with either of these trendlines, its variation is comparable to what is predicted based on such linear interpolations.

cross section at 450 nm (pump LED) and at the wavelength of the band-edge photoluminescence will be similar, InP/ZnSe based nanocomposites are prone to self-absorption and the concomitant efficiency loss. Similar to CdSe/CdS QDs where the CdS shell enhances the QD absorption absorption cross section below 500 nm. Figure 5.5a shows that alloyed (Zn,Cd)Se shells can overcome this issue in the case of InP core/shell QDs.

To demonstrate this point, we synthesized InP/ZnSe and InP/$Cd_{0.06}Zn_{0.94}Se$ core/shell QDs, where different InP core diameters were selected to attain a similar band-edge absorption and photoluminescence. Absorption and emission spectra of both QDs, dispersed in toluene, are represented in Figure 5.6a. The spectra confirm that both samples exhibit an almost identical band-edge absorbance and a highly similar PL spectrum with a peak intensity $\lambda_{max}$ at around 631 nm. Admixing Cd, however, results in a somewhat lower PLQY of 45 % as compared to the 60 % measured for InP/ZnSe with rhodamine 6G as reference. Possibly, this reflects the enhanced delocaliza-

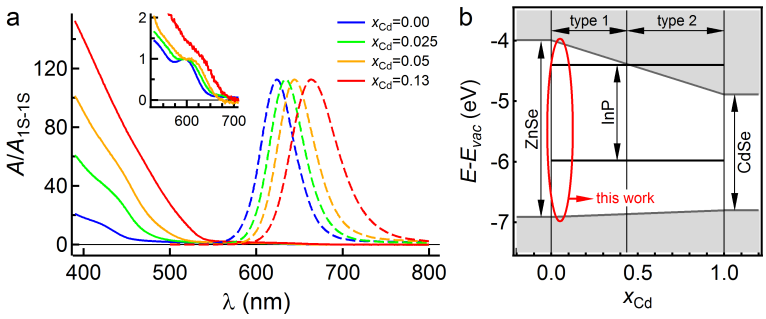


**Figure 5.5:** (**a**) Overview of (full lines) absorption and (dashed lines) emission spectra of InP/(Zn,Cd)Se core/shell QDs with $x_{Cd}$ as indicated. All spectra are recorded on reaction aliquots taken at the end of the reaction as described in Experimental Section. All spectra have been normalized relative to the absorbance maximum $A_{1S-1S}$ of the band-edge feature. The inset shows a zoom on the band-edge transition. (**b**) Simplified energy gap and band alignment diagram of (Zn,Cd)Se alloys constructed as a linear interpolation between the energy levels of ZnSe and CdSe as calculated in ref[47]. The bold horizontal lines represent the energy levels of InP, showing a transition from type I to type II alignment when changing from InP/ZnSe to InP/CdSe.

tion of the electron wavefunction in the shell, which makes charge carrier trapping at the QD outer surface more likely, and higher PLQYs may result from further ZnSe or ZnS shell growth. Moreover, the selective boosting of the absorbance of blue light as compared to red and green makes such core/shell QDs ideal as light convertors for devices pumped by blue LEDs.

## 5.5 Remote phosphor characterization

Both types of QDs were processed in remote phosphor coatings by dispersing a predetermined amount of QDs in Kraton FG1901X, a triblock copolymer based on styrene and ethylene/butylene, with a polystyrene content of 30 %, see Figure 5.6b. Figure 5.7a shows the emission spectrum obtained when pumping such layers containing InP/ZnSe QDs in a remote phosphor configuration with a blue LED and recorded in an integrating sphere. Here, the bands at around 450 and 640 nm correspond to the transmitted blue pump light and the QD photoluminescence, respectively. As expected, less blue light is transmitted and more red light emitted upon increasing the QD loading in the film. However, the emission spectra already indicate that the

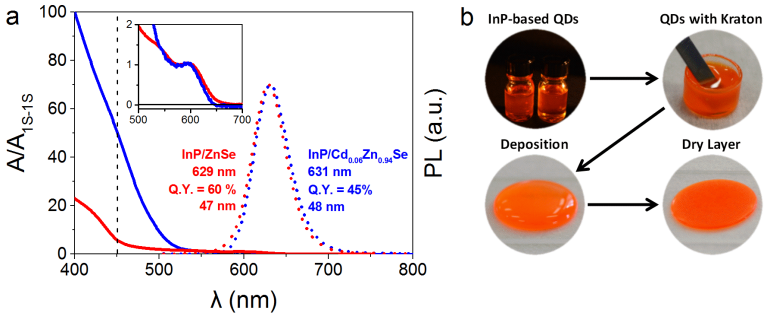


**Figure 5.6:** (**a**) Overview of (full lines) absorption and (dotted lines) emission spectra of (red) InP/ZnSe QDs and (blue) $x_{Cd}$=0.06 InP/(Zn,Cd)Se QDs (abbreviated here as InP/$Cd_{0.06}Zn_{0.94}$Se). The absorbance spectra have been normalized relative to the absorbance maximum $A_{1S\text{-}1S}$ of the band-edge feature. The inset shows a zoom on the band-edge transition. (**b**) Scheme outlining the preparation of remote phosphor disks. InP-based QDs are mixed with kraton to form a solvent-based dispersion that is casted and dried to obtain a solid remote phosphor disk. The dry remote phosphor disks have a surface area of 2.54 $cm^2$.

increase of the integrated emission intensity from the QDs does not match the reduction in the intensity of the blue pump light, while at the same time $\lambda_{max}$ exhibits a progressive redshift. Both trends can be seen more clearly in Figures 5.7b-c, showing that at an absorptance of 94.5 %, the internal PLQY of the InP/ZnSe emission (see the Experimental Section for a definition of internal and external PLQY) has dropped from the originally 60 % in suspension to a mere 38 %, whereas $\lambda_{max}$ has shifted to 650 nm, 21 nm to the red as compared to a suspension of the same InP/ZnSe QDs. Both effects are a signature of self-absorption, where QDs absorb the luminescent light emitted by other QDs. Indeed, after each absorption and re-emission cycle, only a fraction of the light intensity, corresponding to the PLQY measured in solution, is retained. Moreover, the reduced QD absorbance at longer wavelengths makes that self-absorption mostly affects the blue side of the QD photoluminescence. Hence the efficiency drops and the spectral redshift.

In contrast to the layers containing InP/ZnSe QDs, the InP/(Zn,Cd)Se QD layers show no dropping internal PLQY and feature a strongly reduced redshift of $\lambda_{max}$ with increased QD loading, see Figures 5.7a-c. For a 91 % absorptance, a PLQY of 43 % is measured, while $\lambda_{max}$ has shifted to the red by only 8 nm as compared to the emission of dilute QD suspensions.

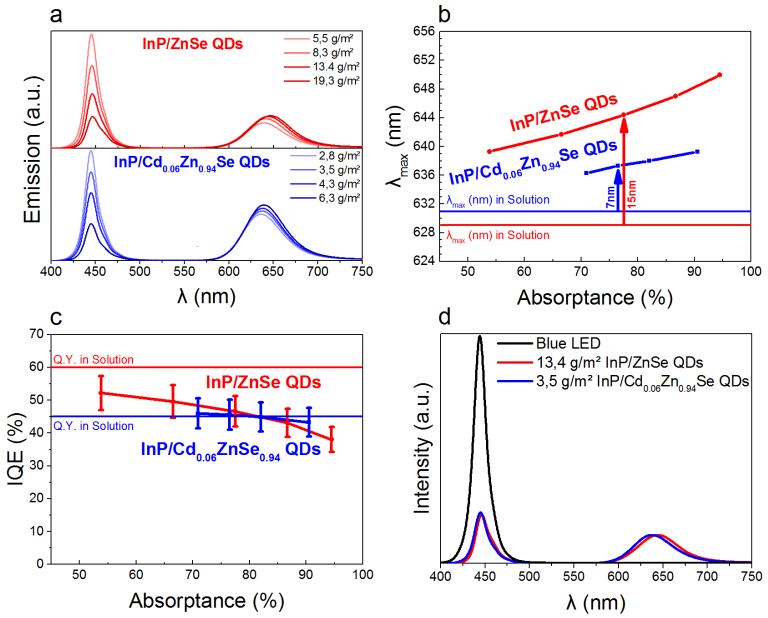


**Figure 5.7:** (**a**) Emission spectra upon excitation by a blue pump LED of remote phosphor disks containing (red) InP/ZnSe and (blue) $x_{Cd}$=0.06 InP/(Zn,Cd)Se QDs (abbreviated here as InP/$Cd_{0.06}Zn_{0.94}$Se) with different solid loadings as indicated in the legend. (**b**) Variation of the wavelength of maximum emission intensity as a function of the absorptance of blue pump light by the remote phosphor disk of layers containing (red) InP/ZnSe or (blue) InP/$Cd_{0.06}Zn_{0.94}$Se QDs. (**c**) The same for the internal quantum efficiency. The error bars represent the estimated uncertainty of 5 % on the internal quantum efficiency determination. (**d**) Emission spectra of ≈ 77 % absorptance layers of (red) InP/ZnSe and (blue) InP/$Cd_{0.06}Zn_{0.94}$Se with respective solid loadings of 13.4 and 3.5 g/$m^2$.

Both effects point towards an effective suppression of self-absorption, in line with the enhanced absorption cross-section due to Cd admixing at 450 nm. The consequence of this is best appreciated by focusing on the example of ≈ 77 % absorptance layers. Despite the original difference in PLQY – 60 % vs. 45 % – both remote phosphor layers effectuate a similar color conversion, see Figures 5.7d. Moreover, thanks to the absorption-enhancing alloyed shells, InP/(Zn,Cd)Se layers with $x_{Cd}$ = 0.06 achieve this with a solid loading, *i.e.*, the sheer weight of the QDs incorporated, that is only 26 % of what InP/ZnSe layers need. Clearly, this weight saving directly translates into a reduced use of InP in InP/(Zn,Cd)Se-based remote phosphors.

Moreover, a solid loading of 3.5 g/m$^2$ as needed here for InP/(Zn,Cd)Se QDs is comparable to the 0.5-1.5 g/m$^2$ solid loading needed in CdSe/CdS based color convertors.[15] Hence, while not entirely Cd-free, a 20-fold reduction of the Cd content in remote phosphor disks can be attained by the approach presented here, while preserving the exquisite self-absorption suppressing characteristics of CdSe/CdS-based QDs.

## 5.6 Conclusion

Summing up, we have presented an approach to enhance the absorption cross section of InP-based QDs in the blue region of the visible spectrum by shelling InP core QDs with a (Zn,Cd)Se alloy. The optical properties of these core/shell QDs point towards a reduced shell band gap and an enhanced electron delocalization, similar to the seminal CdSe/CdS core/shell QDs. We have demonstrated the impact of shell-enhanced absorption on the economy of QD-based color conversion by studying QD-loaded polymer films as remote phosphors. Comparing InP/ZnSe and InP/(Zn,Cd)Se loaded films, we find that the latter significantly suppresses the detrimental effects of self-absorption and can achieve the same color conversion using 74 % less QDs by mass. Often acclaimed as an alternative for Cd-based QDs, InP QDs face issues for widespread use as color convertors in view of the cost and scarcity of indium. Hence, a strategy such as shell-enhanced absorption that lowers the amount of InP QD-based color convertors need makes a difference. Moreover, the approach leaves ample room for further progress. Either increasing the shell volume or raising the Cd fraction in the shell will further enhance the shell absorption. In addition, admixing other elements can have similar effects, where especially a partial replacement of selenium by tellurium is a possible alternative.

# References

[1] Eunjoo Jang, Shinae Jun, Hyosook Jang, Jungeun Lim, Byungki Kim, and Younghwan Kim. *White-Light-Emitting Diodes with Quantum Dot Color Converters for Display Backlights.* Advanced Materials, 22(28):3076–3080, 2010.

[2] J. Lee, V. C. Sundar, J. R. Heine, M. G. Bawendi, and K. F. Jensen. *Full Color Emission from II–VI Semiconductor Quantum Dot–Polymer Composites.* Advanced Materials, 12(15):1102–1105, 2000.

[3] S Nizamoglu, T Ozel, E Sari, and H V Demir. *White light generation using CdSe/ZnS core–shell nanocrystals hybridized with InGaN/GaN light emitting diodes.* Nanotechnology, 18(6):065709, 2007.

[4] Q. Sun, Y. A. Wang, L. S. Li, D. Y. Wang, T. Zhu, J. Xu, C. H. Yang, and Y. F. Li. *Bright, multicoloured light-emitting diodes based on quantum dots.* Nature Photonics, 1(12):717–722, 2007.

[5] Ho Seong Jang, Heesun Yang, Sung Wook Kim, Ji Yeon Han, Sang-Geun Lee, and Duk Young Jeon. *White Light-Emitting Diodes with Excellent Color Rendering Based on Organically Capped CdSe Quantum Dots and $Sr_3SiO_5$:$Ce^{3+}$,$Li^+$ Phosphors.* Advanced Materials, 20(14):2696–2702, 2008.

[6] Jeonghun Kwak, Wan Ki Bae, Donggu Lee, Insun Park, Jaehoon Lim, Myeongjin Park, Hyunduck Cho, Heeje Woo, Do Y. Yoon, Kookheon Char, Seonghoon Lee, and Changhee Lee. *Bright and Efficient Full-Color Colloidal Quantum Dot Light-Emitting Diodes Using an Inverted Device Structure.* Nano Letters, 12(5):2362–2366, 2012.

[7] S. A. McDonald, G. Konstantatos, S. Zhang, P. W. Cyr, E. J. Klem, L. Levina, and E. H. Sargent. *Solution-processed PbS quantum dot infrared photodetectors and photovoltaics.* Nature Materials, 4(2):138–42, 2005.

[8] Xiaogang Peng, Michael C. Schlamp, Andreas V. Kadavanich, and A. P. Alivisatos. *Epitaxial Growth of Highly Luminescent CdSe/CdS Core/Shell Nanocrystals with Photostability and Electronic Accessibility.* Journal of the American Chemical Society, 119(30):7019–7029, 1997.

[9] J. Jack Li, Y. Andrew Wang, Wenzhuo Guo, Joel C. Keay, Tetsuya D. Mishima, Matthew B. Johnson, and Xiaogang Peng. *Large-Scale Synthesis of Nearly Monodisperse CdSe/CdS Core/Shell Nanocrystals Us-*

*ing Air-Stable Reagents via Successive Ion Layer Adsorption and Reaction.* Journal of the American Chemical Society, 125(41):12567–12575, 2003.

[10] D. Pan, Q. Wang, S. Jiang, X. Ji, and L. An. *Synthesis of Extremely Small CdSe and Highly Luminescent CdSe/CdS Core–Shell Nanocrystals via a Novel Two-Phase Thermal Approach.* Advanced Materials, 17(2):176–179, 2005.

[11] J. Lim, S. Jun, E. Jang, H. Baik, H. Kim, and J. Cho. *Preparation of Highly Luminescent Nanocrystals and Their Application to Light-Emitting Diodes.* Advanced Materials, 19(15):1927–1932, 2007.

[12] O. Chen, J. Zhao, V. P. Chauhan, J. Cui, C. Wong, D. K. Harris, H. Wei, H. S. Han, D. Fukumura, R. K. Jain, and M. G. Bawendi. *Compact high-quality CdSe-CdS core-shell nanocrystals with narrow emission linewidths and suppressed blinking.* Nat Mater, 12(5):445–451, 2013.

[13] Jana Bomm, Andreas Büchtemann, Angela Fiore, Liberato Manna, James H. Nelson, Diana Hill, and Wilfried G. J. H. M. van Sark. *Fabrication and spectroscopic studies on highly luminescent CdSe/CdS nanorod polymer composites.* Beilstein Journal of Nanotechnology, 1:94–100, 2010.

[14] Zachar Krumer, Suzanne J. Pera, Relinde J.A. van Dijk-Moes, Yiming Zhao, Alexander F.P. de Brouwer, Esther Groeneveld, Wilfried G.J.H.M. van Sark, Ruud E.I. Schropp, and Celso de Mello Donegá. *Tackling self-absorption in luminescent solar concentrators with type-II colloidal quantum dots.* Solar Energy Materials and Solar Cells, 111:57–65, 2013.

[15] Sofie Abe, Jonas J. Joos, Lisa I. D. J. Martin, Zeger Hens, and Philippe F. Smet. *Hybrid remote quantum dot/powder phosphor designs for display backlights.* Light: Science & Applications, 6(e16271), 2017.

[16] S. Tamang, C. Lincheneau, Y. Hermans, S. Jeong, and P. Reiss. *Chemistry of InP Nanocrystal Syntheses.* Chemistry of Materials, 28(8):2491–2506, 2016.

[17] Renguo Xie, David Battaglia, and Xiaogang Peng. *Colloidal InP Nanocrystals as Efficient Emitters Covering Blue to Near-Infrared.* Journal of the American Chemical Society, 129(50):15432–15433, 2007.

[18] Liang Li and Peter Reiss. *One-pot Synthesis of Highly Luminescent InP/ZnS Nanocrystals without Precursor Injection.* Journal of the American Chemical Society, 130(35):11588–11589, 2008.

[19] Jan Ziegler, Shu Xu, Erol Kucur, Frank Meister, Miroslaw Batentschuk, Frank Gindele, and Thomas Nann. *Silica-Coated InP/ZnS Nanocrystals as Converter Material in White LEDs.* Advanced Materials, 20(21):4068–4073, 2008.

[20] Sunghoon Kim, Jaehyun Park, Sungwoo Kim, Won Jung, Jaeyoung Sung, and Sang-Wook Kim. *The effects of staggered bandgap in the InP/CdSe and CdSe/InP core/shell quantum dots.* Journal of Colloid and Interface Science, 346(2):347–351, 2010.

[21] Christian Ippen, Tonino Greco, and Armin Wedel. *InP/ZnSe/ZnS: A Novel Multishell System for InP Quantum Dots for Improved Luminescence Efficiency and Its application in a Light-Emitting Device.* Journal of Information Display, 13(2):91–95, 2012.

[22] Sungwoo Kim, Taehoon Kim, Meejae Kang, Seong Kwon Kwak, Tae Wook Yoo, Lee Soon Park, Ilseung Yang, Sunjin Hwang, Jung Eun Lee, Seong Keun Kim, and Sang-Wook Kim. *Highly Luminescent InP/GaP/ZnS Nanocrystals and Their Application to White Light-Emitting Diodes.* Journal of the American Chemical Society, 134(8):3804–3809, 2012.

[23] D. Gal and G. Hodes. *Electrochemical Deposition of ZnSe and (Zn,Cd)Se Films from Nonaqueous Solutions.* Journal of the Electrochemical Society, 147(5):1825–1828, 2000.

[24] D.S Sutrave, G.S Shahane, V.B Patil, and L.P Deshmukh. *Microcrystallographic and optical studies on $Cd_{1-x}Zn_xSe$ thin films.* Materials Chemistry and Physics, 65(3):298 – 305, 2000.

[25] Zeger Hens and Iwan Moreels. *Light absorption by colloidal semiconductor quantum dots.* Journal of Materials Chemistry, 22(21):10406–10415, 2012.

[26] Myriam Protière and Peter Reiss. *Highly Luminescent $Cd_{1-x}Zn_xSe$/ZnS Core/Shell Nanocrystals Emitting in the Blue–Green Spectral Range.* Small, 3(3):399–403, 2007.

[27] Shu-Ru Chung, Kuan-Wen Wang, Hong-Shuo Chen, and Hong-Hong Chen. *Novel red-emission of ternary ZnCdSe semiconductor nanocrystals.* Journal of Nanoparticle Research, 17(2):101, Feb 2015.

[28] Xinhua Zhong, Mingyong Han, Zhili Dong, Timothy J. White, and Wolfgang Knoll. *Composition-Tunable $Zn_xCd_{1-x}Se$ Nanocrystals with High Luminescence and Stability.* Journal of the American Chemical Society, 125(28):8589–8594, 2003.

[29] Y. Zheng, Z. Yang, and J.Y. Ying. *Aqueous Synthesis of Glutathione-Capped ZnSe and $Zn_{1-x}Cd_xSe$ Alloyed Quantum Dots.* Advanced Materials, 19(11):1475–1479, 2007.

[30] Xinhua Zhong, Yaoyu Feng, Yuliang Zhang, Zhenyu Gu, and Lei Zou. *A facile route to violet- to orange-emitting $Cd_xZn_{1-x}Se$ alloy nanocrystals via cation exchange reaction.* Nanotechnology, 18(38):385606, 2007.

[31] Olga I. Mićić, Barton B. Smith, and Arthur J. Nozik. *Core–Shell Quantum Dots of Lattice-Matched $ZnCdSe_2$ Shells on InP Cores: Experiment and Theory.* The Journal of Physical Chemistry B, 104(51):12149–12156, 2000.

[32] S. Leyre, E. Coutino-Gonzalez, J. J. Joos, J. Ryckaert, Y. Meuret, D. Poelman, P. F. Smet, G. Durinck, J. Hofkens, G. Deconinck, and P. Hanselaer. *Absolute determination of photoluminescence quantum efficiency using an integrating sphere setup.* Review of Scientific Instruments, 85(12):123115, 2014.

[33] Philippe F. Smet, Anthony B. Parmentier, and Dirk Poelman. *Selecting Conversion Phosphors for White Light-Emitting Diodes.* Journal of The Electrochemical Society, 158(6):R37–R54, 2011.

[34] L. Vegard. *Die Konstitution der Mischkristalle und die Raumfüllung der Atome.* Zeitschrift für Physik, 5(1):17–26, 1921.

[35] Woo-Seuk Song, Hye-Seung Lee, Ju Chul Lee, Dong Seon Jang, Yoonyoung Choi, Moongoo Choi, and Heesun Yang. *Amine-derived synthetic approach to color-tunable InP/ZnS quantum dots with high fluorescent qualities.* Journal of Nanoparticle Research, 15(6):1750, 2013.

[36] Mickael D. Tessier, Dorian Dupont, Kim De Nolf, Jonathan De Roo, and Zeger Hens. *Economic and Size-Tunable Synthesis of InP/ZnE (E = S, Se) Colloidal Quantum Dots.* Chemistry of Materials, 27(13):4893–4898, 2015.

[37] Mickael D. Tessier, Kim De Nolf, Dorian Dupont, Davy Sinnaeve, Jonathan De Roo, and Zeger Hens. *Aminophosphines: A Double Role in the Synthesis of Colloidal Indium Phosphide Quantum Dots.* Journal of the American Chemical Society, 138(18):5923–5929, 2016.

[38] Kyungnam Kim, Dongsuk Yoo, Hyekyoung Choi, Sudarsan Tamang, Jae-Hyeon Ko, Sungwoo Kim, Yong-Hyun Kim, and Sohee Jeong. *Halide–Amine Co-Passivated Indium Phosphide Colloidal Quantum Dots in Tetrahedral Shape.* Angewandte Chemie International Edition, 55(11):3714–3718, 2016.

[39] Aude Buffard, Sébastien Dreyfuss, Brice Nadal, Hadrien Heuclin, Xiangzhen Xu, Gilles Patriarche, Nicolas Mézailles, and Benoit Dubertret. *Mechanistic Insight and Optimization of InP Nanocrystals Synthesized with Aminophosphines.* Chemistry of Materials, 28(16):5925–5934, 2016.

[40] Jennifer L. Stein, Elizabeth A. Mader, and Brandi M. Cossairt. *Luminescent InP Quantum Dots with Tunable Emission by Post-Synthetic Modification with Lewis Acids.* The Journal of Physical Chemistry Letters, 7(7):1315–1320, 2016.

[41] Hyeokjin Lee, Heesun Yang, and Paul H. Holloway. *Single-step growth of colloidal ternary ZnCdSe nanocrystals.* Journal of Luminescence, 126(2):314–318, 2007.

[42] Esther Groeneveld, Leon Witteman, Merel Lefferts, Xiaoxing Ke, Sara Bals, Gustaaf Van Tendeloo, and Celso de Mello Donega. *Tailoring ZnSe–CdSe Colloidal Quantum Dots via Cation Exchange: From Core/Shell to Alloy Nanocrystals.* ACS Nano, 7(9):7913–7930, 2013.

[43] Mee Rahn Kim, Jae Hun Chung, Mihee Lee, Seonghoon Lee, and Du-Jeon Jang. *Fabrication, spectroscopy, and dynamics of highly luminescent core–shell InP@ZnSe quantum dots.* Journal of Colloid and Interface Science, 350(1):5–9, 2010.

[44] V. A. Fedorov, V. A. Ganshin, and Yu. N. Korkishko. *Determination of the Point of the Zincblende-to-Wurtzite Structural Phase Transition in Cadmium Selenide Crystals.* physica status solidi (a), 126(1):K5–K7, 1991.

[45] Chin-Yu Yeh, Z. W. Lu, S. Froyen, and Alex Zunger. *Zincblende–wurtzite polytypism in semiconductors.* Physical Review B, 46(16):10086–10097, 1992.

[46] Benoît Mahler, Nicolas Lequeux, and Benoît Dubertret. *Ligand-Controlled Polytypism of Thick-Shell CdSe/CdS Nanocrystals.* Journal of the American Chemical Society, 132(3):953–959, 2010.

[47] Yoyo Hinuma, Andreas Grüneis, Georg Kresse, and Fumiyasu Oba. *Band alignment of semiconductors from density-functional theory and many-body perturbation theory.* Physical Review B, 90(15):155405, 2014.

[48] Daniel Mourad, Gerd Czycholl, Carsten Kruse, Sebastian Klembt, Reiner Retzlaff, Detlef Hommel, Mariuca Gartner, and Mihai Anastasescu. *Band gap bowing of binary alloys: Experimental results compared to theoretical tight-binding supercell calculations for* $Cd_xZn_{1-x}Se$. Physical Review B, 82(16):165204, 2010.

# 6

# Enhanced Emission Photostability of InP/ZnSe Quantum Dots by Controlled Surface Chemistry

*We investigate the surface chemistry of InP/ZnSe QDs and demonstrate by using nuclear magnetic resonance spectroscopy, X-ray fluorescence spectroscopy and photostability measurements that photostability of InP/ZnSe QDs can be considerably improved by adding thiol molecules to oleylamine-capped InP/ZnSe QDs*

## 6.1 Introduction

Efficient QD-based luminescent down-convertors require QDs that are photostable. It then means that the QDs photoluminescence quantum yield (PLQY) should not drop under prolonged illumination with excitation light. For colloidal QDs, a photo-induced decrease of the PLQY or photobleaching has often been reported, especially in the case of single QD spectroscopy, where the excitation pump power per QD is high (up to 20 kW/cm$^2$).[1] In

general, photobleaching has been attributed to the light-induced oxidation of QDs by oxidizing agents such as water.[2] In the particular case of InP-based QDs, Kim *et al.* showed that the emission of InP/ZnS QDs decreases with time upon UV irradiation.[3] They demonstrated that an external indium oxide coating can increase the emission photostability. In this chapter, we demonstrate that in the case of InP/ZnSe QDs, the emission photostability can be enhanced by changing the surface chemistry. We show that the ligands initially present at the InP/ZnSe QD surface can be replaced by dodecanethiol (DDT). The thus obtained thiol-capped QDs have been incorporated into polymer layers in order to test their emission properties. Both in the case of InP/ZnSe and InP/(Zn,Cd)Se QDs, this amine for thiol ligand exchange markedly improves the resistance to photobleaching and results in a higher emission efficiency after prolonged light exposure. This last chapter underlies the importance of surface chemistry with a view of obtaining highly efficient QD-based light emitting devices.

## 6.2 Experimental section

**Chemicals:** Indium(III) chloride (99.999 %), zinc(II) bromide ($\geq$ 98 %), tris(diethylamino)phosphine $P(NEt_2)_3$ (97 %), selenium powder 100 mesh (99.99 %) and 1-dodecanethiol ($\geq$ 98 %) were purchased from Sigma Aldrich. Trioctylphosphine (TOP; >97 %) were purchased from Strem Chemicals. Oleylamine (OLA; 80-90 %) was purchased from Acros Organics (NB: Oleylamine is stored under inert atmosphere). 1-octadecene (ODE; technical 90 %) was purchased from Alfa Aesar.

**InP/ZnSe QDs synthesis with zinc stearate:** See the synthesis protocol of 629 nm emitting core/shell InP/ZnSe QDs in the Experimental Section of Chapter 5. Here, at the end of the reaction, InP/ZnSe QDs were precipitated once in ethanol and suspended in toluene. Then, 0.5 mL of dodecanethiol was added to this solution and a final precipitation/resuspension cycle was performed.

**InP/ZnSe QDs synthesis without zinc stearate:** 50 mg (0.225 mmol) of indium(III) chloride and 1 g (2.2 mmol) of zinc(II) bromide were mixed in 5 mL (15 mmol) of technical oleylamine. The reaction mixture was stirred and degassed at 120 ℃ for an hour and then heated to 230 ℃ under inert atmosphere. Upon reaching 180 ℃, a volume of 0.23 mL (0.8 mmol) of tris(diethylamino)phosphine was quickly injected in the above mixture and InP nanocrystals synthesis proceeded. The reaction occurred during 3 min.

After the InP core formation, at 3 min, 1.5 mL of stoichiometric TOP-Se (2.24 M) was injected at 230 ℃. Then temperature was increased from 240 to 320 ℃. At 30 min the reaction was stopped and the temperature was lowered. InP/ZnSe QDs were then precipitated once in ethanol and suspended in toluene. Then, 0.5 mL of dodecanethiol was added to this solution and a final precipitation/resuspension cycle was performed.

**QD-doped remote phosphor layers - formation:** See the QD-doped remote phosphor layers - formation in the Experimental Section in Chapter 5. Additional 20 $\mu$L of dodecanethiol were added during the QD-doped remote phosphor layers formation.

**QD-doped remote phosphor layers - characterization:** See the QD-doped remote phosphor layers - characterization in the Experimental Section in Chapter 5.

**NMR spectroscopy:** Nuclear magnetic resonance (NMR) spectra were recorded on a Bruker Avance II spectrometer operating at a $^{1}$H frequency of 500 MHz and using a TXO-Z probe. Samples were prepared by evaporating InP/ZnSe QD dispersions to dryness under a continuous nitrogen flow, redispersing the QDs in 500 $\mu$L of dry deuterated toluene and transferring the solution to an NMR tube (5 mm). Quantitative $^{1}$H spectra were recorded with a 20 s delay between scans to allow for full relaxation of all NMR signals and with the spectral width set to 16 ppm. The quantification was done by using the Digital ERETIC method in Topspin 3.5. The NOESY mixing time was set to 300 ms and 2048 data points in the direct dimension for 512 data points in the indirect dimension were typically sampled, with the spectral width set to 11.5 ppm. Diffusion measurements (2D $^{1}$H DOSY) were performed using a double stimulated echo sequence for convection compensation and with monopolar gradient pulses. Smoothed rectangle gradient pulse shapes were used throughout.

**X-Ray fluorescence spectroscopy:** InP QDs were first drop-cast on paper filter. The X-ray fluorescence spectrum were measured using a Rigaku NEX CG.

**Rutherford backscattering spectroscopy:** Rutherford backscattering spectrometry was performed by measuring backscattered $He^{+}$ ions accelerated to an energy of 1.57 MeV with an NEC 5SDH-2 Pelletron tandem accelerator with a semiconductor detector at a backscattering angle of 168°.

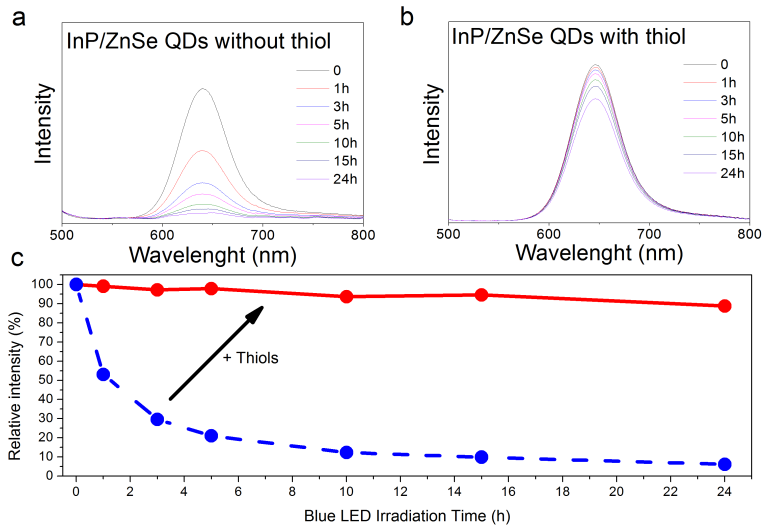


**Figure 6.1:** (**a**) Photoluminescence spectra of InP/ZnSe QDs without any thiol addition dispersed in polymer layer under blue LED excitation during 24 hours. (**b**) Photoluminescence spectra of InP/ZnSe QDs with a thiol treatment dispersed in polymer layer under blue LED excitation during 24 hours. (**c**) Evolution of the integrated photoluminescence intensity of both sample as a function of time.

## 6.3 Results

InP/ZnSe QDs were produced by the aminophosphine-based method, using zinc stearate for shell growth. The protocol is outlined in the Experimental Section. The QDs were mixed with a triblock copolymer (Kraton FG1901X, see Experimental Section) in order to obtain a solid luminescent layer by dropcasting. As shown in Figure 6.1a, we observed a pronounced drop of the luminescence intensity with time when this luminescent layer was exposed to the light of a blue pump light emitting diode (LED). As mentioned in the introduction, this so-called photobleaching has been described before in the literature, and it is a major issue for making efficient luminescent devices based on QDs. On the other hand, we found that photobleaching could be considerably reduced by exposing InP/ZnSe QDs to DDT prior to the formation of the QD-in-polymer films (see Figure 6.1b). As outlined in the Experimental Section, thiol-exposure involves the addition of dodecanethiol to a dispersion of purified, as-synthesized InP/ZnSe QDs, followed by a single precipitation/resuspension cycle and the further addition of 20 $\mu$L dodecanethiol during the remote phosphor layer preparation. Figure 6.1c,

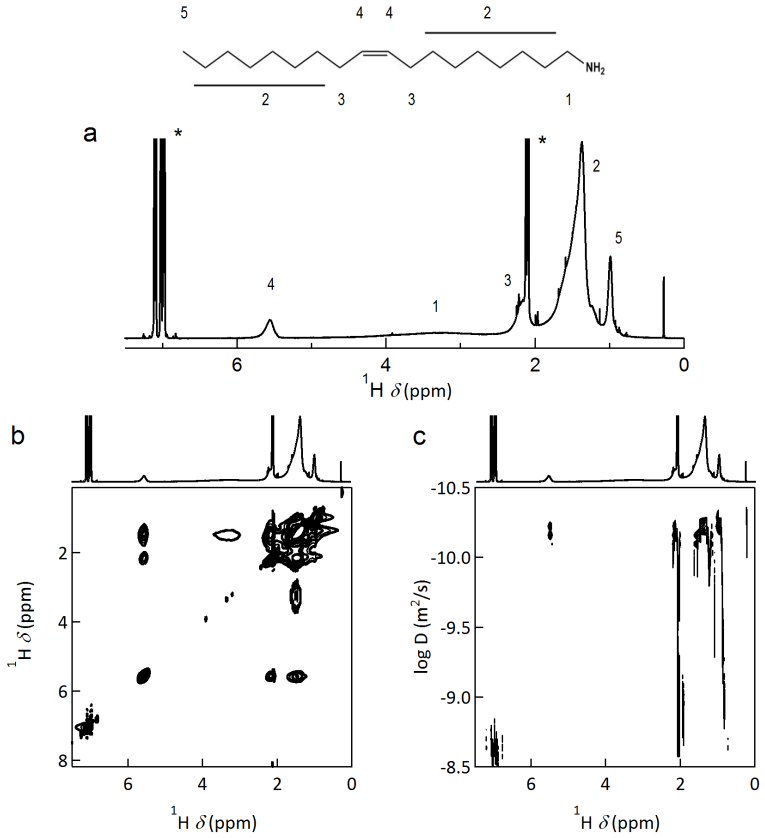


**Figure 6.2:** (**a**) 1D $^{1}$H NMR spectrum of InP/ZnSe (8 nm) QDs stabilized by OLA in toluene-$d_8$. The protons of OLA are denoted by the numbers. * denotes the solvent resonances. (**b**) 2D NOESY spectrum of InP/ZnSe QDs stabilized by OLA in toluene-$d_8$. (**c**) 2D DOSY spectrum of the same solution.

represents in more detail the integrated emission intensities of as-synthesized InP/ZnSe QDs and the same QDs after dodecanethiol exposure as a function of light exposure time. One sees that after 24 hours of exposure to blue light, the intensity of the original QDs was quenched almost completely, while the QDs processed with thiols retained up to 90 % of their initial emission intensity.

To address the effect thiol exposure has on the photobleaching behavior of InP/ZnSe QDs in more detail, we analyzed InP/ZnSe QD dispersions prior to and after a dodecanethiol treatment using solution NMR spectroscopy.

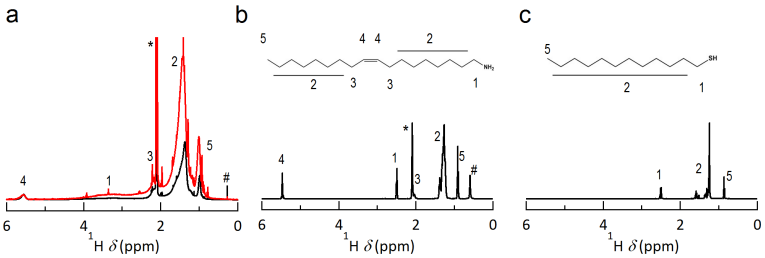


**Figure 6.3:** (**a**) 1D $^1$H NMR spectra of InP/ZnSe QDs stabilized by OLA (black spectrum) and DDT (red spectrum) in toluene-$d_8$. The protons of OLA and DDT are denoted by the numbers. * denotes the solvent resonances. (**b**) 1D $^1$H NMR spectra of free OLA. (**c**) 1D $^1$H NMR spectra of free DDT.

Solution NMR is well established as a technique to analyze the interaction of ligands with QD surfaces, where especially the combination of 1D $^1$H, diffusion ordered spectroscopy (DOSY) and nuclear Overhauser effect spectroscopy (NOESY) can be used to identify and quantify bound ligands.[4] In order to simplify the study, we developed an InP/ZnSe QDs without zinc stearate (see Experimental Section). Indeed, as zinc stearate can act as a ligand in its own right, a synthesis that only contains oleylamine and zinc chloride for the shell growth can strongly facilitate the interpretation of the different ligand resonances in an NMR study. In this respect, it is important to mention that we observed a similarly enhanced photostability by thiol exposure in the case of InP/ZnSe QDs made without zinc stearate.

Figure 6.2, shows the results of a combined NMR analysis on as-synthesized, purified InP/ZnSe QDs. The 1D $^1$H NMR spectrum represented in Figure 6.2a features broad resonances, corresponding to ligands bound to the nanocrystals.[4] The signature resonance of the alkene protons clearly indicates that oleylamine is the main ligand stabilizing the nanocrystal. We obtain a ratio between the integrated intensities of the alkene resonance on the one hand and the $CH_2$ and $CH_3$ resonances on the other hand of 2/36, which indicates that oleylamine is the only organic ligand. The NOESY confirms that the oleylamine interacts with the surface (see Figure 6.2b). Indeed, the oleylamine resonances all exhibit the negative nuclear Overhauser effects (nOe) expected for species interacting with colloidal nanocrystals. The DOSY spectrum (see Figure 6.2c) yields a diffusion coefficient of 60.5 $\pm$ 0.3 $m^2/s$, which corresponds to a hydrodynamic diameter of 12 nm. The diffusion coefficient corresponds to oleylamine bound to the surface of the nanocrystals.

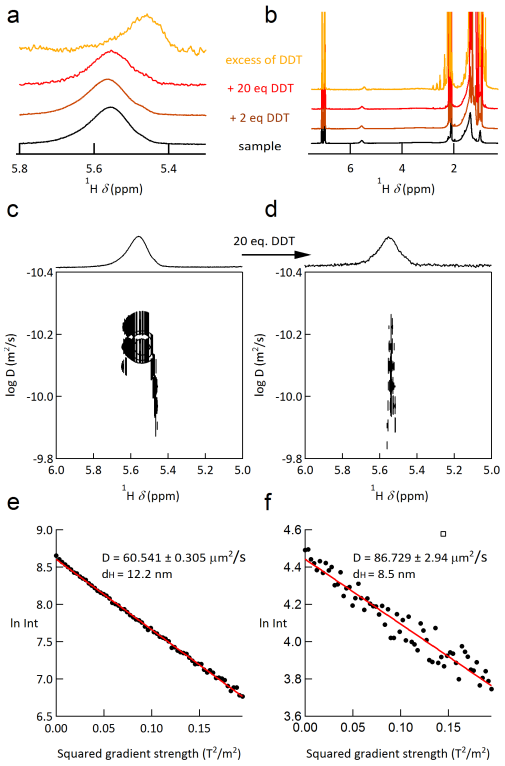


**Figure 6.4:** (**a**) 1D $^1$H NMR spectra of a dispersion of InP/ZnSe QDs stabilized by OLA after addition of different amount of DDT. (**b**) Zoom on a region of the alkene resonance. (**c**) Zoom on a region of the alkene resonance on the 2D DOSY spectrum of InP/ZnSe QDs stabilized by OLA. (**d**) Zoom on a region of the alkene resonance on the 2D DOSY spectrum of InP/ZnSe QDs stabilized by OLA and with excess of DDT. (**e**) DOSY monoexponential decay of the alkene resonance on the bound oleylamine. (**f**) DOSY monoexponential decay of the alkene resonance with excess of DDT.

Figure 6.3a represents the $^1$H NMR spectra of as-synthesized InP/ZnSe QDs (InP/ZnSe-OLA) and the InP/ZnSe QDs after dodecanethiol addition and purification (InP/ZnSe-DDT). Both spectra have been rescaled so as to match the intensity of the alkene resonance. This simple rescaling makes clear that the InP/ZnSe-DDT sample has a significantly larger signal intensity in the aliphatic region (1.5-1.0 ppm) than expected for a ligand shell consisting merely of OLA. Moreover, this additional signal intensity is linked to broadened resonances, not to narrow resonances that would character-

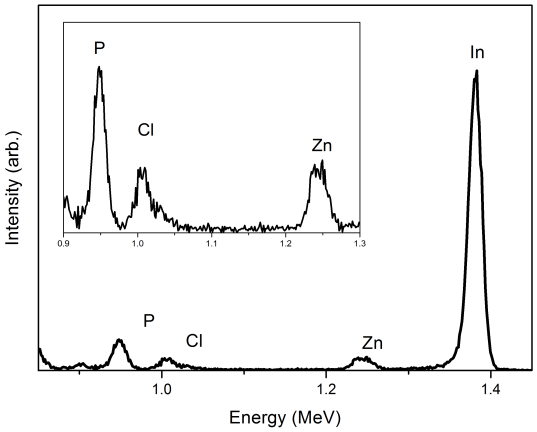


**Figure 6.5:** RBS spectrum of InP QDs made with $InCl_3$ and $ZnCl_2$.

ized free species. In addition, the integration of the alkene resonance in the 1D $^1$H NMR spectra of InP/ZnSe QDs stabilized by OLA and DDT reveals that 50 % OLA is left after a dodecanethiol treatment. This indicates that the dodecanethiol exposure results in InP/ZnSe nanocrystals that have a ligand shell containing both oleylamine and dodecanethiol. We thus conclude that dodecanthiol binds to the ZnSe surface, possibly replacing a part of the originally bound oleylamine.

Figure 6.4a shows 1D $^1$H NMR spectra of a set of dispersions that were obtained by adding 2 and 20 equivalents of dodecanethiol, followed by addition of an even larger excess ($>$ 100 equivalents) of dodecanethiol to a dispersion of purified, as-synthesized InP/ZnSe-OLA QDs. Focusing on the alkene resonance at around 5.55 ppm, it can be seen that the alkene resonance exhibits a pronounced upfield shift (see Figure 6.4b). This indicates that the local environment of OLA changes upon DDT addition, where the observed upfield shift would agree with the change from an aliphatic to an aromatic environment that accompanies desorption of OLA. The tentative conclusion that DDT addition induces OLA desorption is corroborated by pulsed field gradient spectroscopy. Figure 6.4c and 6.4d represent the 2D DOSY spectrum of InP/ZnSe-OLA before and after addition of 20 equivalents of DDT, respectively. In both cases, the signal intensity exhibits a single exponential decay as a function of the square of the gradient strength. DDT addition, however, leads to a slight increase of the diffusion coefficient linked to OLA, where the corresponding solvodynamic diameter drops from 12.2 to 8.5 nm. This suggests that DDT addition changes OLA from a tightly bound to a rapidly exchanging ligand, where it switches between a

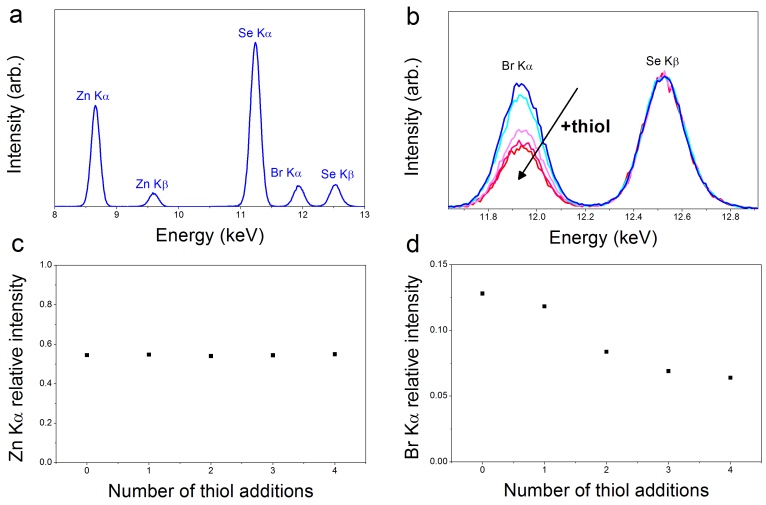


**Figure 6.6:** (**a**) XRF spectrum of InP/ZnSe QDs made with $InCl_3$ and $ZnBr_2$. (**b**) XRF Br K$\alpha$ and Se K$\beta$ lines of InP/ZnSe QDs after several addition of thiol followed by a washing step. (**c**) Zn K$\alpha$ lines intensity relative to Se K$\alpha$ intensity. (**d**) Br K$\alpha$ lines intensity relative to Se K$\alpha$ intensity

bound and a free state with a time constant shorter than the diffusion delay. This is consistent with a release of bound OLA from the QD surface.

In literature, it has already been shown that the surface of InP QDs made with the aminophosphine-based can be enriched in halides.[5] To investigate this in more detail, we analyzed the composition of core InP QDs using Rutherford backscattering spectrometry (RBS). Figure 6.5 represents on RBS spectrum, recorded on a thin film of as-synthesized, purified InP QDs that were synthesized using $InCl_3$ and $ZnCl_2$. It can be seen that the spectrum features 4 signals, which correspond to backscattering on P, Cl, Zn and In nuclei. From the integrated signal intensity, we estimate the composition of the core InP QDs as 41 % of In, 37 % of P, 16 % of Cl and 5 % of Zn. Focusing first on In and P, the elements constituting the actual inorganic core QDs, we thus find an In/P ratio of 1.1. In line with several metal chalcogenide nanocrystals, such as CdSe, CdTe, PbS and PbSe, we thus find that the InP nanocrystal is enriched in cations - indium in this case - which are probably present as a surface excess. In addition, the RBS spectrum indicates that a purified InP nanocrystal sample also contains Zn and Cl. We know from Raman spectroscopy that Zn is most likely not incorporated into the InP core,[6] suggesting that the InP nanocrystals have

a surface enriched in Zn. The charge on the excess surface cations – both $In^{3+}$ and $Zn^{2+}$ in this case – must be compensated by anions. In the case of CdSe nanocrystals synthesized in the presence of carboxylic acids, this anions typically involve carboxylates that bind as X-type ligands to the nanocrystal surface. Here, on the other hand, we find that the 16 % of Cl present almost compensates the charge on the excess In and Zn. This indicates that the InP surface can be best seen as terminated by an excess of $InCl_3$ and $ZnCl_2$, which makes for overall charge neutral nanocrystals.

InP/ZnSe core/shell QDs feature a similar cation excess. In this case, we used X-ray fluorescence spectroscopy (XRF) to analyze their composition. Figure 6.6a shows that purified, as-synthesized InP/ZnSe QDs made using with indium chloride and zinc bromide contain mostly Zn, Se and Br. From the XRF intensities, we estimate a relative composition of 50 % Zn, 45 % Se and 5 % Br. Hence, also in this case, the surface can be well described as terminated by $ZnBr_2$. This conclusion is in line with the previous observation that such InP/ZnSe QDs are capped with oleylamine, which is an L-type ligand that typically binds as a neutral moiety to nanocrystal surfaces. Interestingly, we find that after several repeated exposures of InP/ZnSe QDs to dodecanethiol, the amount of bromide in the samples decreased (see Figure 6.6b-d) while the relative amount of Zn and Se remains constant (see Figure 6.6b-c). This indicates that part of dodecanthiol binds to the ZnSe outer surface as dodecanethiolate, an X-type ligand that can compensate the positive charge on the excess Zn cations.

## 6.4 Discussion

We have shown that the exposure of InP/ZnSe core/shell QDs to dodecanethiol enhances their photostability. We hypothesize that this effect is related to a different termination of the ZnSe outer surface, induced by the exposure to dodecanethiol. According to NMR spectroscopy, as-synthesized InP/ZnSe nanocrystals are stabilized by tightly bound oleylamine. Amines are L-type ligand, *i.e.* Lewis bases, that interact with Lewis acidic surface sites. In addition, elemental analysis showed that as-synthesized InP/ZnSe nanocrystals are enriched in Zn and contain Br; a combination we attributed to the binding of $ZnBr_2$ to the ZnSe outer surface. We summarize both observations in the structural model of the ZnSe outer surface as shown in Figure 6.7.

The NMR analysis further confirmed that dodecanethiol can bind to the ZnSe surface and displace oleylamine. This indicates that oleylamine and

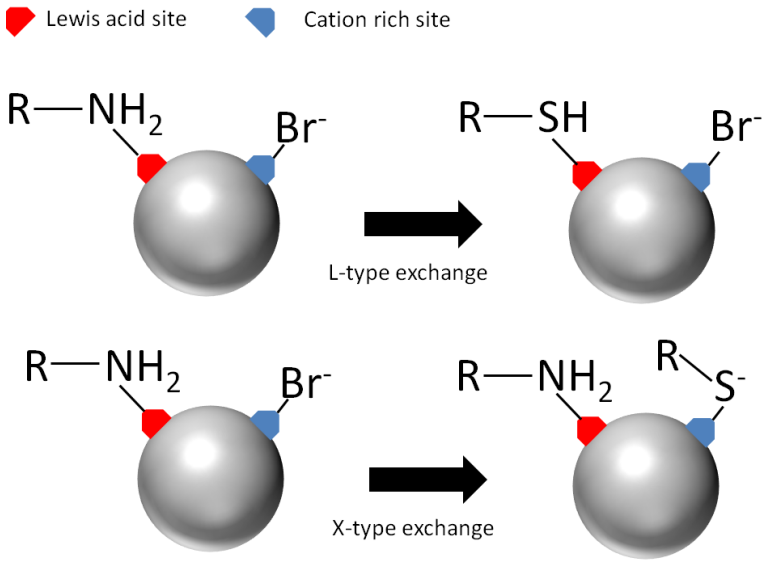


**Figure 6.7:** Two proposed exchange mechanism

dodecanethiol are involved in a L-for-L exchange reaction, where dodecanthiol acts as an L-type ligand by means of its two lone pairs. Such an exchange reaction has been described before, for example in the case of CdSe QDs.[7] According to XRF, exposure of InP/ZnSe QDs to dodecanethiol also displaces bromide from the ZnSe surface. Such a reaction cannot be the action of an L-type ligand, since this would result in a nanocrystal carrying a net positive charge. On the other hand, an exchange of bromide for thiolate – a proper X-type ligand – can explain this observation. We therefore propose a set of 2 exchange reactions that account for the effect of dodecanethiol exposure on the surface chemistry of InP/ZnSe QDs (see figure 6.7).

Both reactions have been depicted in Figure 6.7a-b, showing that after dodecanthiol exposure, InP/ZnSe nanocrystals with a mixed dodecanethiol/-dodecanethiolate ligand shell are obtained. Note that this double role of thiols – acting both as L and X-type ligands – has been described before in the case of CdSe QDs.[7] Finally, it should be noted that we never obtained a full thiol exchange, nor a full displacement of bromide. Consequently, dodecanethiol exposure will lead to a complex ligand shell, composed of dodecanthiol/dodecanethiolate, oleylamine and the halide used in the synthesis.

The effect of thiols on the emission properties of colloidal QDs have already been discussed before in the literature. In the case of single CdSe/ZnS QDs, for example, it was shown that blinking can be suppressed in the presence of $\beta$-mercaptoethanol.[8] It was also demonstrated that the effect on the CdSe/ZnS PLQY can depend on the amount of $\beta$-mercaptoethanol used, where a small amount leads to an increase of the PLQY and larger amounts result in a decrease.[9] On the other hand, it was demonstrated that 11-mercapto-1-undecanol reduces the PLQY of CdSe/ZnS, whereas a thiol functionalized with a benzophenone chromophore leads to a PLQY increase.[10] On ZnSe QDs solubilized in water, it was shown that the addition of thiols, such as thioglycerol, thioglycolic acid, or 3-mercapto-propionic acid, results in a strong increase of the QDs PLQY.[11] Importantly, it has been also shown that the photo-oxidation of CdSe QDs can be prevented by the addition of thiol excess. It has been proposed that surface-bound thiols are oxidized at the CdSe QDs surface, which results in the formation of disulfides.[12] This thiol oxidation would than act as a sacrificial reaction, preventing the CdSe QDs oxidation. Here, a similar role of dodecanethiol on InP/ZnSe QDs can be envisaged.

## 6.5 Conclusion

In this chapter, we have first shown that an addition of dodecanethiol to InP/ZnSe QDs dispersions strongly suppresses the photobleaching of the QD emission. This enhanced photostability can be observed in polymer layers. We have then demonstrated by an extended NMR study that dodecanethiol can bind to the InP/ZnSe QDs surface. Upon binding, it can displace both the oleylamine and halide ions that make up the surface termination of the as-synthesized InP/ZnSe QDs. In this process, a mixed ligand shell containing dodecanethiol and dodecanethiolate together with residual oleylamine and halide is formed.

# References

[1] Wilfried G. J. H. M. van Sark, Patrick L. T. M. Frederix, Ageeth A. Bol, Hans C. Gerritsen, and Andries Meijerink. *Blueing, Bleaching, and Blinking of Single CdSe/ZnS Quantum Dots.* ChemPhysChem, 3(10):871–879, 2002.

[2] S. R. Cordero, P. J. Carson, R. A. Estabrook, G. F. Strouse, and S. K. Buratto. *Photo-Activated Luminescence of CdSe Quantum Dot Monolayers.* The Journal of Physical Chemistry B, 104(51):12137–12142, 2000.

[3] Jung-Ho Jo, Jong-Hoon Kim, Sun-Hyoung Lee, Ho Seong Jang, Dong Seon Jang, Ju Chul Lee, Ko Un Park, Yoonyoung Choi, Chunghun Ha, and Heesun Yang. *Photostability enhancement of InP/ZnS quantum dots enabled by $In_2O_3$ overcoating.* Journal of Alloys and Compounds, 647(Supplement C):6 – 13, 2015.

[4] Zeger Hens and José C. Martins. *A Solution NMR Toolbox for Characterizing the Surface Chemistry of Colloidal Nanocrystals.* Chemistry of Materials, 25(8):1211–1221, 2013.

[5] Kyungnam Kim, Dongsuk Yoo, Hyekyoung Choi, Sudarsan Tamang, Jae-Hyeon Ko, Sungwoo Kim, Yong-Hyun Kim, and Sohee Jeong. *Halide–Amine Co-Passivated Indium Phosphide Colloidal Quantum Dots in Tetrahedral Shape.* Angewandte Chemie International Edition, 55(11):3714–3718, 2016.

[6] M. Rafipoor, H. Tornatzky, D. Dupont, M. D. Tessier, Z. Hens, J. Maultzsch, and H. Lange. *Strain Engineering in InP/(Zn,Cd)Se Core/Shell Alloys.* Manuscript under preparation, 2017.

[7] Jonathan S. Owen, Jungwon Park, Paul-Emile Trudeau, and A. Paul Alivisatos. *Reaction Chemistry and Ligand Exchange at Cadmium-Selenide Nanocrystal Surfaces.* Journal of the American Chemical Society, 130(37):12279–12281, 2008.

[8] Sungchul Hohng and Taekjip Ha. *Near-Complete Suppression of Quantum Dot Blinking in Ambient Conditions.* Journal of the American Chemical Society, 126(5):1324–1325, 2004.

[9] Sohee Jeong, Marc Achermann, Jagjit Nanda, Sergei Ivanov, Victor I. Klimov, and Jennifer A. Hollingsworth. *Effect of the ThiolThiolate Equilibrium on the Photophysical Properties of Aqueous CdSe/ZnS*

*Nanocrystal Quantum Dots.* Journal of the American Chemical Society, 127(29):10126–10127, 2005.

[10] Jordi Aguilera-Sigalat, Simon Rocton, Raquel E.Galian, and Julia Pérez-Prieto. *Fluorescence enhancement of amine-capped CdSe/ZnS quantum dots by thiol addition.* Canadian Journal of Chemistry, 89(3):359–363, 2011.

[11] Alexey Shavel, Nikolai Gaponik, and Alexander Eychmüller. *Efficient UV-Blue Photoluminescing Thiol-Stabilized Water-Soluble Alloyed ZnSe(S) Nanocrystals.* The Journal of Physical Chemistry B, 108(19):5905–5908, 2004.

[12] Jose Aldana, Y. Andrew Wang, and Xiaogang Peng. *Photochemical Instability of CdSe Nanocrystals Coated by Hydrophilic Thiols.* Journal of the American Chemical Society, 123(36):8844–8850, 2001.

# 7

# Summary and perspectives

## 7.1 Summary

Colloidal semiconductor nanocrystals (NCs) or quantum dots (QDs) are a new class of materials that offer various promising applications in fields related to light emission and absorption. Monodisperse ensembles of QDs feature a narrow, size-tunable emission spectrum in combination with a broad absorption and excitation spectrum and are suitable for solution-based processing. These characteristics make QDs emitting in the visible of particular interest for lighting and display applications. In the latter, the white backlight is replaced by the combination of a blue light-emitting diode (LED) and a remote phosphor film that contains QDs emitting in the green and the red part of the visible spectrum. The QDs absorb part of the blue LED light and convert it into narrow green and red light. In this way, the white spectrum is composed of three narrow lines: a blue line from the pump LED and red and green lines from the QD emission. The use of QDs as luminescent wavelength converters strongly enhances the color gamut of an LCD as compared to similar displays with a backlight characterized by a broad, white spectrum.

In this respect, cadmium-based QDs stand out as they exhibit excellent optical properties and are relatively easy to synthesize. However, stringent restrictions on the use of cadmium in consumer products have initiated a shift from the well characterized Cd-based QDs to Cd-free alternatives such as InP QDs where the latter combine emission characteristics that come close to CdSe QDs with a reduced toxicity. Still, InP-based core/shell QDs generally have a reduced absorption cross section as well as a poor photo-stability with respect to Cd-based QDs. Therefore, it is important to understand how to control the core/shell interface, the shell composition and the shell surface in order to optimize the performance of InP-based QDs. In addition, the widespread use of InP-based QDs is hampered by the more difficult synthesis, which often involves expensive and hazardous phosphorous precursors. Hence, there is also a need to find more efficient and cheaper synthesis methods to promote the use of InP-based QDs into product application. The thesis aimed at addressing these issues.

In chapter 3, we first developed an economical way to produce InP QDs using aminophosphine, an approach that was derived from initial literature results presented in chapter 2. We found that the conversion of the indium precursor into InP QDs strongly depends on the P/In molar ratio, where an excess of the aminophosphine (P:In ratio of 4) leads to a full conversion of the indium precursor into InP QDs. This view is supported by an investigation on the reaction mechanism. We demonstrated by an analysis of the exhaust of an InP QD synthesis in combination with a nuclear magnetic resonance spectroscopy (NMR) study that the reaction is initiated by a transamination reaction. This corresponds to an exchange between the amines used as the solvent in the synthesis and the amino groups coordinating to phosphorus in the original precursor. Next, we showed that an excess of aminophosphine is required to attain a full chemical yield as the latter acts both as the reducing agent and the phosphorous precursor in the synthesis. It has been confirmed by mass spectroscopy and NMR measurements that one aminophosphine is reduced from $P^{III}$ to $P^{-III}$ to form one InP unit, whereas the three remaining aminophosphines serve as reducing agents and are transformed into phosphonium salts ($P^{V}$) during the reaction.

In chapter 4, we show that size of InP core QDs synthesized using a full yield reaction involving aminophosphines can be tuned by changing the indium halide used as the indium precursor. However, InP core QDs produced with this method show a low luminescence. If a II-VI shell material with a wider band gap is grown around InP core QDs, photoluminescent core/shell QDs can be obtained that emit visible light. This, in combination with the high chemical reaction yield, enabled photoluminescent InP/ZnS and InP/ZnSe

core/shell QDs to be formed that emit from 510 to 630 nm. Furthermore, we point out that the emission properties depend on the nature of the shell material. For example, a ZnS shell coating leads to an emission linewidth broader than for a ZnSe shell coating, yet tends to result in better quantum yields.

In chapter 5, we present a method to embed InP-based QDs into polymer layer and analyzed their emission properties in a remote phosphor configuration. We show that InP/ZnSe QDs have a relatively low absorption coefficient at 450 nm, the central wavelength of the blue LEDs typically used in displays or lighting applications. This raises the amount of material needed to achieve a predefined color conversion and makes InP/ZnSe QDs prone to self-absorption, two elements that have a negative impact on the performance and the cost of color-converter films. We show that this problem can be addressed by admixing small amounts of Cd in the ZnSe shell since the resulting (Zn,Cd)Se shells have a smaller band gap than the original ZnSe shells. Comparing the photoluminescence efficiency of InP/ZnSe and InP/(Zn,Cd)Se QD layers, we find that the latter exhibit a significantly larger absorptance of blue LED light – they achieve the same color conversion as InP/ZnSe QDs loaded films with $\approx$ 74 % less QDs by mass – and do not suffer from an efficiency loss due to self-absorption.

In chapter 6, we show that the exposure of InP/ZnSe QDs to dodecanthiol results in an enhanced photostability. Using NMR spectroscopy and elemental analysis, we show that dodecanethiol exposure changes the composition of the ligand shell; from the original combination of oleylamine and excess halide to a mixture of dodecanethiol and dodecanethiolate with residual oleylamine and halide. While the relation between this change in ligand shell composition and the enhanced photostabiliy remains unclear, we speculate that the inclusion of dodecanethiol suppresses the photo-oxidation of the ZnSe outer surface.

## 7.2 Prospects

In this thesis we presented synthesis methods that make possible the economical production of InP-based QDs, including size control at full chemical yield, shell growth and surface engineering. We showed that the thus obtained InP-based QDs can be used as materials for luminescent wavelength conversion for both general lighting and display backlighting. However, to realize such applications, several challenges linked to optical properties, nanocrytals synthesis and material composition remain to be addressed.

As shown in the literature overview given in chapter 2 and throughout the experimental results presented in this thesis, InP QDs typically have emission lines with a full width at half maximum (FWHM) higher than 45 nm. This is broad as compared to Cd-based QDs, perovskite nanocrystals, or CdSe-based nanoplatelets, which can reach a FWHM of only 10 nm and it is a borderline value in view of most applications that rely on the photoluminescence of colloidal QDs. Addressing this, however, is not easy since it remains unclear as to why some hot injection syntheses attain narrow size dispersions and others do not. At least, it will require a more in-depth study on the factors tha affect the balance between nucleation and growth during the synthesis of colloidal nanocrystals.

To be successfully applied in consumer products, QDs must exhibit a highly efficient photoluminescence that is stable against external influences such as the prolonged exposure to light, heat, humidity, and air. The PLQY of InP/ZnS and InP/ZnSe QDs synthesized along the lines discussed in this thesis can be as high as 75-80 %, still photostability remains an issue. Even after exposure to dodecanethiol, a measurable drop of the PLQY occurs after only 24 hours of permanent illumination. To address this issue – and further enhance the PLQY of as-synthesized InP-based QDs – an in-depth study of defects at the core/shell interface and the shell outer surface is needed. At best, such a study combines experimental data on interface or surface composition with theoretical approaches to model the energy-level spectrum of pristine and purposefully distorted nanocrystals, similar to what has been done recently in the case of CdSe QDs.

A further issue the possible widespread use of InP-based QDs for luminescent down-conversion faces is the indium. Indium is scarce and expensive and therefore not well suited for mass products. Here, Ga- and Al-based III-V semiconductors can offer a useful alternative. Within this material family, a broad range of bulk band gaps can be addressed and the lattice mismatch with, for example, ZnSe is minimal. Unfortunately, no synthesis recipes are available today that lead to high quality Ga- and Al-based III-V nanocrystals. Possibly, the use of aminophosphines and aminoarsines – which were successfully used to synthesize InAs QDs – opens new possibilities in this direction.

Finally, using InP-based QDs in lighting and display applications will require an upscaling of the production volume achievable at laboratory scale to volumes in line with industrial demands. Upscaling can be envisaged through a larger volume batch process, or by implementing the synthesis in a flow reactor. For both implementations, the aminophosphine-based approach is highly attractive. As can be seen in each method section, it

relies on hazard-free precursors and shell growth is accomplished by adding additional reagents to the core reaction mixture. Moreover, one can see that such core/shell syntheses are executed at an exceptionally high solid loading. Consequently, low amount of solvent is needed per gram of QD-material synthesized, which reduces reactor volumes and synthesis cost. Hence, in view of the above mentioned points, synthesis upscaling may be the easiest challenge to address.